

MASSIVE STARS IN MOLECULAR CLOUDS RICH IN HIGH-ENERGY SOURCES: THE BRIDGE OF G332.809–0.132 AND CS 78 IN NGC 6334.

MARIA MESSINEO¹, KARL M. MENTEN², DONALD F. FIGER³, J. SIMON CLARK⁴

Draft version July 23, 2020

ABSTRACT

Detections of massive stars in the direction of the HII region CS 78 in NGC 6334 and of G332.809–0.132 are here presented. The region covered by the G332.809–0.132 complex coincides with the RCW 103 stellar association. In its core (40' in radius), approximately 110 OB candidate stars ($K_s < 10$ mag and $0.4 < A_{K_s} < 1.6$ mag) were identified using 2MASS, DENIS, and GLIMPSE data. This number of OB stars accounts for more than 50% of the observed number of Lyman continuum photons from this region. Medium-resolution K -band spectra were obtained for seven early types, including one WN 8 star and one Ofpe/WN 9 star; the latter is located near the RCW 103 remnant and its luminosity is consistent with a distance of ≈ 3 kpc. The area analyzed encloses 9 of the 34 OB stars previously known in RCW 103, as well as IRAS 16115–5044 which we reclassify as a candidate luminous blue variable. The line of sight is particularly interesting, crossing three spiral arms; a molecular cloud at -50 (with RCW 103 in the Scutum-Crux arm) and another at -90 km s⁻¹ (in the Norma arm) are detected, both rich in massive stars and supernova remnants.

We also report the detection of a B supergiant as the main ionizing source of CS 78, 2MASS J17213513–3532415. Medium-resolution H and K -band spectra display H I and He I lines, as well as Fe II lines. By assuming a distance of 1.35 kpc, we estimate a bolometric magnitude of -6.16 , which is typical of supergiants.

Subject headings: Stellar evolution — Infrared sources — Supergiant stars — Early-type emission stars — Supernova remnants

1. INTRODUCTION

Massive stars ($< \approx 8 M_\odot$) are key contributors to the chemical enrichment of the Milky Way with their high mass-loss rates. They explode as supernovae creating neutron stars and black holes, and are believed to be sources of γ -ray bursts, which are the most energetic explosions in the Universe. Much of what we know about the masses of supernova progenitors and the fates of massive stars come from theoretical work (Heger et al. 2003). Ideally, progenitor masses could be measured by studying young pulsars and supernova remnants associated with young stellar clusters/massive stars. However, because of their short life spans, massive stars are rare and predominantly observed in young (a few megayear) massive ($\sim 10^4 M_\odot$) clusters. Stellar clusters are important building blocks of a Galaxy, and the best natural laboratories to test theories of star formation and stellar evolution. However, in recent years, analyses of open clusters and of their surroundings have revealed the enigmatic existence of several massive stars in isolation (Gvaramadze et al. 2012). Massive stars seen in isolation could be either stars born in isolation, or in an already dissolved cluster, or ejected from a nearby cluster. Theoretical simulations show that a cluster may lose up to 25% of massive stars via ejection, including its most

massive members (e.g., Oh et al. 2014). A fraction of stars may be born by hierarchical star formation and not by monolithic collapses, such as stars in the Cyg OB1 association (e.g., Wright et al. 2015).

Ideally, one should analyze the content of evolved massive stars per region, where “region” is the environmental unit in which the cluster was formed, i.e., the parental molecular cloud. Eventually, the comparison between various units will yield new insights into the distribution of various types of massive stars and the remnants of core-collapse supernovae (SNRs). Currently, this topic is widely discussed, and several works have been published (e.g., Humphreys et al. 2017; Smith & Tombleson 2015).

A total of 295 SNRs (Green 1991) are known in the Milky Way. Almost 80 very-high-energy γ -ray emitters have been discovered with the High Energy Stereoscopic System (HESS) (H. E. S. S. Collaboration et al. 2018); they are mostly found associated with young pulsar wind nebulae and SNRs. Several new high-mass X-ray binaries have been discovered in Chandra and XMM data. However, very few collapsed objects (pulsars and black holes) and remnants are currently confirmed to be associated with young stellar clusters rich in massive stars. For example, the soft gamma repeater SGR 1806–20 is associated with the massive cluster Cl 1806–20 (Figer et al. 2005); an X-ray pulsar was detected in Westerlund 1 by Muno et al. (2006); the TeV source HESS J1837–069 was likely originated from a member of the Red Supergiant cluster 1 (RSGC 1) (Figer et al. 2006; Gotthelf & Halpern 2008); the magnetar SGR 1900+14 is found to be associated with a cluster of two red supergiants (RSGs) (Davies et al. 2009); the TeV gamma-ray source HESS 1640–465 is located a few arcminutes away from the stellar cluster Mercer 81 (Davies et al. 2012), and SGR J1745–29 is located near the Galactic center (GC) cluster (Mori et al. 2013).

Based on observations collected at the European Southern Observatory (ESO Programmes 087.D-09609).

MM is currently employed by USTC. This work was designed during her ESA fellowship (2010), and partially carried out at the MPIR.

¹ Key Laboratory for Researches in Galaxies and Cosmology, University of Science and Technology of China, Chinese Academy of Sciences, Hefei, Anhui, 230026, China

² Max-Planck-Institut für Radioastronomie, Auf dem Hügel 69, D-53121 Bonn, Germany

³ Center for Detectors, Rochester Institute of Technology, 54 Memorial Drive, Rochester, NY 14623, USA

⁴ Department of Physics and Astronomy, The Open University, Walton Hall, Milton Keynes, MK7 6AA, UK

With regard to SNRs, a letter from Pauls (1977) reports the serendipitous discovery of the positional coincidence of SNR G127.1+00.5 with the open cluster NGC 559. A longer discussion of positional coincidences of SNRs with stellar clusters is given by Kumar (1978). The author concluded that most coincidences are random, while he suggested that SNR G291.0-0.1 is located in the open cluster Trumpler 18. While the first-mentioned association (NGC 559 with an SNR) still holds, that of Trumpler 18 could not be confirmed (Acero et al. 2016; Kharchenko et al. 2016). More recently, Safi-Harb et al. (2007) investigated the likelihood of an association between the NGC 5281 cluster, which contains the enigmatic X-ray emitter HD 119682, and the SNR G309.2-00.6, with the result that it could not be established. Messineo et al. (2008) reported that the SNR G12.72-0.00 positionally coincided with the massive stellar cluster Cl 1713-178. However, we estimated that almost 90% of the celestial superpositions of clusters and SNRs are chance coincidences (see the Appendix).

Certainly, it is important to carefully examine stellar associations and giant molecular cloud complexes with care for their content of massive stars, pulsars, and SNRs. Examples include the Cygnus region that contains about 10 SNRs and 14 pulsars, along with some of the most massive stellar associations of the Milky Way (9 OB associations) (Abeysekera et al. 2018). Sparse massive stars and one young stellar cluster (GLIMPSE9) are found to populate the G23.3-0.3 ([23,78]) complex (Messineo et al. 2014), which contains four SNRs: W41 (which hosts the TeV emitter HESS J1834-087), G22.7-0.2 (SNR2), G22.7583-0.4917 (SNR3), and G22.9717 - 0.3583 (SNR4).

Comparisons of the spatial distribution of different types of evolved massive stars (e.g. Wolf-Rayet stars (WRs), B supergiants, RSGs) have recently been reported (e.g., Smith & Tombleson 2015). The rarity of known massive stars and the mounting evidence that a large fraction of them is found in isolation (loose associations or ejected stars) motivate us to look for them also outside stellar clusters, by using other tracers, such as molecular clouds rich in high-energy sources and SNRs. Inspired by this idea and by the availability of large surveys of the Galactic plane at near- and mid-infrared wavelengths, we searched for massive stars in the direction of a few regions rich in high-energy sources.

In Sections 2 and 3, we describe the targets, the spectroscopic observations, and available photometric data. In Section 4, we analyze the infrared spectra. In Sections 5 and 7, we briefly describe the core of the giant molecular complex G332.809-0.132 and the HII region CS 78 in NGC 6334, and we discuss the likely association of the massive stars detected with these regions.

2. THE SAMPLE

In this work, we present bright infrared stars in the direction of two prominent Galactic star-forming regions that have a remarkable number of high-energy sources associated with them: the core of the giant HII region G332.809-0.132 (hereafter called “The Bridge”) (Rahman & Murray 2010) and CS 78 in NGC 6334 (Churchwell et al. 2007). The two regions are listed in Table 1.

The list of observed targets is provided in Tables 2 (8 early-type stars), **3, and 4** (76 late-type stars). K_s magnitudes of the targets and serendipitous detections range from 3.9 mag to 12.05 mag; $H-K_s$ colors are mostly from 0.5 mag to 1.2 mag. The majority of the targets were selected as infrared-bright

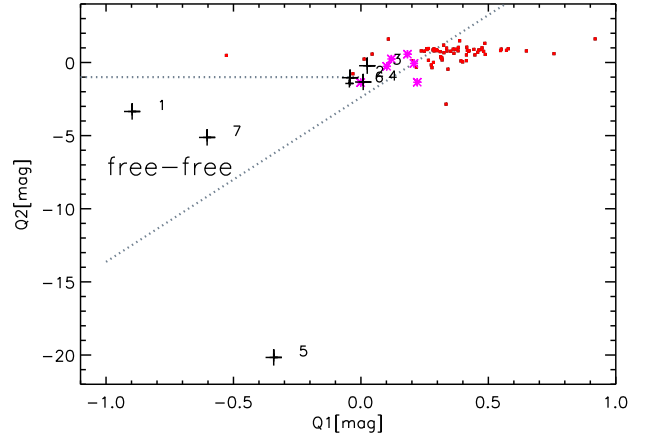


FIG. 1.— $Q1$ versus $Q2$ diagram of targets. Plus signs indicate the early-type stars from Table 2; those with emission lines are marked with larger crosses. Small red boxes mark the late-type stars in Table 4, and magenta asterisks those with water absorption (Mira-like stars). The two gray lines are from Messineo et al. (2012) and mark the region where free-free emitters resides.

and obscured stars in the directions of the chosen regions. In Fig. 1, we plot their $Q2$ versus the $Q1$ values, as defined in Messineo et al. (2012)⁵. In the $J-H$ versus $H-K_s$ plane, $Q1$ is equivalent to the distance on the y-axis of a datapoint to a vector that passes through the origin and follows the vector of interstellar extinction (e.g., Messineo et al. 2012, 2014). In the $J-K_s$ versus $K_s-[8.0]$ plane, $Q2$ is equivalent to the distance on the y-axis of a datapoint to a vector that passes through the origin and follows the vector of interstellar extinction. $Q2$ is a measure of the $8.0 \mu\text{m}$ excess. The area below $Q2 = -1$ mag and to the left of the oblique line is rich in free-free emitters (e.g., Messineo et al. 2012; Mauerhan et al. 2011). This diagram is a powerful diagnostic for locating free-free emitters (84% of the Wolf-Rayet stars, WRs, and 67% of known luminous blue variables, LBVs, are located in this area). Normal OB stars are located to the right of the oblique line and late-type stars to its left side. Due to stellar variability and nonsimultaneity of the measurements, additional criteria are required to identify OB stars, for example, the classical $J-H$ versus $J-K_s$ diagram or the $I-J$ versus $J-K_s$ diagram. Details on the number of candidate OB stars are given in Section 5.5.

3. DATA

3.1. Spectroscopic Observations and Data Reduction

Observations were made with the Son of Isaac (SofI) instrument on the ESO New Technology Telescope (NTT) on La Silla on 2011 June 10-12 (under ESO Program 087.D-09609, see also Messineo et al. (2014)). Spectra with the medium-resolution grism, a slit width of $1''$, and the K_s filter that covers from $2.0 \mu\text{m}$ to $2.3 \mu\text{m}$ at a resolving power $R \sim 2200$, were obtained for all targets. Additionally, low-resolution spectra covering from $1.53 \mu\text{m}$ to $2.52 \mu\text{m}$ with $R \sim 980$ were taken for a few targets. Medium-resolution spectra in the H -band with a slit width of $1''$, covering from $1.5 \mu\text{m}$ to $1.8 \mu\text{m}$ with a resolving power of ~ 1250 , were taken for one interesting target (star E1).

Pairs of frames were subtracted and flat-fielded. One to three stellar traces were identified in each frame and extracted. Wavelength calibration was performed with Xe and

⁵ $Q1 = (J - H) - 1.8 \times (H - K_s)$; $Q2 = (J - K_s) - 2.69 \times (K_s - [8.0])$.

TABLE 1
LIST OF OBSERVED REGIONS.

ID	Molecular Cloud	Radio/X-rays	Ra[J2000] (hh mm ss)	Dec[J2000] (dd mm ss)	Radius (arcmin)
1	G332.809–0.132-Bridge	3 SNRs + 1 PWN + 6 PSRs	16 16 08	–51 01 04	40
2	NGC 6334/CS 78 ^a	PSR B1718-35	17 21 35	–35 32 41	2

Notes. CS 78 (with a radius of 2') is a bubble identified with GLIMPSE data (Churchwell et al. 2007). It is detached from the bulk of emission of the molecular complex NGC 6334 (which has a radius about 20'), and it is located in its northeastern periphery (e.g., see figures in Willis et al. 2013).

Ne arc spectra. Correction for atmospheric and instrumental responses was performed by dividing the target spectrum by spectra of B-type stars taken in the same manner and at a similar air mass to the target. Telluric lines were removed with linear interpolation.

Observed targets are listed in Tables 2, 3, and 4.

3.2. Photometric Data

For every spectroscopically observed star, we searched for counterparts in the Two Micron All Sky Survey (2MASS) Catalog of Point Sources (Cutri et al. 2003; Skrutskie et al. 2006), in the third release of Deep Near Infrared Survey of the Southern Sky (DENIS) data available at CDS (catalog B/denis) (Epchtein et al. 1994), in the Galactic Legacy Infrared Midplane Survey Extraordinaire (GLIMPSE) catalog (Churchwell et al. 2009), and in the Wide-field Infrared Survey Explorer (WISE) catalog (Wright et al. 2010) using the closest match within a search radius of 2". The II/293 GLIMPSE catalog from CDS is a combination of the original GLIMPSE-I (v2.0), GLIMPSE-II (v2.0), and GLIMPSE-3D catalogs. WISE counterparts were retained only if their signal-to-noise ratios were larger than 2.5. We searched for counterparts in the Version 2.3 of the The Midcourse Space Experiment (MSX) Point Source Catalog (PSC) (Price et al. 2001) using a search radius of 5". MSX upper limits were removed.

Due to their brightness, targets are mostly saturated in the VISTA Variables in the Via Lactea (VVV) dataset (Saito et al. 2012). For a few fainter targets with 2MASS upper limits, VVV photometric measurements were adopted.

Using 2MASS positions, we searched for *BVR* photometry in The Naval Observatory Merged Astrometric Dataset (NOMAD) (Zacharias et al. 2004) and for Gaia data in the second release (DR2) (Gaia Collaboration et al. 2018). The photometric data are listed in the Appendix A.

In the following sections, Gaia DR2 parallactic distances will be considered, but only for those objects with fractional error on the parallax (ϖ) smaller than 20% and with weighed errors (UWE) within the limits advised by Luri et al. (2018). A zero point of +0.029 mas was used.

4. ANALYSIS

4.1. Spectra of Early-type Stars

We detected eight early-type stars, with associated spectra shown in Figs. 2 and 3, and listed in Table 2.

Star E1 was observed in both *H* and *K* bands, as shown in Fig. 3 and Table 3. The *K* band shows the He I line at 2.058 μm in emission, the iron line at 2.089 μm in emission, and the Br_γ in emission. The *H*-band spectrum displays the H I lines in emission, along with two Fe II lines at 1.5778 and 1.6878 μm (Morris et al. 1996; Steele & Clark 2001). There is also a hint of [FeII] at 1.6642 μm . The absence of He I emission at 2.112 μm and the lack of Mg

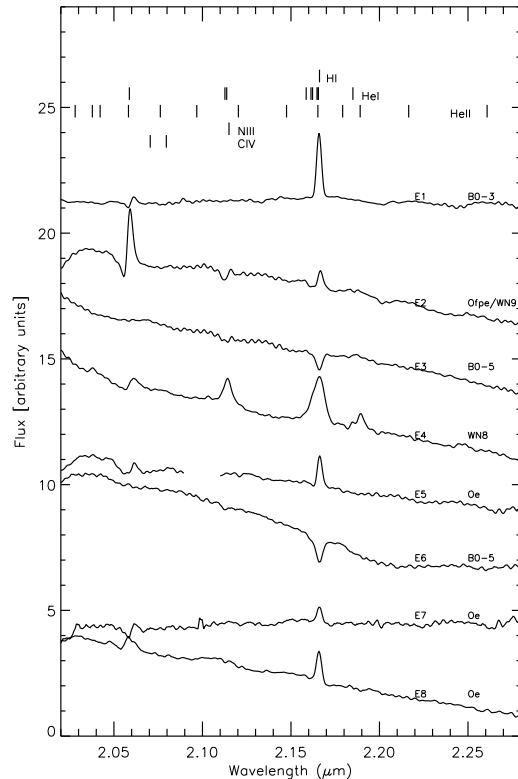


FIG. 2.— *K*-band spectra of detected early-type stars.

II lines 2.138 μm and 2.144 μm suggest T_{eff} lower than that of [OMN2000]LS1 (≈ 13000 K Clark et al. 2009) and [MDF2011]15 (≈ 16000 K Messineo et al. 2011). On the other hand, star E1 has infrared spectral features similar to those seen in the low-resolution spectra of S Dor taken in 1993 September by Morris et al. (1996). Its spectrum also lacks He I emission. S Dor is an LBV and has a variable spectral type that ranges from B3 to F type (Massey 2000). The spectrophotometric work of Wolf & Kaufer (1997) reports a minimum of S Dor between the beginning of 1993 and the end of 1994. van Genderen et al. (1997) provide a spectral type of B3 (16000 K) for observations taken on 1993, April 22. We conclude that the temperature of star E1 must be in the range of 13000–16000 K (B5–B3).

The spectrum of star E2 shows a strong He I line at 2.058 μm , a Br_γ line in emission, a He I line at 2.112 μm in absorption, and NIII at 2.115 μm in emission. The ratio of the He I and Br_γ lines is typical of Ofpe/WN 9 stars, which are massive evolved stars in transition to the WR phase (e.g., Najarro et al. 1997; Messineo et al. 2009).

The spectra of stars E3 and E6 have He I lines at 2.112 μm (in absorption), and Br_γ lines (in absorption). The lack of

TABLE 2
LIST OF DETECTED EARLY-TYPE STARS.

ID	α [J2000]	δ [J2000] (hh mm ss)	Sp. type (deg mm ss)	T_{eff} (K)	Field	2MASS ID/Alias
E1	17 21 35.13	-35 32 41.60	B3-5	14600± 900	CS 78	J17213513-3532415
E2	16 17 42.92	-50 54 25.14	Ofpe/WN 9	26500± 6500	G332.809-0.132	J16174291-5054251
E3	16 17 42.04	-50 56 37.26	B0-5	20600± 6900	G332.809-0.132	J16174204-5056372
E4	16 20 16.07	-50 58 07.68	WN 8	45000± 5000	G332.809-0.132	J16201606-5058076
E5	16 17 02.20	-50 47 03.18	Oe	37700± 6700	G332.809-0.132	J16170220-5047031/[RA2004a] IRS 1
E6	16 20 09.03	-50 48 58.84	B0-5	20600± 6900	G332.809-0.132	J16200902-5048588/TYC 8324-906-1
E7	16 17 09.23	-50 47 14.70	Oe	37700± 6700	G332.809-0.132	J16170923-5047147/[RA2004a] IRS 2
E8	16 17 03.01	-50 47 30.84	Oe	37700± 6700	G332.809-0.132	J16170300-5047308

Notes. Identification numbers are followed by coordinates, spectral types, effective temperatures, T_{eff} , and field name. Sources are listed per field and are sorted by K_s magnitude within each field.

TABLE 3
LIST OF LINES DETECTED IN THE SPECTRUM OF STAR E1.

Line	Vacuum λ (μm)	Obs. λ (μm)	EW (\AA)	FWHM (\AA)
H I 18-4	1.53460 ^b	1.53409	2.1 ± 0.8	30 ± 2
H I 17-4	1.54432 ^b	1.54389	2.6 ± 0.7	27 ± 2
H I 16-4	1.55605 ^a	1.55600	5.0 ± 1.5	37 ± 2
H I 15-4	1.57050 ^b	1.57051	1.6 ± 0.3	23 ± 2
FeII z^2 I _{11/2} -3 d ⁵ 4 s ² I _{11/2}	1.5776 ^c	1.57624	1.1 ± 0.1	18 ± 3
H I 14-4	1.58849 ^b	1.58865	2.9 ± 0.3	32 ± 2
H I 13-4	1.61138 ^b	1.61145	3.2 ± 0.6	28 ± 2
H I 12-4	1.64114 ^a	1.64089	3.8 ± 0.6	27 ± 1
H I 11-4	1.68111 ^a	1.68108	3.1 ± 0.6	22 ± 2
FeII z^4 F _{9/2} -c ⁴ F _{9/2}	1.68778 ^c	1.68840	3.6 ± 0.8	34 ± 2
H I 10-4	1.73669 ^a	1.73644	4.9 ± 0.5	32 ± 1
He I	2.05869 ^a	2.06190	..	25 ± 8
Fe II z^4 F _{3/2} ⁰ -c ⁴ F _{3/2} ?	2.091 ^c	2.08911	0.6 ± 0.4	18 ± 3
H I 7-4	2.16612 ^a	2.165871	8.2 ± 1.4	27 ± 3

Notes. ^a from the NIST line list. ^b Storey & Hummer (1995). ^c Morris et al. (1996), Clark et al. (1999).

He II lines suggests that these are B0-5 stars (B0-8I or B0-3V).

The spectrum of star E4 has the He I line at 2.058 μm in emission, the N III complex at 2.115 μm in emission, the Br_γ line in emission, and the He II line at 2.189 μm in emission. This broad-line spectrum resembles that of WR 130 (Figer et al. 1997), which is classified as a WN 8 star by van der Hucht (2001).

The spectra of stars E5, E7, and E8 display Br_γ lines in emission. Because H -band spectra are not available, we will call them OBe stars. Star E5 appears as a blend of two stars, which are surrounded by a gaseous ring (see charts in Appendix C). Stars E5 ([RA2004a] IRS 1), E7 ([RA2004a] IRS 2), and L74 ([RA2004a] IRS 9) have been analyzed with infrared photometry by Roman-Lopes & Abraham (2004). For stars E5 and E7, the authors have inferred spectral types O5 and mid-O, respectively.

4.2. Spectra of Late Types

K_s -band spectra of late-type stars are characterized by CO bands in absorption. The equivalent widths of the CO bands, $\text{EW}(\text{CO})$, linearly increase with decreasing temperatures. EWs were determined with a line taken from 2.285 μm to 2.307 μm (high-resolution) or from 2.285 μm to 2.315 μm (low-resolution) and using two estimates of the continuum; one continuum was taken as the average flux density

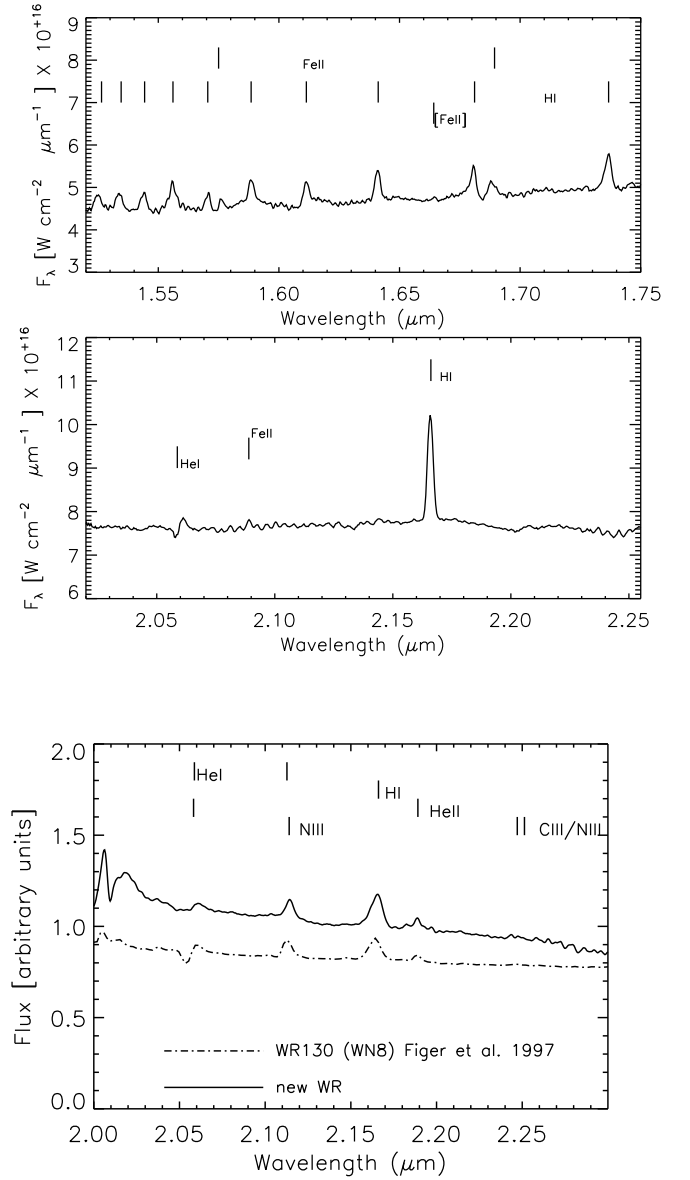


Fig. 3.— Upper and middle panels: H - and K -bands spectra of star E1. Bottom panel: K -band spectrum of star E4, a newly discovered WR star, of WN 8 type. For a comparison, a spectrum of WR 130 from the atlas of Figer et al. (1997) is shown with a dotted line.

from 2.285 μm to 2.290 μm (Figer et al. 2006) and a second

TABLE 4
SPECTRA OF DETECTED LATE-TYPE STARS.

ID	RA(J2000) [hh mm ss]	DEC(J2000) (deg mm ss)	EW(CO)-high* (K)	EW(CO)-low (K)	Sp[rgb]	Sp[rsg]	Type	Field	2MASS-ID/Alias
L1	16 17 29.76	-50 55 39.64	41± 2	..	M7	K5	..	G332.809-0.132	J16172975-5055396/IRAS 16137-5048
L2	16 20 20.86	-50 53 37.21	51± 1	51± 4	..	M2	..	G332.809-0.132	J16202085-5053372
L3	16 16 58.67	-51 04 01.69	49± 2	M2	..	G332.809-0.132	J16165866-5104016/IRAS 16132-5056
L4	16 18 14.49	-50 56 13.45	41± 2	..	M7	K5	Mira	G332.809-0.132	J16181449-5056134
L5	16 18 25.88	-51 02 05.56	48± 3	M1	Mira	G332.809-0.132	J16182588-5102055/IRAS 16145-5054
L6	16 17 30.93	-50 58 35.12	30± 3	..	M2	K2	..	G332.809-0.132	J16173092-5058351/TYC 8323-726-1
L7	16 17 08.76	-51 02 17.22	28± 1	..	M1	K2	Mira	G332.809-0.132	J16170875-5102172/TYC 8323-928-1
L8	16 16 52.03	-51 05 33.59	46± 2	M1	..	G332.809-0.132	J16165202-5105335
L9	16 17 18.77	-51 01 36.43	27± 3	..	M1	K2	..	G332.809-0.132	J16171876-5101364
L10	16 16 58.27	-50 50 47.40	30± 3	..	M2	K2	..	G332.809-0.132	J16165827-5050474
L11	16 17 18.06	-50 57 29.24	40± 6	..	M7	K5	..	G332.809-0.132	J16171805-5057292
L12	16 16 49.59	-50 51 17.24	44± 2	..	M7	M0	..	G332.809-0.132	J16164958-5051172
L13	16 17 04.73	-50 59 41.71	34± 2	..	M4	K3	..	G332.809-0.132	J16170473-5059417
L14	16 16 16.69	-51 14 59.81	37± 3	..	M6	K4	..	G332.809-0.132	J16161669-5114598
L15	16 19 08.56	-50 45 09.09	40± 4	..	M7	K5	Mira	G332.809-0.132	J16190855-5045090
L16	16 22 28.57	-50 49 28.07	44± 3	..	M7	M0	..	G332.809-0.132	J16222857-5049280
L17	16 17 24.47	-51 03 32.02	37± 2	..	M6	K4	..	G332.809-0.132	J16172446-5103320/GSC 8323-1211
L18	16 19 37.96	-50 57 29.86	38± 5	..	M6	K5	..	G332.809-0.132	J16193796-5057298
L19	16 19 16.22	-51 02 17.65	41± 4	..	M7	K5	..	G332.809-0.132	J16191621-5102176
L20	16 21 58.62	-51 05 14.86	46± 1	M1	Mira	G332.809-0.132	J16215861-5105148
L21	16 17 38.73	-50 59 38.32	49± 2	M2	..	G332.809-0.132	J16173873-5059383
L22	16 18 43.30	-50 56 40.10	43± 3	..	M7	M0	..	G332.809-0.132	J16184330-5056401
L23	16 18 13.16	-51 02 10.65	31± 3	..	M3	K3	Mira	G332.809-0.132	J16181315-5102106
L24	16 21 56.79	-51 01 14.53	40± 2	41± 1	M7	K5	..	G332.809-0.132	J16215678-5101145
L25	16 17 03.52	-50 55 02.68	39± 3	..	M7	K5	..	G332.809-0.132	J16170351-5055026
L26	16 22 25.10	-50 48 35.90	44± 4	..	M7	M0	..	G332.809-0.132	J16222509-5048358
L27	16 18 01.46	-50 55 58.85	37± 2	..	M6	K4	..	G332.809-0.132	J16180145-5055588
L28	16 17 36.17	-50 55 23.64	39± 3	..	M7	K5	..	G332.809-0.132	J16173617-5055236
L29	16 16 19.70	-51 14 01.78	35± 2	..	M4	K4	..	G332.809-0.132	J16161970-5114017
L30	16 17 45.40	-50 58 02.02	36± 4	..	M5	K4	..	G332.809-0.132	J16174539-5058020
L31	16 17 35.34	-50 57 09.18	19± 3	..	K2	K0	..	G332.809-0.132	J16173534-5057091
L32	16 17 06.52	-51 00 05.84	47± 2	M1	..	G332.809-0.132	J16170651-5100058
L33	16 19 24.79	-51 08 20.98	38± 1	40± 1	M7	K5	..	G332.809-0.132	J16192478-5108209
L34	16 16 41.97	-51 06 05.57	36± 1	..	M5	K4	..	G332.809-0.132	J16164196-5106055
L35	16 20 22.94	-50 53 29.08	46± 2	47± 4	..	M1	..	G332.809-0.132	J16202293-5053290
L36	16 16 50.14	-51 12 23.61	39± 3	..	M7	K5	..	G332.809-0.132	J16165014-5112236
L37	16 18 57.81	-50 52 29.36	39± 1	..	M7	K5	..	G332.809-0.132	J16185780-5052293
L38	16 16 43.75	-51 11 13.24	43± 2	..	M7	M0	..	G332.809-0.132	J16164375-5111132

Notes. Sources are sorted by K_s magnitude. Identification numbers are followed by celestial coordinates, EW(CO) from the high-resolution mode, EW(CO) from the low-resolution mode, inferred spectral types (for giants and supergiants), comment on the type, and field name. (*) EW(CO) from the high-resolution mode (slit of 1'') have been multiplied by a factor 1.85 to match those from the low-resolution mode (slit of 0.6'').

continuum was taken as a linear fit to the flux densities from 2.250 μm to 2.257 μm , from 2.270 μm to 2.277 μm , and from 2.285 μm to 2.290 μm (Ramírez et al. 2000). Spectral types were derived by comparing the obtained EWs with those of stellar templates of K and M types (Kleinmann & Hall 1986). Spectral types derived from the seven low-resolution spectra are typically accurate within two subclasses (Figer et al. 2006; Messineo et al. 2017).

For the 76 spectra with the high-resolution mode, the transmission quickly drops down longward of 2.3 μm , so EW(CO) from the high-resolution mode are more uncertain than those from the low mode. We recalibrate the EW from the high-resolution spectra with those measurements in common with the low-resolution spectra. Because the EW(CO) and temperatures of giants and supergiants follow two different linear relations (Blum et al. 2003; Figer et al. 2006), spectral types were derived for giants and supergiants. Detected late-type stars are listed in Table 4. A few targets with spectra that show curved continua are marked in the Table as Mira stars.

In the catalog by Skiff (2014), GSC 8323-1211 (L17) is reported as an M2 star; we estimated an M6 type by assuming a giant. L48 (M5) coincides with [BRA2016]-DBS100-Obj4 and L71 (M7) with the candidate young stellar object [BRA2016]-DBS100-ysoc (Borissova et al. 2016).

5. THE CORE OF G332.809-0.132: "THE BRIDGE"

Because of the estimated number of Lyman continuum photons, Rahman & Murray (2010) reported G332 as one of the 14 extended giant complexes of the Galaxy identified with WMAP data (with a semi-major axis of 93.6), where one-third of Galactic free-free emission resides. G332.809-0.132 is the associated star forming complex at 3.4 kpc (with a semi-major axis of 48'), object n. 34 in Table 2 of Rahman & Murray (2010). We estimated that the 14 extended regions (Table 1 of Rahman et al.) cover 27% of the disk ($360^\circ \times 1^\circ$) and include 50% of the Conti & Crowther giant HII regions, while the identified star-forming (SF) complexes (Table 2 of Rahman et al.) cover 4% of the disk and include

TABLE 4
CONTINUATION OF TABLE 4.

ID	RA(J2000) (hh mm ss)	DEC(J2000) (deg mm ss)	EW(CO)-high (K)	EW(CO)-low (K)	Sp[rgb]	Sp[rsg]	Type	Field	2MASS-ID/Alias
L39	16 16 46.98	-51 08 43.46	36± 3	..	M5	K4	..	G332.809-0.132	J16164698-5108434
L40	16 19 29.03	-50 42 25.71	38± 2	..	M6	K5	..	G332.809-0.132	J16192903-5042257
L41	16 16 56.37	-50 54 26.34	40± 2	..	M7	K5	..	G332.809-0.132	J16165636-5054263
L42	16 21 56.89	-51 03 56.01	33± 0	36± 0	M3	K3	..	G332.809-0.132	J16215688-5103560
L43	16 18 05.17	-50 54 35.53	37± 3	..	M6	K4	..	G332.809-0.132	J16180517-5054355
L44	16 17 29.04	-51 00 23.50	43± 1	..	M7	M0	..	G332.809-0.132	J16172904-5100234
L45	16 16 40.40	-51 07 32.75	17± 2	..	K1	K0	..	G332.809-0.132	J16164039-5107327/TYC 8323-2680-1
L46	16 17 26.06	-51 02 56.05	43± 1	..	M7	M0	..	G332.809-0.132	J16172605-5102560
L47	16 16 44.17	-51 04 08.21	35± 2	..	M5	K4	..	G332.809-0.132	J16164417-5104082
L48	16 20 27.39	-50 54 42.00	35± 1	34± 1	M5	K4	..	G332.809-0.132	J16202739-5054420/[BRA2016]-DBS100-Obj4
L49	16 18 43.49	-50 56 11.19	35± 2	..	M4	K4	..	G332.809-0.132	J16184348-5056111
L50	16 18 10.35	-51 01 57.36	33± 2	..	M4	K3	..	G332.809-0.132	J16181035-5101573
L51	16 17 51.06	-50 53 14.34	30± 4	..	M2	K2	..	G332.809-0.132	J16175105-5053143
L52	16 19 37.74	-50 58 13.68	41± 4	..	M7	K5	..	G332.809-0.132	J16193774-5058136
L53	16 17 58.23	-51 00 59.49	36± 1	..	M5	K4	..	G332.809-0.132	J16175823-5100594
L54	16 16 48.47	-51 08 39.38	30± 1	..	M2	K2	..	G332.809-0.132	J16164846-5108393
L55	16 17 44.77	-50 57 45.13	39± 2	..	M7	K5	..	G332.809-0.132	J16174477-5057451
L56	16 20 16.21	-50 58 52.28	36± 3	..	M5	K4	..	G332.809-0.132	J16201621-5058522
L57	16 17 46.28	-50 58 23.54	40± 2	..	M7	K5	..	G332.809-0.132	J16174628-5058235
L58	16 17 01.80	-50 47 30.49	21± 2	..	K3	K0	..	G332.809-0.132	J16170180-5047303
L59	16 17 14.37	-50 47 18.83	40± 2	..	M7	K5	..	G332.809-0.132	J16171437-5047188
L60	16 20 07.49	-50 47 12.40	30± 0	..	M2	K2	..	G332.809-0.132	J16200749-5047123
L61	16 18 57.83	-50 51 53.86	30± 0	..	M2	K3	..	G332.809-0.132	J16185783-5051538
L62	16 20 09.46	-50 49 25.61	16± 0	..	K1	K0	..	G332.809-0.132	J16200945-5049256
L63	16 20 28.27	-50 54 49.35	27± 0	..	M0	K1	..	G332.809-0.132	J16202826-5054493
L64	16 17 34.73	-50 55 10.61	27± 1	..	M1	K2	..	G332.809-0.132	J16173473-5055106
L65	16 20 20.94	-50 54 46.75	34± 1	..	M4	K4	..	G332.809-0.132	J16202094-5054467
L66	16 20 18.66	-50 55 11.53	40± 1	..	M7	K5	..	G332.809-0.132	J16201866-5055114
L67	16 16 12.48	-51 16 21.77	29± 2	..	M1	K2	..	G332.809-0.132	J16161247-5116217
L68	16 20 23.06	-50 52 32.90	32± 0	30± 3	M3	K3	..	G332.809-0.132	J16202305-5052328
L69	16 20 26.32	-50 55 10.07	37± 1	..	M6	K4	..	G332.809-0.132	J16202632-5055100
L70	16 17 13.60	-50 48 11.98	49± 2	M1	..	G332.809-0.132	J16171360-5048119
L71	16 20 24.71	-50 54 04.46	39± 1	..	M7	K5	..	G332.809-0.132	J16202470-5054044/[BRA2016]-DBS100-ysoc
L72	16 17 07.84	-50 46 45.47	25± 0	..	K5	K1	..	G332.809-0.132	J16170784-5046454
L73	16 20 27.69	-50 54 56.21	43± 3	..	M7	M0	..	G332.809-0.132	J16202772-5054564
L74	16 17 04.37	-50 47 16.44	29± 2	..	M2	K2	..	G332.809-0.132	J16170437-5047164/[RA2004a] IRS 9
L75	16 17 06.11	-50 47 31.61	39± 4	..	M7	K5	..	G332.809-0.132	J16170610-5047314
L76	16 20 08.90	-50 48 51.17	40± 0	..	M7	K5	..	G332.809-0.132	J16200887-5048510

TABLE 5
LIST OF THE THREE SNRS AND OF ONE CANDIDATE PULSAR WIND NEBULA PROJECTED OVER G332.809-0.132-BRIDGE.

Name	Ra[J2000] [hh mm ss]	Dec [J2000] [hh mm ss]	Diam [']	Related pulsar	PSR distance	Ref.
SNR RCW 103 (G332.4-0.4)	16 17 33	-51 02 00	10	1E 1613.7-5055	3.3 ^{+1.3} _{-0.2}	2,5,6,7,9,10,11, 13
	16 16 29.89	-50 17 14.9		PSR J1616-5017	3.5	12
G332.0+00.2	16 13 17	-50 53 00	12			2,5
Kes 32/G332.4+00.1	16 15 20.0	-50 42 00	15	PSR J1614-5048/ PSR B1610-50 (?)	7.3, 7.5 ^{+3.5} _{-0.9}	2,5,8,11, 12, 13
HESS J1616-508	16 16 23	-50 53 48	8.16	CXOU J161729.3-505512/PSR J1617-5055 (?)	6.5	1,2,3,4, 12
	16 14 45.7	-51 44 49		PSR J1614-5144	6.1	12
	16 16 30.9	-51 09 17		PSR J1616-5109	6.8	12

References. 1 = Aharonian et al. (2006); 2 = Hare et al. (2017); 3 = Kargaltsev et al. (2009); 4 = Chang et al. (2008); 5 = Green (2014); 6 = Liu et al. (2015); 7 = Rea et al. (2016); 8 = Brinkmann et al. (1999); 9 = Ho & Andersson (2017); 10 = Borghese et al. (2018); 11=Acero et al. (2016); 12= Manchester et al. (2005); 13=Stafford et al. (2019).

TABLE 6
PARAMETERS OF DETECTED EARLY-TYPE STARS.

ID	Sp. Type	K_{so}	$J-H$	$H-K_s$	$A_{K_s}(JH)$	$A_{K_s}(JK_s)$	$A_{K_s}(HK_s)$	BC_{K_s}	M_{bol1}	$Q1$	$Q2$	MD	MD(ϖ)
		[mag]	[mag]	[mag]	[mag]	[mag]	[mag]	[mag]	[mag]	[mag]	[mag]	[mag]	[mag]
E1	B3-5	5.24	0.00	-0.02	1.54	1.81	2.30	-0.75	-6.16 ± 0.57	-0.90 ± 0.17	-3.35 ± 0.00	10.65 ± 0.18	..
E2	Ofpe/WN 9	5.12	-0.10	-0.07	0.93	0.94	0.98	-2.91	-10.45 ± 0.71	-0.04 ± 0.16	-1.04 ± 0.01	12.66 ± 0.26	..
E3	B0-5	5.13	-0.03	-0.02	0.95	0.94	0.93	-2.12	-9.64 ± 0.71	0.02 ± 0.10	-0.22 ± 0.01	12.66 ± 0.41	..
E4	WN 8	6.90	0.02	0.11	0.53	0.47	0.37	-3.40	-9.16 ± 0.71	0.01 ± 0.09	-1.33 ± 0.01	12.66 ± 0.50	..
E5	Oe	8.53	-0.11	-0.10	1.20	1.32	1.53	-4.38	-8.51 ± 0.71	-0.34 ± 0.14	..	12.66 ± 0.41	..
E6	B0-5	9.91	-0.03	-0.02	0.19	0.20	0.23	-2.12	-4.87 ± 0.71	-0.05 ± 0.07	-1.43 ± 0.03	12.66 ± 0.50	12.51
E7	Oe	8.56	-0.11	-0.10	1.59	1.79	2.14	-4.38	-8.48 ± 0.71	-0.60 ± 0.11	-5.12 ± 0.04	12.66 ± 0.41	..
E8	Oe	9.48	-0.11	-0.10	0.81	0.78	0.73	-4.38	-7.56 ± 0.71	0.16 ± 0.16	..	12.66 ± 0.50	..
P1 ^a	WC 8	9.69	0.05	0.38	1.85	1.66	1.30	-3.60	-6.57 ± 0.71	0.01 ± 0.21	-1.88 ± 0.02	12.66 ± 0.41	..
P2 ^a	WN 7	8.40	0.02	0.11	0.40	0.43	0.47	-3.90	-8.16 ± 0.71	-0.26 ± 0.10	-2.72 ± 0.01	12.66 ± 0.50	..

endtabular

Notes. Identification numbers, which are taken from Table 2, are followed by spectral types, de-reddened K_s magnitudes, three estimates of total extinction ($A_{K_s}(JH)$, $A_{K_s}(JK)$, $A_{K_s}(HK_s)$), BC_{K_s} , bolometric magnitudes ($M_{bol} = K_{sabs} + BC_{K_s}$), $Q1$ and $Q2$ parameters. Appended to the table, are the values for the two previously known WR stars.

(^a) P1 = [SMG2009] 1059-34, 2MASS J16143723-5126263; P2 = WR 74, 2MASS J16161381-5136417.

TABLE 7
LIST OF ISOLATED KNOWN MASSIVE STARS IN THE DIRECTION OF “THE BRIDGE”.

ID	2MASS-ID	Ra[J2000] (hh mm ss)	Dec[J2000] (dd mm ss)	Sp. type	References
P1	J16143723-5126263	16:14:37.24	-51:26:26.33	WC 8	1,2
P2	J16161381-5136417	16:16:13.81	-51:36:41.77	WN 7	1,3
P3	J16125464-5044510	16:12:54.65	-50:44:50.99	K3Ib-II	1,4
P4	J16151992-5026463	16:15:19.94	-50:26:46.12	M2Iab	1,4
P5	J16164067-5014370	16:16:40.70	-50:14:37.12	M3I	1,4
P6	J16191454-5024243	16:19:14.53	-50:24:24.45	M5.5I	1,4
P7	J16191948-5131264	16:19:19.48	-51:31:26.52	M3Ia	1,4
P8	J16202307-5104580	16:20:23.06	-51:04:58.12	M1Ib	1,4

References. 1 = Skiff (2014); 2 = Shara et al. (2009); 3 = Houk (1978); 4 = Messineo & Brown (2019).

33% of Conti & Crowther giant HII regions.⁶ Later, in Section 6, we will see that this complex coincides with the Nor OB4/RCW 103 association (with 34 stellar members listed in Mel’nik & Dambis 2017). At mid-infrared wavelengths, the complex appears shaped like “Santa Claus’s sled”. In the MSX composite image, warm dust emission (*A* band) traces the right and left tracks of “the sled”, while the central area (hereafter called “the Bridge”) is particularly rich in high-energy sources (see Figs. 4 and 5). We defined “the Bridge” by visually inspecting of the MSX composite image and locations of the three SNRs, by wanting to center and delineate a good portion of the complex and to exclude the two strong ridges of $8 \mu\text{m}$ emission on the two sides. The radius used ($40'$) would allow us to sample the evolved massive stars along the line of sight and to avoid regions of higher nebulosity, which could be perhaps younger – triggered seeds of star formation. One can imagine that supernova explosions and ionizing flux from massive stars dominate the central area.

For this complex, Rahman & Murray (2010) estimated a total number of Lyman continuum photons, Q_0 , $5.0 \times 10^{51} \text{ s}^{-1}$. This number corresponds to an incredibly large number of OB stars; it is equivalent to 1000 O7 dwarfs (Martins et al. 2005) or 250 O7 supergiants (Martins et al. 2005), or 200 O7 supergiants (Panagia 1973). *Where are they?* Only 34 massive stars have been reported in RCW 103 (Mel’nik & Dambis 2017). Because the complex is bubbling with supernova explosions (see Section 5.1), we can assume that a large fraction is made up of evolved massive stars. The quest to detect the earlier generation of massive stars that is undergoing final destruction via supernovae is an imperative to understand the intricate mechanism of sequential star formation and the possible overlap along the same line of sight of multiple clouds. With this aim in mind, we tried to identify candidate massive OB stars in this complex and to count them. Indeed, a second smaller molecular cloud (a few arcminutes wide) was detected along the same line of sight by Rahman & Murray (2010); it is object number 35 with $V_{LSR} \approx -91 \text{ km s}^{-1}$, i.e. with a near-kinematic distance of about 5 kpc. Furthermore, by looking at the original velocity measurements around -52 km s^{-1} , covering this complex and listed in Caswell & Haynes (1987), we notice two groupings of velocities along the structure; in most positions, velocities are from -41.0 to -48.4 km s^{-1} , but in the southern central area there are four posi-

⁶ The giant HII region complexes identified by Conti are strong radio and mid-infrared (MIR) emitters. The presence of MIR emission identifies a radio source as an HII region (with thermal emission). SNRs, which are associated with nonthermal (synchrotron) radiation, show no or very little MIR emission.

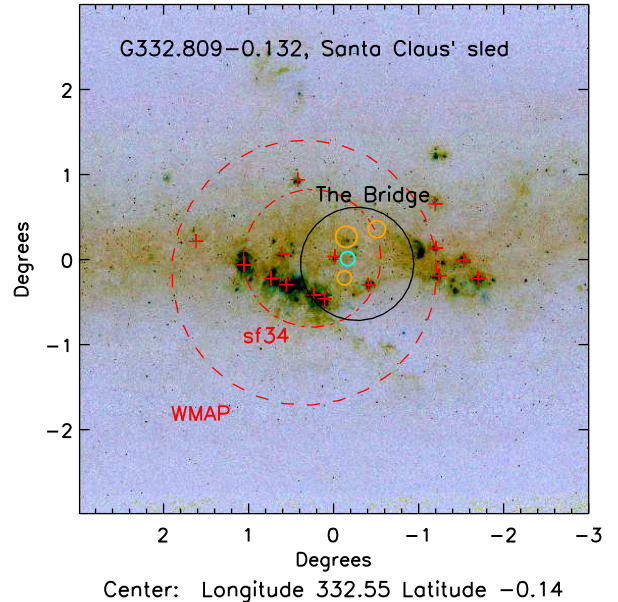


Fig. 4.— Composite map of the G332.809–0.132 region with MSX data in Galactic coordinates. Longitude is on the *x*-axis and latitude on the *y*-axis. The blue is the *A* band, the green is the *D* band, and the red is the *E* band. Orange circles indicate SNRs listed by Green (1991, 2014). The cyan circle shows the positional uncertainty of the γ -ray source HESS J1616–508. The large black circle encloses the central area ($r = 40'$), referred to as “The Bridge”. Red circles show the locations and semimajor axis of the WMAP source from Table 1 of Rahman & Murray (2010) and the associated SF region n.34 from their Table 2. V_{lsr} from -38 to -60 km s^{-1} from Caswell & Haynes (1987) are marked with red plus sign symbols.

tions with velocities from -52.0 to -57.3 km s^{-1} with only one position with both velocities. Toward IRAS 16132–5039, two absorption lines appear in the HI spectrum of Corti et al. (2016), one at ≈ -52 and the second deeper one at -42 km s^{-1} , with a map of the -42 km s^{-1} component centered on the IRAS source. $V_{\text{lsr}} = -46.7 \pm 2.6 \text{ km s}^{-1}$ for the high-density tracing CS molecule was measured toward the IRAS source (Bronfman et al. 1996). $V_{\text{lsr}} = -42$ or -47 yields a near-kinematic distance of 2.9 or 3.1 kpc (Reid et al. 2009). This is a relative shift in velocity of $5\text{--}10 \text{ km s}^{-1}$ relative to that used by Murray & Rahman ($-52 \pm 7.0 \text{ km s}^{-1}$, $\approx 3.4 \text{ kpc}$, 2010) to identify the G332.809–0.132 complex. It is unclear at this stage if the two velocities (-46 and -52) are tracing two different clouds along the same line of sight, or a peculiar velocity structure of the same complex like in W33 (Immer et al. 2014). Both velocity components are here regarded as belonging to the same complex in the Scutum–Crux arm (Fig. 6).

5.1. High-energy Sources in “The Bridge”

“The Bridge” region is rich in high-energy sources, with three known SNRs and one TeV emitter, HESS J1616–508 (Green 2014; Hare et al. 2017), as listed in Table 5.

The SNR RCW 103 has a diameter of $10'$ and is reported to be at the likely distance of 3.3 kpc (e.g., Caswell et al. 1975; Xing et al. 2014), and therefore, associated with the star-forming complex G332.809–0.132. RCW 103 is a young SNR ($\approx 2000 \text{ yr}$) with a known central compact object, 1E 161348–5055. The recently detected X-ray-burst activity points to a magnetar (Ho & Andersson 2017; Borghese et al. 2018) and therefore to a massive star progenitor of $18\text{--}20 M_{\odot}$ (Frank et al. 2015).

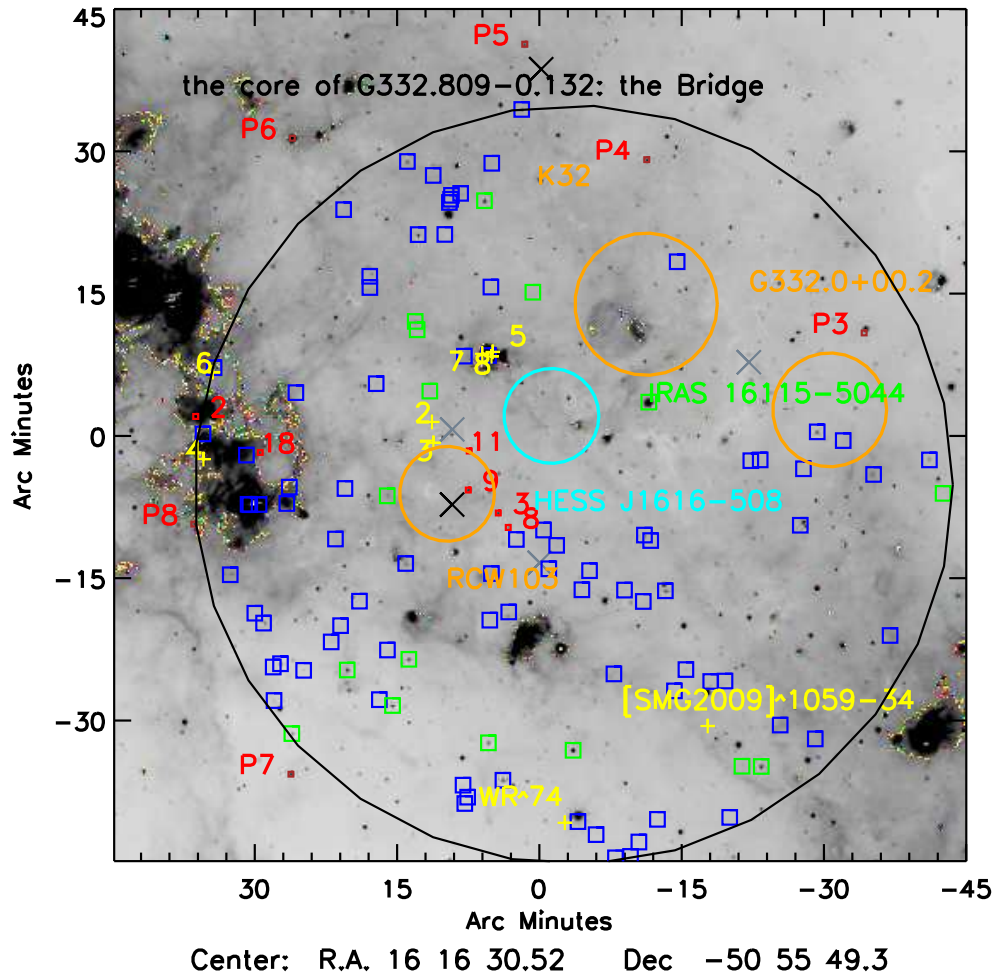


FIG. 5.— A zoomed-in image of the central $1^\circ \times 1^\circ$ of G332.809-0.132 (“The Bridge”). The gray image represents the WISE W3 band. North is up and East to the left. Detected early-type stars are marked with yellow crosses (Table 6), late-type stars with red boxes (Table 9). Green squares indicate free-free emitters with $K_s < 10.0$ mag and $J-K_s$ from 0.7 to 3.0 mag (from Tables 8 and 10), while blue squares indicate normal early-type stars with $K_s < 10.0$ mag and $J-K_s$ from 0.7 to 3.0 mag (from Tables 8 and 11). Orange circles indicate SNRs listed by Green (1991, 2014). The cyan circle shows the positional uncertainty of the γ -ray source HESS J1616-508. Black crosses (at ≈ 3 kpc) and gray crosses (at ≈ 6 kpc) mark the location of X-ray point sources listed in Table 5.

Kes 32 (G332.4+00.1) is an SNR with a diameter of $15'$, about $20'$ north of RCW 103, while SNR G332.0+00.2 is $15'$ west of Kes 32 and has a diameter of $12'$. The PSR J1614-5048 is located between Kes 32 and SNR G332.0+00.2. The high column density indicates that PSR J1614-5048 is located behind “The Bridge” at 7.3 kpc (Brinkmann et al. 1999), or it could experience massive local extinction (in “The Bridge”).

The HESS source J1616-508, detected by Aharonian et al. (2006), is one of the brightest HESS sources with a flux (1-10 TeV) of 1.7×10^{-11} erg cm^{-2} s^{-1} . It is possible that the TeV emission is associated with a pulsar wind nebula powered by the off-centered PSR, PSR J1617-5055, which coincides with CXOU J161729.3-505512 (Chang et al. 2008; Kargaltsev et al. 2009; Hare et al. 2017). In any case (pulsar wind nebula or hadronic processes in SNR), the HESS J1616-508 is another tracer for a massive evolved star. It is located only a few arcminutes away from RCW 103 (see Fig. 5), and both sources are likely to contribute to the γ -

ray emission detected by Fermi (Xing et al. 2014). For PSR J1617-5055, Kargaltsev et al. (2009) estimated a distance of 6.5 kpc from the dispersion measure and the Galactic electron density distribution model by Taylor & Cordes (1993). This confirms the superposition of two molecular clouds along the line of sight (≈ 3 and ≈ 6 kpc). The ATNF pulsar catalog provides three additional pulsars (Manchester et al. 2005)⁷. PSR J1616-5017 is at an estimated distance of 3.5 kpc, compatible with that of RWC 103 in the Scutum-Crux arm. PSRs J1614-5144 and J1616-5109 are at 6.1 and 6.8 kpc, which means they may be in the Norma arm along with HESS J1616-508.

5.2. Newly Detected Evolved Massive Stars in “The Bridge”

We targeted stars in “The Bridge” area, mainly in isolation and in the direction of the HESS J1616-508 source. Only a

⁷ About 2500 pulsars are listed in the catalog of Manchester et al. (2005).

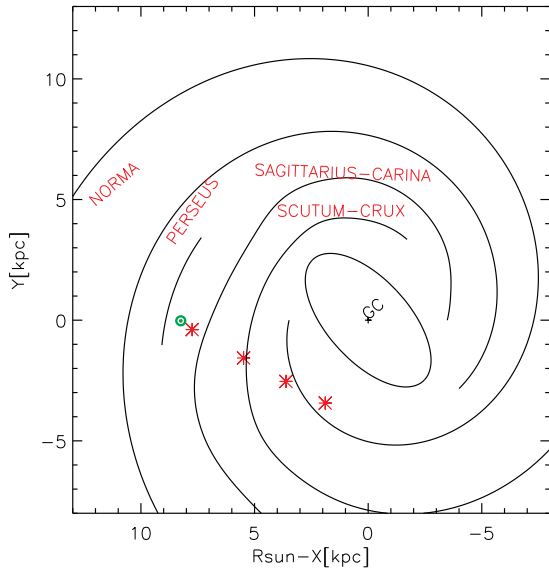


FIG. 6.— Top view of the Galactic disk, with a sketch of the central Bar and spiral arms. Spiral arms are taken from Cordes & Lazio (2002). The Galactic center is marked with a cross and our location with a green dot. Red asterisks mark distances of 850 pc (≈ -8 km s $^{-1}$), 3400 pc (-52 km s $^{-1}$), 5500 pc (-102 km s $^{-1}$), and 7450 pc (-140 km s $^{-1}$) along the line of sight of G332.809–0.132.

few targets are located within 5' from known clusters – star E4 is near the [DBS2003]-100 cluster and E5, E7, and E8 are in [DBS2003]-160/[DBS2003]-161.

5.2.1. Detected Early-type Stars

Star E2 is a rare transitional object on its way to the WR stage, an Ofpe/WN 9. Ofpe/WN 9 stars were first recognized in the GC by their strong He I lines (e.g., Najarro et al. 1997; Blum et al. 1995; Figer et al. 1995). They have masses from 25 to 60 M_{\odot} and may be the progenitors of WN 8 stars (Martins et al. 2007). E2 is located in isolation between SNR RCW 103 and the circle error of HESS J1616–508. By assuming the distance of G332.809–0.132 (DM = 12.66 mag), $A_{K_s} = 0.94$ mag, and $BC_K = -2.91 \pm 0.19$ (Martins et al. 2007), we derived $M_K = -7.54$ mag, $M_{bol} = -10.45$ mag, i.e., $L = 1.2 \times 10^6 L_{\odot}$. This luminosity is consistent with that of the Ofpe/WN 9 stars in the Quartet cluster (Messineo et al. 2009), in the Quintuplet (Figer et al. 1999), and in the GC (Martins et al. 2007). Star E2 is possibly associated with G332.809–0.132 and with the progenitor of SNR RCW 103. For a distance of 6 kpc, M_{bol} would be -11.68 mag, which would make E2 brighter than the Ofpe/WN 9 stars in the GC (min = -8.5 , max = -11.3 mag, Martins & Plez 2006). Its Gaia DR2 parallax, $\varpi = 0.57 \pm 0.14$ mas (corresponding to a distance from 1.3 to 2.2 kpc), has a fractional error larger than 20%. With the current Gaia DR2, deviations up to 50% from the actual distance are measured for OB stars (> 1.5 kpc, Shull & Danforth 2019).

Star E3 (B0–5 I) is 2'2 (about 2 pc) away from star E2 and has a similar value of K_s and interstellar extinction (dereddened $K_s = 5.13$ mag and $A_{K_s} = 0.94$). Its colors are consistent with those of normal early-type stars and its magnitude suggests a supergiant for a distance between 1.5 and 3.5 kpc. By assuming DM = 12.66 mag, for star E3 we estimate an absolute $M_K = -7.53$ mag, which is a value typical for B5 supergiants. This indicates that star E3 is another evolved

massive star (B0–5 I) associated with the progenitor of SNR RCW 103 in G332.809–0.132. For a distance of 6 kpc, M_K would be -8.76 mag, a value that is too bright for a B0–5 star (Martins & Plez 2006). The Gaia DR2 parallax is of poor quality.

Star E4 is a WR of WN 8 type. It is located in isolation on the southwest side of “The Bridge”, about 4' away from the center of the cluster [DBS2003]-100 (see Borissova et al. 2016), and it was targeted because of its free-free excess. By assuming intrinsic $J - H = 0.02$ mag and $H - K_s = 0.11$ mag, and a bolometric correction $BC_K = -3.4$ mag from the work by Crowther et al. (2006), we derived $A_{K_s} = 0.46$ mag, and a dereddened $K_s = +6.90$ mag, and apparent bolometric magnitude $m_{bol} = 3.5$ mag. The two WN 8 stars detected in Westlund1 have $M_K \approx -5.8$ mag, while WR66 (WN 8) has $M_K = -4.89$ mag (Crowther et al. 2006). By assuming $M_K = -5.8$ mag, we obtain a distance modulus of DM = 12.66 mag, i.e., a distance of 3.5 kpc. By assuming an average $M_K = -5.34$ mag, we obtain DM = 12.25 mag (2.8 kpc). The Gaia DR2 parallax is of poor quality. It is plausible that star E4 is associated with the giant molecular complex G332.809–0.132 (and SNR RCW 103). Typical initial masses of WN 8 stars are larger than 40 M_{\odot} .

In the direction of the stellar cluster [DBS2003]-160/[DBS2003]-161 (Dutra et al. 2003), we detected three emission line stars (E5, E7, and E8 in Table 2). This cluster was analyzed by Roman-Lopes & Abraham (2004) and is centered on IRAS 16132–5039. IRAS 16132–5039 harbors two MSX components. From near-infrared (NIR) and mid-infrared photometry, by assuming that it is on the zero-age main sequence (ZAMS), Roman-Lopes & Abraham (2004) have inferred an O5 type for the star E5, which is the brightest star in the MSX A component (E5 coincides with star IRS 1 in their Table 2). The obtained low-resolution K -band spectra do not allow a class refinement. With $A_{K_s} = 1.27, 1.74,$ and 0.74 mag, stars E5, E7, and E8 have dereddened $K_s = 8.57, 8.60,$ and 9.52 mag. By assuming DM = 12.66 mag, we derive $M_K = -4.09, -4.06, -3.14$ mag, typical values for O5, O5, and O8 stars on the ZAMS (or O6, O6, and O9.5 dwarfs; Martins & Plez 2006). The Gaia DR2 parallaxes have large errors. By assuming a conservative BC_K of -4.38 mag (average of the values for O2–O8 stars, Martins & Plez 2006), we obtained $M_{bol} = -8.51$ mag, -8.48 mag, and -7.56 mag. Their massive nature is also confirmed by the finding of Roman-Lopes et al. (2009). They analyzed the brightest stars of the MSX B component, which has K_s magnitude similar to that of stars E5 and E7, and obtained the spectrum of an O3If $^{+}$ or O3–5V.

Star E6 is a dwarf with $A_{K_s} = 0.20$ mag; Gaia DR1 gives a proper motion of $\varpi = 0.74 \pm 0.29$ mas yr $^{-1}$ and a distance of ≈ 1.5 kpc. Gaia DR2 lists $\varpi = 0.31 \pm 0.04$ mas yr $^{-1}$ and a distance of ≈ 2.9 kpc.

Inferred parameters of detected early-type stars are given in **Table 6**.

5.3. Previous Spectroscopic Information from the Literature

By searching the catalog of Skiff (2014), we were able to collect spectral types of 63 OB stars (47 of which are above $K_s = 10$ mag) and 2 WR stars, 20 yellow stars, and 24 late-type stars located in the direction of G332.809–0.132. Among the 24 late-type stars, 6 stars are reported as class I stars and are included in the catalog of class I stars detected in Gaia DR2 (Messineo & Brown 2019) and listed in Table 7.

The 63 OB stars are listed in Table 8. All but two of the

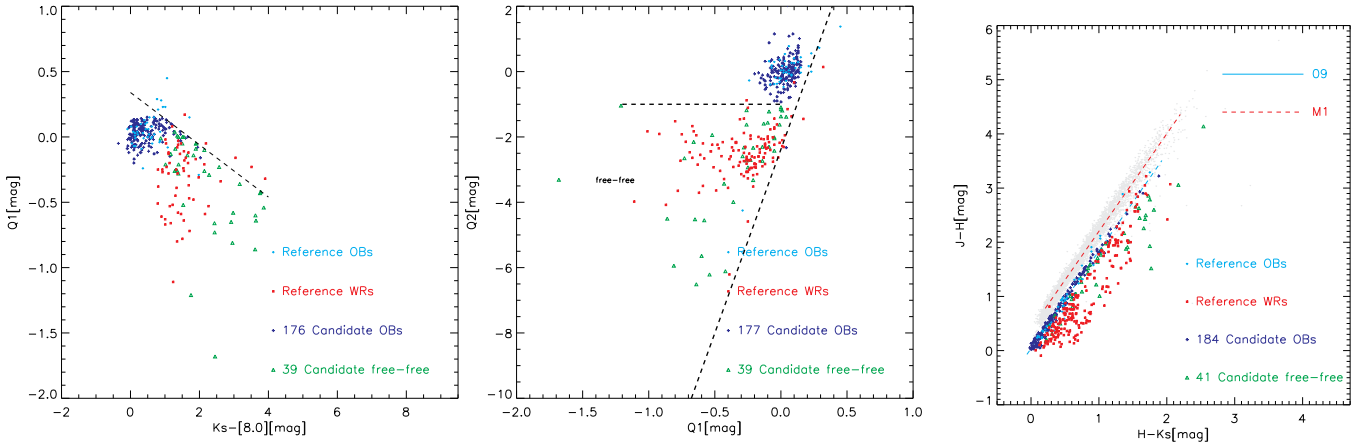


FIG. 7.— *Left panel:* $Q1$ versus $K_s-[8.0]$ diagram. The dashed curve marks the line below which free-free emitters are located. The region above it is mainly populated by late-type stars (for more details, see Messineo et al. 2012). *Middle panel:* $Q2$ versus $Q1$ diagram. Free-free emitters are located below the line $Q2 = -1$ mag and to the left of the oblique curve (for more details see Messineo et al. 2012). *Right panel:* $J-H$ versus $H-K_s$ diagram. The location of M1 stars with A_{K_s} from 0 to 3 mag is marked with a long-dashed red line. The location of O9 stars with A_{K_s} from 0 to 3 mag is indicated with a long-dashed cyan line. Gray dots show 2MASS datapoints in “The Bridge” area with $K_s < 10$ mag. In all panels, red squares indicate the positions of reference WRs and cyan diamonds those of reference OB stars (Messineo et al. 2012). Thirty-five new, very probable, free-free emitters from Table 10 are located and marked with green triangles; the other 122 stars that are likely early-type stars from Table 11 are indicated with blue crosses.

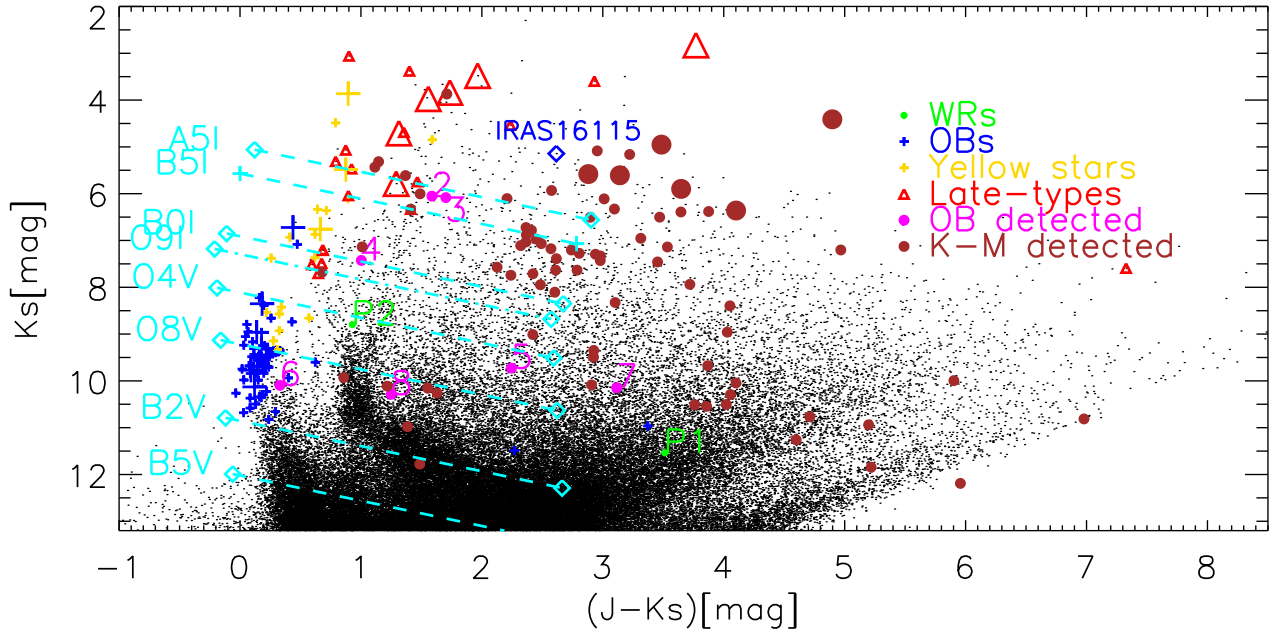


FIG. 8.— K_s versus $J-K_s$ diagram of 2MASS stars in the direction of “The Bridge”. The locations of O4, O8, B2, and B5 dwarfs for $DM = 12.66$ mag and $A_{K_s} = 0.0$ mag are marked with cyan diamonds (Messineo et al. 2011, 2014, and references therein). Dashed lines connect the zero-extinction locations to those at $A_{K_s} = 1.5$ mag. Red triangles indicate the locations of previously known late-type stars, gold pluses those of yellow stars, and blue plus signs those of known early-type stars, (see Table 8). OB stars from Table 2 are marked and labeled in magenta and K-M stars from Table 4 are indicated with brown filled circles. Bigger symbols are used for stars of class I. The position of the candidate free-free emitter IRAS 16115–5044 is indicated with a blue diamond and labeled.

known OB stars have A_{K_s} smaller than 0.4 mag, with a mean of $A_{K_s} = 0.18$ mag and a $\sigma = 0.07$ mag. Their parallactic distances ranges from 0.2 to 3.9 kpc. Fifteen stars out of the 63 have Gaia DR2 distances from 2.0 to 4 kpc, and among them seven have been previously reported as members of a population of massive stars at the distance of G332.809–0.132 (see Section 6).

The two WR stars are listed in Table 7. SIMBAD reports WR 74 (P2) as a WN 7 detected by Shara et al. (2009) and

van der Hucht (2001). It is located on the Southern periphery of “The Bridge”, and has a $K_s = 8.7$ mag. By assuming intrinsic $J-H = 0.02$ mag and $H-K_s = 0.11$ mag, and $BC_K = -3.9$ mag from the work by Crowther et al. (2006), we derived a moderate extinction, $A_{K_s} = 0.43$ mag, and a dereddened K_s of $+8.40$ mag, and apparent bolometric magnitude $m_{bol} = 4.5$ mag. For $DM = 12.66$, we obtained $M_K = -4.3$ mag, and $M_{bol} = -8.2$ mag. In the work of Hamann et al. (2006), for this WR, it is reported that $DM = 13.0$ mag and $M_{bol} = -8.76$

mag, which, for $DM = 12.66$ mag, implies $M_{bol} = -8.46$ mag and $M_K = -4.56$ mag. Its interstellar extinction agrees with the A_{K_s} measurements of star E4 (WN 8), which has a spectrophotometric distance of about 3 kpc; therefore, it supports the association with G332.809–0.132. WN 7 stars in Westerland 1 have brighter M_K from -5.0 to -6.0 mag. The Gaia parallax from DR2 has high uncertainty (0.14 ± 0.05 mas); a larger distance cannot be excluded.

[SMG2009] 1059–34 (P1) is another WR of WC 8 type (Shara et al. 2009). By assuming $J - H = 0.05$ mag, $H - K_s = 0.38$ mag, and $BC_K = -3.6$ mag (Crowther et al. 2006), we estimate A_{K_s} of about 1.7 mag, and with a $DM = 12.66$ mag and $M_{bol} = -6.57$ mag. M_{bol} can span several orders of magnitudes in WC 8 types from -4.65 mag (WR135) to -8.5 mag (star in Westerland 1). Its parallax has not been measured.

5.4. Late-type Stars

In Table 9, we summarize some properties of the brightest observed late-type stars and of the six K-M I stars reported by Skiff (2014) and Messineo & Brown (2019) in the direction of G332.809–0.132, as listed in Table 7.

For four of the known K-M I stars Gaia radial velocities⁸ are available. Stars P3 and P8 at $A_{K_s} = 0.16$ mag $\sigma = 0.1$ mag have $V_{lsr} = -39$ km s⁻¹ with $\sigma = 2$ km s⁻¹, and stars P4 and P7 at $A_{K_s} = 0.41$ mag with $\sigma = 0.1$ mag have $V_{lsr} = -53$ mag with $\sigma = 7$ mag, which again indicate kinematic distances of 2800 and 3490 kpc, respectively. For stars P3 and P8, the distance inferred from their average Gaia DR2 parallaxes is 2628 kpc in good agreement with the kinematic ones, but for stars P4 and P7 the parallactic distances are anomalously small (918 pc). From the radial velocities, we conclude that stars P3, P8, P4, and P7 are associated with the Scutum-Crux arm and the G332.809–0.132 complex; by assuming a $DM = 12.66$ mag, we infer M_{bol} from -4.5 mag (K3 I) to -6.90 mag (M2 I). Star P5 has $A_{K_s} = 0.3$ mag, Gaia MD = 9.29 mag, but its velocity is not available. Star P6 is an RSG (M5.5 I) at $A_{K_s} = 1.49$ mag and $M_{bol} = -8.30$ mag when assuming the distance to G332.809–0.132 (its velocity is not available and the Gaia DR2 parallax is of poor quality).

The 76 late-type stars we observed are mostly in the direction of the center of this complex; for a putative distance of 3.4 kpc, six of them were brighter than $M_{bol} < -5.26$ mag (see Table 9), with three highly probably RSGs owing to their large $EW_{2.29 \mu m}(CO)$; their A_{K_s} ranges from 1.01 mag to 2.10 mag. The high values of interstellar extinction are still compatible with the A_{K_s} of stars in IRAS 16132–5039, which belongs to the 3.4 kpc complex. However, we cannot exclude a larger distance; the near HESS 1640–465 source is reported at the likely distance of 6.5 kpc by Kargaltsev et al. (2009). Radial velocities are demanded for a clearer scenario.

5.5. Candidate Evolved Early-type Stars

As seen in the previous sections, G332.809–0.132 hosts a number of massive transitional objects and WRs, as expected for being a region rich in remnants. Stars E2 (Ofpe/WN 9), E4 (WN 8), and WR74 (WN 7) have K_s of 6.05, 7.43, and 8.80 mag and $A_{K_s} = 0.94$, 0.47, and 0.43 mag, respectively. We searched for other candidate massive stars with free-free excess and that are brighter than $K_s = 10.0$ mag, which for

⁸ Gaia DR2 velocities in the solar barycentric reference frame were transformed into V_{lsr} using $(U_o, V_o, W_o) = (10.27, 15.32, 7.74)$ km s⁻¹. These are the same values used in the fortran code that Reid et al. (2009) present to infer kinematic distances with their rotation curve.

a $DM = 12.66$ mag and $A_{K_s} = 0.5$ mag roughly corresponds to the observed magnitudes for an O9 dwarf (Martins & Plez 2006), as shown in Table 12, as described in Sect. 5.6.

We adopted the criteria described in Section 2 and Messineo et al. (2012), which should yield a fraction larger than 80% of the Wolf-Rayet star population, and retrieved 35 targets (other than the two known WRs), which are listed in Table 10, and illustrated in Fig. 7. Six of them are reported in the literature as possible late-type stars (one carbon, four candidate asymptotic giant stars (AGBs) and one planetary nebula, PN). Thirty-four (out of 35) objects are in Gaia DR2 with V_{lsr} measurements available only for two stars (radial velocities are fitted with templates spectra with $T_{eff} < 10000$ k). This suggests that 83% of the sample consists of genuine windy massive stars with free-free emission. Among the spectroscopically known OB stars listed in Table 8, there are five stars photometrically classified as free-free emitters. They all have emission lines.

Having excluded those stars classified as late-type stars and free-free emitters based on their 2MASS and GLIMPSE magnitudes (Messineo et al. 2012), by using the classical $J - H$ versus $H - K_s$ diagram with 2MASS datapoints and $I - J$ versus $J - K_s$ diagram of DENIS datapoints, 184 other likely OB stars are found. SIMBAD provides a spectral type for 46 of them, with 37 being early types, 8 (17%) yellow stars, and one (2%) late-type. For 179 (out of 184) selected OB stars, Gaia DR2 parallaxes exist, but only 22 Gaia DR2 radial velocities have been measured with 6 of them associated with SIMBAD F-types and one C-type. This confirms the early nature of the bulk of the sample. By excluding those already known or with Gaia DR2 velocities (e.g., cooler than 10,000 K), we remain with 122 likely new OB stars, which are listed in Table 11. In Fig. 7, these targets are shown along with a comparison sample of known early-type stars in the inner Galaxy.

5.5.1. Notes on IRAS 16115–5044

IRAS 16115–5044 is a candidate free-free emitter that is marked in SIMBAD as a PN. IRAS 16115–5044 was spectroscopically observed in the JHK bands during the IRAS survey for late-type stars by Weldrake et al. (2003). In this conference proceeding contribution, the authors estimated a B4I spectral type from the H band. Suárez et al. (2006) also concluded that this source is not a PN, but a young star. The K band spectrum in Fig. 1 of Weldrake et al. (2003) – with Bry in emission with a P-Cygni profile and a FWHM velocity of about 300 km s⁻¹, Fe II at 2.091 μm , Mg II at 2.138 and 2.144 μm , and Na I at 2.206 and 2.209 μm in emission – recalls the spectra of the LBV Pistol (11800 K), of G24.73+0.69 (12000 K), and G26.47+0.02 (17000 K) (Clark et al. 2003; Najarro et al. 2009). By assuming a B4 type (14000 K), the 2MASS magnitudes $J = 7.76$ mag, $H = 6.13$ mag, and $K_s = 5.14$ mag, and the extinction curve n.3 of Messineo et al. (2005), we estimate $A_{K_s}(J - H) = 1.4$ mag ($A_{K_s}(H - K) = 1.5$ mag). The Gaia DR2 parallax ($\varpi = 0.69 \pm 0.19$ mas yr⁻¹) has a fractional error larger than 27%, and the Gaia distance ranges from 1.1 to 2 kpc. For a distance of 1.5 kpc, by integrating under the stellar energy distribution (SED) and extrapolating with a blackbody curve, we infer a $BC_K = -1.16 \pm 0.49$ mag and $M_{bol} = -8.3$ mag ($\log_{10} \frac{L_*}{L_\odot} = 5.2$), which confirms a supergiant class. The A_{K_s} value is suggestive of a larger distance. For a distance of 3.4 kpc, $M_{bol} = -10.08$ mag ($\log_{10} \frac{L_*}{L_\odot} = 5.9$). A more detailed study of this source will be

TABLE 8
KNOWN OB STARS .

ID	Ra	Dec	I _{den}	<i>J</i>	<i>H</i>	<i>K_s</i>	[8.0]	Q1	Q2	<i>A_{K_s}</i>	plx	DM	VR	DMv	Sp. Type ^d	Sp.(adopt)	DM(sp) ^b	DM(adopt)	<i>M_K</i> ^b	2MASS-ID/Alias	Ref ^c	Sp. year
	(hh mm ss)	(deg mm ss)	(mag)	(mag)	(mag)	(mag)	(mag)	(mag)	(mag)	(mag)	(mas)	(mag)	(km s ⁻¹)	(mag)			(mag)	(mag)	(mag)		(RCW 103)	
1	16 13 00.73	-51 03 20.39	8.49	7.16	6.93	6.72	6.52	-0.14	-0.11	0.35	0.30 ± 0.05	12.43[12.14-12.76]	B4Ie	B3-5 I	12.64	12.43	-6.06	J16130073-5103203/LS 3508		2003
2	16 18 43.72	-51 27 57.72	8.86	7.55	7.29	7.08	6.80	-0.12	-0.29	0.36	0.23 ± 0.04	12.96[12.62-13.37]	A3II/A2Ib	A2 (I)	(13.91)	12.96	-6.24	J16184372-5127577/LS 3544.Ly431	3	1971/1987
3	16 19 08.34	-51 05 38.56	9.03	8.38	8.31	8.22	8.10	-0.08	-0.17	0.18	4.66 ± 0.04	6.64[6.62-6.66]	OB+	6.64	1.40	J16190833-5105385/HD 146522		1971
4	16 16 37.70	-50 36 26.50	..	8.53	8.44	8.35	8.32	-0.08	0.11	0.20	0.27 ± 0.04	12.60[12.32-12.91]	A8-9V	A8 V	..	12.60	-4.45	J16163769-5036264/LS 3529.HD 146058	1	1978
5	16 13 49.36	-50 52 12.56	9.29	8.58	8.42	8.39	8.25	0.09	-0.17	0.16	0.82 ± 0.05	10.36[10.24-10.48]	O9II/B2V/B0-2I-II	O9-B2 (I)	(14.29)	10.36	-2.13	J16134935-5052125/CPD-50 9063		1969/1977/1978/1987
6	16 17 23.73	-50 51 53.49	9.41	8.92	8.71	8.66	8.50	0.11	-0.19	0.19	2.79 ± 0.04	7.75[7.72-7.79]	-24.15	11.26	A2	7.75	0.72	J16172373-5051534/HD 146184		1939
7	16 14 40.40	-50 48 22.65	..	9.17	8.97	8.74	7.35	-0.21	-3.32	0.36	0.61 ± 0.05	10.97[10.80-11.14]	A9-F0IV-V	A9 V	..	10.97	-2.59	J16144040-5048226/LS 3518.CD-50 10263	1	1978
8	16 15 27.45	-50 59 01.00	9.21	8.85	8.80	8.79	8.57	0.03	-0.55	0.10	0.38 ± 0.05	11.97[11.73-12.23]	27.00	..	B0.5III-IV/B2:Ve	B0-3 V	11.07	11.97	-3.28	J16152744-5059010/HD 145828.HD 145828.Ly407	1,2	1969/1987
9	16 14 25.41	-51 11 02.79	9.38	9.02	8.97	8.95	8.87	..	-0.16	0.11	0.77 ± 0.05	10.50[10.36-10.64]	B0III-B0.5III:	B0 III	13.15	10.50	-1.66	J16142541-5111027/HD 145637		1961/1969
10	16 14 09.31	-51 27 35.68	9.44	9.10	9.04	8.96	9.04	-0.07	0.36	0.17	0.63 ± 0.05	10.91[10.76-11.07]	B3II-III	B0-3 III	12.26	10.91	-2.12	J16140930-5127356/HD 145579		1978
11	16 18 57.93	-51 03 29.73	9.62	9.14	9.10	8.96	8.87	-0.20	-0.07	0.23	0.50 ± 0.04	11.38[11.23-11.55]	B7-8Ib-II	B8 (II)	(15.69)	11.38	-2.65	J16185792-5103297/LS 3547		1978
12	16 14 53.58	-51 19 01.05	9.37	9.10	9.06	9.05	8.95	0.03	-0.24	0.09	3.33 ± 0.06	7.37[7.33-7.41]	B2II/O8	O8 (I)	(14.48)	7.37	1.59	J16145358-5119010/HD 145722		1987/1987
13	16 17 03.84	-51 00 43.56	9.56	9.27	9.17	9.17	9.03	0.08	-0.28	0.11	0.80 ± 0.07	10.41[10.23-10.61]	B3II-III	B3 III	11.60	10.41	-1.35	J16170384-5100435/HD 146125		1978
14	16 18 30.56	-51 25 57.87	9.36	9.27	9.25	9.24	9.28	-0.01	0.15	0.10	2.00 ± 0.22	8.46[8.24-8.71]	B7-8III	B8 III	..	8.46	0.68	J16183055-5125578/HD 146373		1978
15	16 18 22.92	-51 26 24.26	9.76	9.46	9.32	9.26	..	0.02	..	0.18	0.34 ± 0.05	12.15[11.88-12.46]	-30.00	..	B9IV-V	B9 V	9.14	12.15	-3.07	J16182291-5126242/LS 3540.CP-51 9232.CPD-51.9	1,2	1978
16	16 16 22.28	-50 26 22.74	9.30	9.11	0.38 ± 0.04	11.93[11.72-12.16]	B0.5III/B3III:	B0-3 III	J16162228-5026227/LS 3526		1961/1969/1987
17	16 15 15.53	-50 30 35.55	9.89	9.52	9.38	9.30	9.18	0.01	-0.13	0.19	1.51 ± 0.04	9.06[9.00-9.12]	B1III/BOV	9.06	0.05	J16151553-5030355/CPD-50 9104		1969/1987
18	16 19 11.04	-51 14 01.92	9.73	9.49	9.39	9.31	..	-0.05	..	0.19	0.98 ± 0.04	9.98[9.89-10.08]	A3	9.98	-0.86	J16191104-5114019/HD 146523		1939
19	16 12 37.85	-50 41 25.85	10.12	9.68	9.48	9.35	9.37	-0.02	0.37	0.26	1.34 ± 0.04	9.32[9.25-9.39]	B8-9II-III	B8 III	..	9.32	-0.23	J16123785-5041258/CPD-50 9031		1978
20	16 13 39.28	-50 29 45.79	10.09	9.64	9.41	9.36	9.28	0.13	0.05	0.19	1.41 ± 0.04	9.22[9.15-9.29]	A5	9.22	-0.05	J16133928-5029457/CPD-50 9058		1939
21	16 13 58.11	-50 54 58.69	10.11	9.69	9.46	9.40	9.38	0.12	0.24	0.20	1.44 ± 0.06	9.17[9.08-9.27]	A7	9.17	0.03	J16135810-5054586/CPD-50 9066		1939
22	16 18 16.43	-51 33 35.18	9.77	9.55	9.47	9.44	9.47	0.02	0.20	0.13	1.28 ± 0.04	9.41[9.34-9.48]	A5	9.41	-0.10	J16181643-5133351/HD 146340		1939
23	16 13 44.57	-51 06 20.10	10.23	9.67	9.51	9.45	9.29	0.04	-0.18	0.19	0.31 ± 0.06	..	-40.00	..	A0III-IV	A0 III	J16134457-5106200/LS 3512.CP-50 9059.CPD-50.9	1,2	1978
24	16 18 49.45	-51 09 27.15	9.91	9.63	9.55	9.47	9.42	-0.07	0.02	0.18	-7.43 ± 1.22	B1III/A5II	B1-A5 II	J16184944-5109271/CPD-50 9205		1961/1987	
25	16 16 40.84	-50 39 20.62	..	9.64	9.50	9.48	9.30	0.11	-0.34	0.13	1.03 ± 0.04	9.88[9.80-9.97]	A5	9.88	-0.53	J16164083-5039206/HD 146074		1939
26	16 15 26.04	-51 09 17.87	10.19	9.66	9.59	9.48	9.54	-0.12	0.31	0.21	0.34 ± 0.04	12.17[11.93-12.45]	-17.00	..	B1:	B0-3 (I)	(15.54)	12.17	-2.90	J16152603-5109178/CD-50 10282.CD-50 10282.Ly4	1,3	1978
27	16 16 07.22	-51 05 21.31	..	9.73	9.55	9.49	9.38	0.06	0.04	0.19	1.88 ± 0.04	8.60[8.56-8.64]	B2-3III	B2 III	12.44	8.60	0.70	J16160722-5105213/CPD-50 9128		1969
28	16 14 11.81	-51 14 51.32	10.03	9.61	9.55	9.50	9.38	-0.02	-0.20	0.15	0.62 ± 0.04	10.94[10.80-11.09]	-26.00	..	A5	10.94	-1.59	J16141180-5114513/LS 3514.CD-50 10251.Ly398	1,2	1939
29	16 20 16.82	-50 59 15.30	10.18	9.73	9.61	9.51	..	-0.05	..	0.21	0.65 ± 0.04	10.85[10.72-11.00]	B1III/O9V/B2V	O9-B2 V	11.90	10.85	-1.55	J16201681-5059152/[L64] 444		1969/1987/1993
30	16 20 00.43	-51 07 32.32	9.96	9.73	9.49	9.57	9.75	0.38	0.65	0.06	1.90 ± 0.05	8.57[8.52-8.63]	..	3.86	15.91	OB-	..	8.57	0.94	J16200043-5107323/HD 146687		1964
31	16 14 53.41	-51 13 37.40	10.34	9.79	9.69	9.59	9.36	-0.08	-0.41	0.21	0.33 ± 0.04	12.24[12.00-12.51]	-61.00	..	A8-9V	A8 V	..	12.24	-2.86	J16145340-5113373/LS 3519.CD-50 10270.Ly401	1,3	1978
32	16 18 36.36	-51 17 16.72	10.27	9.78	9.67	9.59	9.60	-0.02	0.20	0.18	0.51 ± 0.11	B2.5III/B2:	B2 III	12.55	J16183636-5117167/LS 3542		1969/1987	

Notes. Identification numbers are followed by celestial coordinates, *I, J, H, K_s*, and [8.0] magnitudes; the Q1 and Q2 parameters; extinction *A_{K_s}*; Gaia DR2 parallaxes (plx), derived parallactic distance moduli (DM); Gaia DR2 spectroscopic radial velocities in the solar barycentric reference frame (VR); kinematically inferred DMs (DMv) (Reid et al. 2009); spectral types, spectrophotometric DM(sp); DMadopted; obtained absolute *K_s* magnitudes (*M_K*); 2MASS IDs/Alias; references for the members of RCW 103; years of the collected spectral types.

A_{K_s} are estimated by assuming *H-K_s* = -0.10 mag and *J-K_s* = -0.01 mag (values for O stars by Martins & Plez 2006).

Stars #7, #35, #47, #62, and #63 have colors of free-free emitters (Messineo et al. 2012).

^a Sp. type= spectral types collected from Skiff (2014) or SIMBAD.

TABLE 8
KNOWN OB STARS .

ID	Ra	Dec	Iden	<i>J</i>	<i>H</i>	<i>K_s</i>	[8.0]	Q1	Q2	<i>A_{K_s}</i>	pix	DM	VR	DMv	Sp. Type ^d	Sp.(adopt)	DM(sp) ^b	DM(adopt)	<i>M_K^b</i>	2MASS-ID/Alias	Ref ^c	Sp. year	
	(hh mm ss)	(deg mm ss)	(mag)	(mag)	(mag)	(mag)	(mag)	(mag)	(mag)	(mag)	(mas)	(mag)	(km s ⁻¹)	(mag)			(mag)	(mag)	(mag)		(RCW 103)		
33	16 13 17.45	-51 23 40.59	10.75	10.22	9.91	9.60	8.28	-0.25	-2.93	0.48	0.36 ± 0.04	12.03[11.83-12.25]	OB-	12.03	-2.91	J16131745-5123405/LS 3509	1971	
34	16 18 40.65	-51 26 09.36	10.02	9.86	9.74	9.65	..	-0.03	..	0.20	2.62 ± 0.05	7.89[7.84-7.93]	OB+e	7.89	1.56	J16184064-5126093/HD 146424	1971/1976	
35	16 19 24.13	-51 11 37.66	9.84	9.75	9.71	9.68	9.47	-0.03	-0.48	0.13	1.44 ± 0.06	9.16[9.08-9.24]	B9	9.16	0.39	J16192412-5111376/HD 146575	1921	
36	16 13 37.92	-51 16 33.04	10.10	9.83	9.74	9.69	9.77	-0.02	0.37	0.16	0.85 ± 0.04	10.28[10.17-10.39]	B8-9IV	B8 IV	..	9.92	10.28	-0.75	J16133791-5116330/HD 145489	1978	
37	16 13 34.74	-50 53 28.01	10.18	9.81	9.73	9.70	9.66	0.01	0.01	0.14	1.14 ± 0.05	9.67[9.57-9.77]	B8-9II	B8 (II)	(16.52)	..	9.67	-0.11	J16133473-5053280/CPD-509055	1978	
38	16 19 04.50	-50 53 58.80	10.40	9.94	9.85	9.71	9.60	-0.17	-0.04	0.25	0.45 ± 0.04	11.59[11.42-11.78]	-19.00 ^d	..	A0	11.59	-2.13	J16190449-5053587/LS 3548,CP-50 9216.Ly435	1.3	1939
39	16 17 29.67	-50 36 17.19	10.46	9.93	9.81	9.72	9.30	-0.05	-0.90	0.21	0.96 ± 0.04	10.01[9.93-10.10]	B0.5IV/B0:	B0 IV	..	12.55	10.01	-0.50	J16172966-5036171/HD 146222	1971/1987	
40	16 15 01.59	-51 23 50.72	9.98	9.77	9.75	9.75	9.74	0.02	..	0.08	0.94 ± 0.05	10.08[9.97-10.19]	B8	10.08	-0.41	J16150158-5123507/HD 145761	1921	
41	16 13 38.25	-50 35 59.01	10.06	9.86	9.79	9.77	9.64	0.03	-0.27	0.12	0.78 ± 0.05	10.45[10.32-10.58]	B3-6III:(e?)	B3-5 III	..	13.12	10.45	-0.80	J16133824-5035590/HD 145488	1978	
42	16 13 21.63	-51 05 34.08	10.40	10.03	9.90	9.84	9.67	0.01	-0.25	0.18	1.00 ± 0.05	9.93[9.84-10.03]	B7-8IIp:Si	B8 (II)	(16.62)	..	9.93	-0.27	J16132163-5105340/CPD-509049	1978	
43	16 14 05.90	-51 10 52.02	10.18	9.97	9.93	9.84	..	-0.13	..	0.18	0.81 ± 0.05	10.38[10.26-10.52]	A0	10.38	-0.72	J16140589-5110520/CPD-509068	1939	
44	16 18 45.58	-50 44 16.98	10.18	9.93	9.87	9.84	9.81	0.01	0.01	0.12	2.48 ± 0.04	8.00[7.97-8.04]	B9	8.00	1.72	J16184557-5044169/CPD-509203	1939	
45	16 17 23.68	-51 14 27.55	10.94	10.34	10.15	9.94	8.92	-0.21	-2.33	0.35	0.30 ± 0.04	12.44[12.17-12.76]	A5	12.44	-2.85	J16172367-5114275/[M81]1-505	1939	
46	16 18 47.80	-51 06 59.57	9.99	10.01	9.96	9.98	10.00	0.08	0.09	0.07	1.11 ± 0.06	9.71[9.60-9.83]	em	9.71	0.20	J16184779-5106595/HD 146445	1981	
47	16 15 37.39	-51 12 51.75	10.40	10.13	10.07	9.98	9.89	-0.10	-0.10	0.19	1.58 ± 0.06	8.96[8.88-9.05]	B8-9	8.96	0.83	J16153739-5112517/CPD-509114	1978	
48	16 16 55.77	-50 35 45.56	..	10.25	10.18	10.13	10.13	-0.01	0.13	0.15	0.93 ± 0.04	10.09[10.00-10.17]	A5	10.09	-0.11	J16165577-5035455/HD 146105	1939	
49	16 18 48.17	-50 42 29.82	10.60	10.44	10.35	10.22	..	-0.14	..	0.23	1.01 ± 0.17	9.92[9.59-10.30]	B7-9I:	B8 (I)	(16.95)	..	9.92	0.07	J16184817-5042298/CPD-509207	1978	
50	16 14 48.62	-50 59 11.35	10.38	10.23	10.29	10.26	10.48	-0.10	0.55	0.09	1.09 ± 0.07	9.75[9.63-9.88]	A0	9.75	0.42	J16144862-5059113/CPD-509088	1939	
51	16 17 15.74	-51 26 41.11	10.98	10.48	10.34	10.30	10.13	0.07	-0.27	0.16	0.37 ± 0.06	11.98[11.68-12.32]	A0	11.98	-1.84	J16171574-5126411/HPD Nor 34	1939	
52	16 14 36.50	-51 30 03.68	..	10.50	10.37	10.34	10.22	0.07	-0.16	0.14	0.28 ± 0.04	12.56[12.28-12.88]	B	12.56	-2.36	J16143650-5130036/LS 3516	1966	
53	16 15 55.93	-50 27 10.51	10.85	10.53	10.37	10.36	10.33	0.14	0.09	0.13	1.32 ± 0.08	9.35[9.23-9.47]	OB-	9.35	0.88	J16155593-5027105/HD 145922	1971	
54	16 14 00.67	-51 12 59.07	10.76	10.45	10.43	10.37	10.34	-0.09	-0.01	0.15	1.56 ± 0.04	9.00[8.94-9.06]	B/A	9.00	1.22	J16140067-5112590/CPD-509067	1978	
55	16 19 53.00	-51 13 49.19	11.21	10.48	10.44	0.38 ± 0.04	11.94[11.74-12.15]	A0	J16195300-5113491/LS 3554	1939	
56	16 15 18.42	-50 55 37.52	11.00	10.62	10.53	10.49	10.76	0.03	0.84	0.14	0.29 ± 0.06	B4V/O9	B3-5 V	12.73	J16151842-5055375/[L64] 404.Ly404	3	1987/1987
57	16 18 17.00	-51 15 26.94	10.65	..	10.53	10.51	10.66	1.35 ± 0.05	9.31[9.23-9.39]	OB	J16181699-5115269/CPD-509192	1964	
58	16 18 49.64	-51 01 06.93	10.94	10.66	10.64	10.58	10.61	-0.08	0.16	0.14	0.96 ± 0.08	10.03[9.85-10.22]	A0	10.03	0.41	J16184964-5101069/[L64] 432.Ly432	3	1939
59	16 15 51.09	-51 37 29.81	11.50	10.95	10.80	10.66	..	-0.11	..	0.27	0.68 ± 0.04	10.76[10.65-10.88]	OB	10.76	-0.37	J16155109-5137298/HPD Nor 11	1964	
60	16 15 56.02	-50 27 24.03	10.88	10.71	10.69	10.68	10.45	..	-0.58	0.09	1.25 ± 0.05	9.47[9.38-9.56]	B	9.47	1.12	J16155602-5027240/HD 145923	1966	
61	16 17 44.56	-51 01 53.86	11.61	11.06	10.86	10.82	10.39	0.13	-0.93	0.17	0.36 ± 0.04	12.03[11.81-12.26]	B-A	12.03	-1.38	J16174456-5101538/LS 3537	1978	
62	16 17 17.68	-50 28 11.66	..	14.34	12.30	10.96	8.27	-0.38	-3.89	1.99	OB:	J16171767-5028116/[RC2017]A 10	1971	
63	16 16 16.61	-51 12 40.73	..	13.76	12.38	11.49	9.83	-0.23	-2.20	1.36	-0.36 ± 0.73	em	12.66	-2.53	J16161660-5112407/[RC2017]B 139	2018		

TABLE 9
THE MOST LUMINOUS LATE-TYPE TARGETS .

ID	Sp(rsg)	Sp(giant)	A_{K_s} [mag]	BC[rsg] [mag]	Ko [mag]	M_{bol} [rsg] [mag]	M_{bol} [giant] [mag]	M_{bol} [mag]	DM(adopt) [mag]	DM(ϖ) [mag]	DM(V_{lsr}) [mag]
L02	M2	..	2.10± 0.02	2.80	2.31± 0.03	-7.55± 0.71	..	-7.60± 0.00	12.66± 0.50
L03	M2	..	1.34± 0.02	2.80	3.61± 0.03	-6.25± 0.71	..	-6.20± 0.00	12.66± 0.50
L08	M1	..	1.01± 0.02	2.73	4.57± 0.04	-5.36± 0.71	..	-5.25± 0.00	12.66± 0.50
L09	K2	M1	1.15± 0.01	2.53	4.45± 0.02	-5.68± 0.71	-5.47± 0.71	-5.45± 0.00	12.66± 0.50
L11	K5	M7	1.43± 0.01	2.66	4.47± 0.02	-5.53± 0.71	-4.97± 0.71	-5.37± 0.00	12.66± 0.50
L18	K5	M6	1.67± 0.02	2.66	4.69± 0.02	-5.31± 0.71	-4.88± 0.71	-5.16± 0.00	12.66± 0.50
L21	M2	..	1.33± 0.02	2.80	5.17± 0.04	-4.69± 0.71	..	-4.65± 0.00	12.66± 0.50
L32	M1	..	1.37± 0.02	2.73	5.77± 0.02	-4.15± 0.71	..	-4.05± 0.00	12.66± 0.50
L35	M1	..	2.13± 0.02	2.73	5.07± 0.02	-4.86± 0.71	..	-4.75± 0.00	12.66± 0.50
P3	K3	..	0.16± 0.01	2.53	5.63± 0.02	-4.50± 0.71	12.66± 0.50	12.23	12.13
P4	M2	..	0.52± 0.10	2.80	2.96± 0.21	-6.90± 0.74	12.66± 0.50	10.17	12.51
P5	M3	..	0.30± 0.02	2.84	3.67± 0.04	-2.78± 0.71	9.29± 0.50	9.29	..
P6	M5.5	..	1.49± 0.16	3.02	1.33± 0.33	-8.30± 0.78	12.66± 0.50
P7	M3	..	0.40± 0.15	2.84	3.44± 0.31	-6.38± 0.77	12.66± 0.50	9.92	12.80
P8	M1	..	0.17± 0.02	2.73	4.53± 0.03	-5.39± 0.71	12.66± 0.50	11.68	12.26

Top table: Brightest late-type stars observed in this work. Identification numbers are as in Table 4. Stars brighter than $M_{bol} < -5.26$ mag ($L \geq 10^4 L_{\odot}$) or with measure $EW_{2.29 \mu m} > 45 \text{ \AA}$ are listed. *Bottom table:* Known K-M I stars from Skiff (2014). Identification numbers are as in Table 7. Identification numbers (ID) are followed by spectral types estimated for RSGs and giants (Sp(rsg), Sp(giant)), interstellar extinction, A_{K_s} , adopted bolometric correction, BC_K , dereddened K_s magnitudes, Ko, bolometric magnitudes obtained with for RSGs and for giants (M_{bol} [rsg], M_{bol} [giant]), bolometric magnitudes obtained by direct integration under the SED (M_{bol}), adopted distance moduli, DM(adopt), distance moduli from Gaia, DM(ϖ), and distance moduli from Gaia V_{lsr} DM(V_{lsr}).

TABLE 10
CANDIDATE FREE-FREE EMITTERS.

ID	Ra (hh mm ss)	Dec (deg mm ss)	Iden (mag)	J (mag)	H (mag)	K_s (mag)	[8.0] (mag)	Q1 (mag)	Q2 (mag)	A_{K_s} (mag)	plx (mas)	DM (mag)	VR (km s^{-1})	DMv (mag)	DMadopt (mag)	M_K (mag)	VAR	2MASS-ID/Alias	Comments	
1	16 18 10.38	-51 24 17.21	11.40	6.53	5.18	4.46	3.17	0.04	-1.38	1.18	0.42 ± 0.21	12.66	-9.38	..	J16181037-5124172/IRAS 16143-5117	
2	16 16 08.27	-51 29 03.33	..	7.30	5.59	4.61	2.71	-0.05	-2.42	1.53	0.03 ± 0.23	12.66	-9.58	..	J16160826-5129033/IRAS 16123-5121	
3	16 19 26.77	-51 24 31.22	12.90	8.34	6.32	4.88	1.90	-0.58	-4.55	2.09	0.16 ± 0.17	12.66	-9.87	..	J16192677-5124312/CGCS 6631	C
4	16 14 00.75	-51 30 39.81	11.40	6.97	5.88	5.13	3.85	-0.26	-1.62	1.13	0.88 ± 0.14	12.66	-8.66	VAR	J16140074-5130398/IRAS 16102-5123	
5	16 15 17.96	-50 52 19.71	13.05	7.76	6.13	5.14	3.32	-0.14	-2.30	1.52	0.69 ± 0.19	12.66	-9.04	..	J16151795-5052197/IRAS 16115-5044	PN/cLBV
6	16 18 40.78	-51 20 30.95	12.29	7.29	6.01	5.28	3.78	-0.05	-2.04	1.17	0.13 ± 0.21	12.66	-8.55	..	J16184077-5120309	
7	16 17 07.51	-50 31 06.38	12.80	7.60	6.17	5.32	4.02	-0.09	-1.22	1.32	0.35 ± 0.19	12.66	-8.66	..	J16170751-5031063	
8	16 19 18.58	-51 27 09.92	14.10	8.47	6.89	6.01	4.66	0.01	-1.19	1.39	0.15 ± 0.26	12.66	-8.04	..	J16191858-5127099/IRAS 16154-5119	
9	16 17 59.18	-51 19 25.32	..	8.81	7.04	6.01	4.12	-0.09	-2.30	1.60	12.66	-8.25	VAR	J16175917-5119253	
10	16 17 05.61	-51 28 15.67	15.70	8.97	7.11	6.07	4.56	-0.00	-1.15	1.64	-0.73 ± 0.35	12.66	-8.23	..	J16170560-5128156	
11	16 17 53.80	-50 43 48.62	11.10	7.74	6.79	6.19	5.02	-0.13	-1.59	0.94	0.90 ± 0.13	10.16	-4.91	..	J16175380-5043486	
12	16 18 13.16	-51 02 10.65	13.24	9.09	7.57	6.72	5.33	-0.00	-1.37	1.35	-0.38 ± 0.26	12.66	-7.29	..	J16181315-5102106	
13	16 16 49.13	-51 32 46.15	..	10.35	8.17	6.80	4.52	-0.29	-2.59	2.06	-2.38 ± 0.74	12.66	-7.92	..	J16164913-5132461	
14	16 15 24.42	-51 15 53.99	..	11.08	8.45	6.86	4.29	-0.23	-2.70	2.40	-0.21 ± 0.51	12.66	-8.20	..	J16152442-5115539/IRAS 16115-5108	
15	16 17 23.41	-50 45 26.15	16.40	13.67	9.54	7.00	3.24	-0.43	-3.43	3.78	12.66	-9.44	..	J16172340-5045261/IRAS 16136-5038	
16	16 15 06.76	-50 35 49.94	15.81	10.43	8.53	7.11	4.19	-0.65	-4.52	2.04	0.27 ± 0.23	12.66	-7.59	..	J16150676-5035499	
17	16 15 03.54	-51 35 26.35	15.76	10.68	8.70	7.57	5.67	-0.05	-2.01	1.76	0.31 ± 0.34	12.66	-6.85	..	J16150354-5135263	
18	16 12 11.56	-50 53 18.38	..	11.94	9.27	7.73	5.59	-0.10	-1.56	2.36	1.94 ± 3.40	12.66	-7.29	..	J16121156-5053183	
19	16 17 06.78	-51 24 46.78	..	10.92	8.94	7.84	6.29	-0.00	-1.09	1.73	-2.70 ± 0.55	12.66	-6.55	..	J16170678-5124467	
20	16 17 52.51	-50 44 41.75	12.17	10.51	9.50	8.49	5.53	-0.81	-5.94	1.38	0.38 ± 0.03	11.94	-78.43	13.25	J16175251-5044417	
21	16 14 13.82	-51 30 39.40	13.60	10.33	9.28	8.62	6.97	-0.14	-2.73	1.03	-0.14 ± 0.10	12.66	-5.07	..	J16141381-5130393	
22	16 18 14.74	-51 32 04.72	..	12.70	10.24	8.64	4.87	-0.42	-6.11	2.37	0.54 ± 1.05	12.66	-6.39	..	J16181474-5132047/IRAS 16144-5124	
23	16 12 46.71	-50 48 00.56	13.84	12.61	10.35	8.69	6.25	-0.73	-2.65	2.37	0.94 ± 0.04	10.06	J16124671-5048005	
24	16 16 27.36	-51 36 28.48	..	12.88	10.46	8.78	5.15	-0.60	-5.64	2.44	12.66	-6.32	..	J16162735-5136284/MSXGC 6331.9057-00.6572	AB?
25	16 16 25.44	-50 58 31.04	..	12.23	10.72	8.94	6.49	-1.68	-3.31	2.29	0.59 ± 0.04	11.03	J16162543-5058310	
26	16 15 58.26	-50 52 45.37	..	13.36	10.86	9.17	5.31	-0.54	-6.21	2.47	0.11 ± 0.86	12.66	-5.96	..	J16155825-5052453/2MASS J16155825-5052453	AB?
27	16 17 44.25	-50 51 09.87	12.88	11.40	10.19	9.22	7.69	-0.52	-1.94	1.38	0.50 ± 0.03	11.37	J16174425-5051098	
28	16 15 23.44	-51 26 24.49	16.11	14.45	11.40	9.22	5.61	-0.86	-4.50	3.11	0.30 ± 0.09	12.66	-6.55	..	J16152344-5126244	
29	16 13 20.00	-51 23 23.64	16.18	12.53	10.65	9.25	5.61	-0.64	-6.51	2.01	0.13 ± 0.18	12.66	-5.42	..	J16132000-5123236/2MASS J16132000-5123236	AB?
30	16 16 35.42	-50 40 45.99	..	10.14	9.66	9.40	8.52	-0.01	-1.62	0.48	0.18 ± 0.05	12.66	-3.74	..	J16163542-5040459	
31	16 12 00.39	-51 01 38.85	12.49	10.92	10.11	9.51	8.12	-0.28	-2.32	0.91	0.46 ± 0.03	11.55	-2.73	7.24	J16120038-5101388	
32	16 15 00.75	-51 38 33.97	..	14.12	11.33	9.58	6.41	-0.36	-3.99	2.61	-0.92 ± 0.66	12.66	-5.69	..	J16150075-5138339/2MASS J16150075-5138339	AB?
33	16 14 10.41	-51 29 32.30	16.45	14.35	11.50	9.77	7.62	-0.26	-1.18	2.61	0.03 ± 0.16	12.66	-5.50	..	J16141041-5129323	
34	16 18 39.78	-50 46 46.77	15.68	14.22	11.62	9.81	7.38	-0.66	-2.15	2.62	0.42 ± 0.07	11.74	J16183978-5046467	
35	16 16 11.73	-50 38 08.75	..	13.67	11.74	9.99	8.23	-1.21	-1.04	2.38	0.18 ± 0.15	12.66	-5.05	..	J16161172-5038087	

Candidate massive stars ($K_s < 9$ mag) with free-free emission. For a few targets SIMBAD provides information is found as annotated. AB? = Asymptotic Giant Branch Star candidate; C = carbon star; PN = planetary nebula; cLBV = candidate LBV in the present work.

Columns are as in Table 8.

TABLE 11
CANDIDATE NORMAL OB STARS.

ID	Ra(J2000)	Dec(J2000)	Iden	<i>J</i>	<i>H</i>	<i>K_s</i>	[8.0]	Q1	Q2	<i>A_{K_s}</i>	plx	DM	VR	DMv	DMadopt	<i>M_K</i>	VAR	2MASS-ID/Alias	Comments		
	(hh mm ss)	(deg mm ss)	(mag)	(mag)	(mag)	(mag)	(mag)	(mag)	(mag)	(mag)	(mas)	(mag)	(km s ⁻¹)	(mag)	(mag)	(mag)					
1	16 16 55.83	-51 32 12.26	..	6.54	5.28	4.63	3.96	0.10	0.11	1.07	0.17 ± 0.29	12.66	-9.10	..	J16165583-5132122		
2	16 16 42.73	-50 21 29.69	..	6.29	5.20	4.66	4.25	0.12	0.55	0.93	1.17 ± 0.19	12.66	-8.93	..	J16164272-5021296		
3	16 17 51.61	-50 34 39.46	10.86	6.83	5.61	4.99	4.32	0.12	0.01	1.03	1.67 ± 0.16	12.66	-8.70	VAR	J16175160-5034394		
4	16 19 47.26	-50 57 45.72	8.86	5.85	5.31	5.04	4.61	0.05	-0.37	0.50	0.19 ± 0.04	12.66	-8.11	..	J16194726-5057457/TYC 8324-1718-1		
5	16 19 25.80	-51 19 47.51	11.44	7.06	5.80	5.13	4.32	0.06	-0.27	1.09	1.25 ± 0.20	12.66	-8.61	..	J16192580-5119475		
6	16 18 00.98	-51 09 19.27	14.78	8.07	6.26	5.28	4.27	0.03	0.09	1.57	-0.24 ± 0.23	12.66	-8.95	..	J16180098-5109192		
7	16 15 06.28	-51 12 12.76	12.09	7.44	6.04	5.30	4.47	0.08	-0.11	1.20	0.09 ± 0.20	12.66	-8.56	..	J16150628-5112127		
8	16 13 25.20	-50 55 19.93	12.96	7.77	6.21	5.35	4.40	0.01	-0.14	1.37	0.77 ± 0.20	12.66	-8.68	..	J16132519-5055199		
9	16 17 58.45	-50 26 56.50	12.82	7.97	6.25	5.38	4.46	0.14	0.13	1.43	0.70 ± 0.19	12.66	-8.71	..	J16175844-5026565		
10	16 19 36.95	-51 15 29.28	14.68	8.41	6.57	5.60	4.43	0.10	-0.35	1.56	0.66 ± 0.22	12.66	-8.62	..	J16193694-5115292		
11	16 17 18.77	-51 01 36.43	..	8.75	6.74	5.61	4.15	-0.03	-0.77	1.77	0.10 ± 0.32	12.66	-8.82	..	J16171876-5101364		
12	16 15 20.52	-51 06 20.91	14.47	8.66	6.85	5.82	4.43	-0.03	-0.90	1.61	-0.22 ± 0.33	12.66	-8.45	..	J16152052-5106209		
13	16 13 51.52	-50 28 53.75	..	10.50	7.60	5.95	4.00	-0.08	-0.69	2.54	1.87 ± 1.66	12.66	-9.25	..	J16135151-5028537		
14	16 13 46.57	-50 52 57.95	17.54	9.26	7.16	6.00	4.55	0.02	-0.64	1.82	-0.43 ± 0.34	12.66	-8.48	..	J16134657-5052579		
15	16 19 10.20	-51 20 30.50	11.18	7.86	6.62	6.01	5.70	0.14	1.01	1.03	1.02 ± 0.16	12.66	-7.68	..	J16191020-5120304		
16	16 19 39.13	-51 02 59.16	12.28	7.97	6.75	6.10	..	0.06	-0.02 ± 0.15	12.66	J16193912-5102591		
17	16 13 28.78	-50 42 55.18	17.48	9.60	7.45	6.31	5.09	0.09	0.01	1.82	.. ± 0.45	12.66	-8.17	..	J16132878-5042551		
18	16 18 20.03	-50 50 20.73	10.12	7.61	6.83	6.43	5.80	0.05	-0.51	0.70	0.27 ± 0.13	12.66	-6.93	..	J16182003-5050207		
19	16 12 47.18	-50 59 45.21	10.99	7.86	6.98	6.46	5.92	-0.07	-0.03	0.85	0.61 ± 0.10	10.96	-5.36	..	J16124717-5059452		
20	16 17 23.27	-50 30 19.65	11.39	7.99	7.03	6.49	5.93	-0.02	0.02	0.89	1.02 ± 0.15	12.66	-7.06	..	J16172326-5030196		
21	16 18 19.24	-51 23 39.79	9.11	7.26	6.82	6.53	6.20	-0.10	-0.13	0.50	0.20 ± 0.05	12.66	-6.63	..	J16181923-5123397/TYC 8323-2185-1		
22	16 14 52.17	-51 20 29.92	12.56	8.59	7.25	6.58	6.10	0.13	0.73	1.12	0.42 ± 0.16	12.66	-7.20	VAR	J16145216-5120299		
23	16 12 34.67	-51 16 42.24	10.94	7.98	7.18	6.71	6.17	-0.05	-0.16	0.78	0.42 ± 0.10	12.66	-6.73	..	J16123467-5116422		
24	16 18 45.09	-51 15 50.01	9.99	7.76	7.12	6.75	6.30	-0.03	-0.19	0.63	0.28 ± 0.11	12.66	-6.54	..	J16184508-5115500		
25	16 14 03.22	-50 58 20.95	14.35	9.25	7.75	6.96	6.07	0.09	-0.12	1.28	0.20 ± 0.21	12.66	-6.98	..	J16140322-5058209		
26	16 19 20.50	-51 02 54.18	14.07	9.26	7.87	7.08	..	-0.03	0.28 ± 0.18	12.66	J16192049-5102541		
27	16 17 04.50	-51 15 19.68	10.59	8.21	7.54	7.17	6.67	-0.00	-0.30	0.64	0.31 ± 0.09	12.66	-6.13	..	J16170449-5115196		
28	16 17 22.84	-51 32 42.86	14.71	9.59	8.03	7.22	6.18	0.11	-0.45	1.32	-0.96 ± 0.31	12.66	-6.76	..	J16172283-5132428		
29	16 13 54.73	-50 47 41.68	..	10.93	8.57	7.28	5.85	0.04	-0.22	2.02	-0.22 ± 0.91	12.66	-7.40	..	J16135473-5047416		
30	16 19 13.72	-50 51 13.89	14.00	9.70	8.17	7.38	6.68	0.12	0.45	1.29	0.18 ± 0.17	12.66	-6.57	..	J16191372-5051138		
31	16 17 21.71	-51 34 39.26	16.65	10.26	8.42	7.41	6.16	0.02	-0.53	1.60	0.15 ± 0.37	12.66	-6.85	..	J16172170-5134392		
32	16 16 04.91	-51 36 33.96	..	8.18	7.69	7.44	6.96	0.05	-0.56	0.46	0.23 ± 0.07	12.66	-5.68	..	J16160490-5136339		
33	16 14 25.74	-51 21 41.00	10.28	8.35	7.83	7.51	7.23	-0.07	0.09	0.55	0.23 ± 0.07	12.66	-5.70	..	J16142574-5121410		
34	16 14 35.41	-51 21 44.74	..	8.74	7.93	7.53	7.17	0.09	0.25	0.70	0.41 ± 0.08	12.66	-5.83	..	J16143540-5121447		
35	16 19 30.74	-51 20 07.67	14.19	9.66	8.25	7.54	6.87	0.15	0.30	1.18	-0.07 ± 0.19	12.66	-6.30	..	J16193074-5120076		
36	16 19 30.44	-51 23 39.89	15.97	10.07	8.46	7.55	6.62	-0.04	0.03	1.44	0.06 ± 0.27	12.66	-6.55	..	J16193043-5123398		
37	16 17 08.28	-51 27 43.04	9.79	8.29	7.84	7.63	7.32	0.07	-0.15	0.42	0.11 ± 0.07	12.66	-5.45	..	J16170828-5127430		
38	16 15 10.94	-51 36 18.55	11.93	9.01	8.13	7.70	7.10	0.08	-0.30	0.76	-0.04 ± 0.10	12.66	-5.72	..	J16151093-5136185		
39	16 14 21.90	-51 36 03.24	13.19	9.62	8.55	7.98	7.39	0.04	0.07	0.95	0.25 ± 0.12	12.66	-5.63	..	J16142189-5136032		
40	16 14 34.10	-50 33 01.83	..	11.41	9.17	8.00	6.96	0.13	0.63	1.87	12.66	-6.53	..	J16143410-5033018		
41	16 13 08.16	-50 51 28.93	..	11.98	9.46	8.05	6.45	-0.01	-0.36	2.19	12.66	-6.80	..	J16130815-5051289		
42	16 13 13.15	-51 08 37.11	..	12.58	9.65	8.05	7.12	0.05	2.02	2.49	12.66	-7.10	..	J16131315-5108371		
43	16 15 33.81	-51 12 09.05	16.15	10.59	8.94	8.06	7.13	0.08	-0.00	1.41	0.50 ± 0.28	12.66	-6.01	..	J16153381-5112090		
44	16 15 40.77	-51 20 59.33	14.21	10.05	8.78	8.10	7.08	0.06	-0.80	1.11	-0.02 ± 0.18	12.66	-5.67	..	J16154076-5120593		
45	16 20 08.17	-50 48 30.83	10.87	8.96	8.44	8.11	7.73	-0.08	-0.17	0.56	0.28 ± 0.06	12.52	-4.97	..	J16200817-5048308		
46	16 14 09.48	-50 58 25.93	13.84	9.88	8.72	8.14	7.48	0.11	-0.04	0.98	0.33 ± 0.14	12.66	-5.49	..	J16140948-5058259		
47	16 17 41.39	-50 28 25.59	14.85	10.24	8.91	8.22	7.39	0.10	-0.21	1.14	0.84 ± 0.19	12.66	-5.58	..	J16174139-5028255		
48	16 19 24.80	-50 57 51.65	9.70	8.64	8.39	8.22	7.92	-0.06	-0.38	0.32	0.31 ± 0.04	12.36	-4.46	..	J16192480-5057516/TYC 8324-913-1	
49	16 16 19.50	-51 07 27.09	..	10.37	8.98	8.25	7.52	0.09	0.14	1.19	-0.52 ± 0.23	12.66	-5.60	..	J16161949-5107270		
50	16 15 52.56	-51 37 56.41	11.30	9.29	8.73	8.37	7.84	-0.11	-0.49	0.60	12.66	-4.89	..	J16155255-5137564		
51	16 17 30.77	-50 31 16.89	13.12	9.80	8.90	8.41	7.86	0.01	-0.08	0.82	0.51 ± 0.12	12.66	-5.07	..	J16173077-5031168		
52	16 18 23.87	-50 40 12.31	13.47	9.93	8.93	8.42	7.69	0.07	-0.45	0.87	0.20 ± 0.12	12.66	-5.11	..	J16182386-5040123		
53	16 18 51.47	-51 17 32.70	11.83	9.47	8.80	8.43	7.90	0.02	-0.39	0.63	0.08 ± 0.08	12.66	-4.86	..	J16185147-5117326		
54	16 17 02.59	-50 27 09.75	12.18	9.70	8.96	8.54	7.88	-0.02	-0.63	0.70	0.41 ± 0.08	11.80	-3.96	..	J16170258-5027097		
55	16 13 34.20	-50 59 14.17	13.28	10.03	9.03	8.55	8.07	0.15	0.19	0.83	0.27 ± 0.10	12.66	-4.94	..	J16133419-5059141		
56	16 14 33.05	-51 28 30.90	..	13.69	10.47	8.59	6.56	-0.16	-0.35	2.85	0.45 ± 0.06	11.61	-5.87	..	J16143304-5128309	
57	16 18 13.56	-51 18 26.02	..	11.47	9.67	8.59	7.45	-0.15	-0.20	1.66	0.43 ± 0.03	11.68	-4.75	..	J16181355-5118260	
58	16 17 29.97	-50 30 56.67	13.19	9.99	9.09	8.59	7.96	..	-0.31	0.83	0.39 ± 0.13	12.66	-4.90	..	J16172		

TABLE 11
CONTINUATION OF TABLE 11

ID	Ra(J2000) (hh mm ss)	Dec(J2000) (deg mm ss)	l _{den} (mag)	J (mag)	H (mag)	K _s (mag)	[8.0] (mag)	Q1 (mag)	Q2 (mag)	A _{K_s} (mag)	plx (mas)	DM (mag)	VR (km s ⁻¹)	DMv (mag)	DMadopt (mag)	M _K (mag)	VAR	2MASS-ID/Alias	Comments
62	16 19 42.80	-51 14 26.33	11.84	9.66	9.10	8.79	8.45	0.02	-0.05	0.54	0.19 ± 0.07	12.66	-4.41	..	J16194279-5114263	
63	16 14 44.01	-50 44 03.89	10.94	9.49	9.06	8.85	8.52	0.04	-0.22	0.41	0.29 ± 0.06	12.47	-4.03	..	J16144401-5044038	
64	16 18 08.57	-50 28 55.06	10.28	9.40	9.09	8.93	8.78	0.04	0.06	0.32	0.48 ± 0.04	11.45	-2.84	..	J16180856-5028550/TYC 8319-705-1	
65	16 17 50.93	-51 36 34.22	10.67	9.52	9.18	8.95	8.79	-0.06	0.16	0.40	0.24 ± 0.05	12.85	-4.30	..	J16175093-5136342	
66	16 12 09.88	-50 58 08.36	..	10.37	9.44	9.00	..	0.13	0.39 ± 0.03	11.90	J16120988-5058083	
67	16 19 46.48	-51 02 57.04	12.80	10.30	9.55	9.03	..	-0.18	-0.06 ± 0.09	12.66	J16194647-5102570	
68	16 19 45.37	-51 02 59.65	12.82	10.31	9.62	9.12	..	-0.20	12.66	J16194536-5102596	
69	16 17 35.20	-50 31 26.34	11.49	9.78	9.34	9.13	8.80	0.08	-0.24	0.40	-0.64 ± 0.28	12.66	-3.92	..	J16173520-5031263	
70	16 15 39.41	-51 40 22.31	11.78	9.93	9.42	9.14	8.86	0.01	0.03	0.50	0.21 ± 0.06	12.66	-4.02	..	J16153940-5140223	
71	16 13 07.79	-50 56 13.43	16.13	11.44	9.95	9.14	8.46	0.02	0.44	1.30	-0.48 ± 0.23	12.66	-4.82	..	J16130778-5056134	
72	16 19 37.87	-51 18 25.60	11.28	9.82	9.40	9.22	8.96	0.09	-0.09	0.37	0.18 ± 0.05	12.66	-3.81	..	J16193787-5118255	
73	16 16 10.12	-51 38 01.68	..	9.87	9.48	9.27	9.14	0.02	0.24	0.39	0.16 ± 0.05	12.66	-3.78	..	J16161012-5138016	
74	16 18 41.46	-51 01 22.62	14.06	10.83	9.80	9.29	8.88	0.11	0.42	0.87	0.24 ± 0.10	12.66	-4.24	..	J16184146-5101226	
75	16 17 33.89	-50 34 39.21	13.45	10.57	9.71	9.30	8.97	0.12	0.39	0.73	0.54 ± 0.10	11.22	-2.66	..	J16173389-5034392	
76	16 18 23.90	-50 39 01.70	13.93	10.72	9.79	9.30	8.80	0.04	0.06	0.83	0.08 ± 0.12	12.66	-4.19	..	J16182390-5039016	
77	16 19 01.12	-51 10 13.29	10.28	9.65	9.41	9.31	9.20	0.05	0.07	0.25	0.67 ± 0.04	10.78	-1.73	..	J16190111-5110132/TYC 8324-972-1	
78	16 15 16.33	-51 06 55.28	12.98	10.44	9.70	9.33	8.94	0.10	0.05	0.65	0.14 ± 0.11	12.66	-3.98	..	J16151633-5106552	
79	16 15 57.33	-51 10 06.57	12.33	10.29	9.68	9.37	9.07	0.05	0.10	0.56	0.13 ± 0.07	12.66	-3.85	..	J16155732-5110065	
80	16 19 18.73	-51 01 11.04	11.67	10.14	9.63	9.39	9.29	0.06	0.47	0.46	0.35 ± 0.04	12.12	-3.18	..	J16191873-5101110	
81	16 17 29.36	-50 30 31.98	14.56	10.95	9.95	9.45	9.09	0.09	0.53	0.86	0.22 ± 0.14	12.66	-4.07	..	J16172935-5030319	
82	16 18 40.94	-50 31 58.69	14.78	11.07	10.04	9.47	8.89	0.02	0.03	0.93	0.24 ± 0.17	12.66	-4.12	..	J16184094-5031586	
83	16 17 21.14	-50 47 29.44	13.77	10.82	9.96	9.48	9.07	0.01	0.26	0.80	0.36 ± 0.10	12.66	-3.98	..	J16172114-5047294	
84	16 14 44.60	-50 43 30.86	11.16	10.00	9.66	9.50	9.31	0.04	-0.02	1.33	0.32 ± 0.05	12.30	-3.13	..	J16144459-5043308	
85	16 16 24.75	-51 09 55.20	..	11.21	10.18	9.53	8.76	-0.12	-0.41	0.01	0.26 ± 0.04	12.68	-4.15	..	J16162474-5109551	
86	16 13 55.24	-51 26 05.77	..	12.54	10.60	9.54	8.54	0.06	0.31	1.67	-0.15 ± 0.19	12.66	-4.79	..	J16135523-5126057	
87	16 14 59.86	-51 22 45.23	12.81	10.50	9.85	9.55	9.34	0.10	0.39	0.56	0.32 ± 0.10	12.66	-3.67	..	J16145985-5122452	
88	16 17 20.82	-50 50 27.56	10.48	9.84	9.64	9.59	9.51	0.09	0.05	0.19	0.29 ± 0.04	12.46	-3.06	..	J16172081-5050275/TYC 8323-805-1	
89	16 15 21.10	-51 13 20.56	13.88	10.94	10.10	9.60	9.00	-0.08	-0.28	0.82	-0.78 ± 0.72	12.66	-3.88	..	J16152109-5113205	
90	16 16 02.48	-51 12 07.58	..	11.89	10.38	9.60	8.84	0.12	0.22	1.27	-1.28 ± 0.40	12.66	-4.33	..	J16160248-5112075	
91	16 16 51.98	-51 34 04.62	..	10.24	9.81	9.63	9.47	0.10	0.21	0.38	3.25 ± 0.76	12.66	-3.41	..	J16165198-5134046	
92	16 13 48.19	-51 26 16.85	12.88	10.57	9.96	9.65	9.56	0.05	0.70	0.56	-1.73 ± 0.46	12.66	-3.57	..	J16134818-5126168	
93	16 17 19.75	-51 33 59.28	12.43	10.69	10.01	9.65	8.40	0.04	-2.33	0.62	0.10 ± 0.06	12.66	-3.63	..	J16171975-5133592	
94	16 20 14.18	-50 51 43.60	11.91	10.32	9.88	9.66	9.42	0.06	-0.00	0.41	0.20 ± 0.05	12.66	-3.41	..	J16201417-5051435	
95	16 18 35.60	-51 15 46.06	10.57	9.92	9.81	9.67	9.37	-0.12	-0.55	0.25	0.69 ± 0.04	10.72	-1.30	..	J16183560-5115460/TYC 8323-2582-1	
96	16 17 33.34	-51 20 47.19	11.84	10.32	9.91	9.69	9.60	0.02	0.39	0.41	0.15 ± 0.05	12.66	-3.38	..	J16173333-5120471	
97	16 14 59.48	-50 37 30.89	..	12.38	10.62	9.71	9.00	0.13	0.79	1.48	-0.71 ± 0.61	12.66	-4.43	..	J16145947-5037308	
98	16 20 16.11	-50 55 28.32	12.54	10.57	10.02	9.71	9.55	-0.02	0.43	0.54	0.05 ± 0.06	12.66	-3.49	..	J16201610-5055283	
99	16 12 32.85	-50 55 32.67	11.17	10.18	9.89	9.72	9.53	-0.02	-0.06	0.33	0.58 ± 0.04	11.06	-1.67	..	J16123285-5055326/TYC 8323-451-1	
100	16 13 24.35	-51 27 41.89	..	12.60	10.73	9.76	8.91	0.13	0.57	1.57	-0.11 ± 0.58	12.66	-4.47	..	J16132435-5127418	
101	16 16 46.59	-51 06 49.36	..	11.68	10.40	9.77	9.04	0.14	-0.04	1.07	0.28 ± 0.23	12.66	-3.96	..	J16164658-5106493	
102	16 17 35.03	-50 28 46.67	10.46	9.94	9.85	9.77	9.74	-0.04	0.09	0.18	0.52 ± 0.04	11.29	-1.70	..	J16173502-5028466/TYC 8319-954-1	
103	16 20 06.54	-50 52 12.85	10.61	9.98	9.87	9.78	10.13	-0.05	1.15	0.20	0.04 ± 0.15	12.66	-3.08	..	J16200654-5052128/TYC 8324-1509-1	
104	16 17 32.55	-51 30 33.25	10.87	10.17	9.93	9.79	9.78	-0.01	0.34	0.28	0.47 ± 0.23	12.66	-3.15	..	J16173255-5130332/TYC 8323-1405-1	
105	16 16 08.14	-51 37 07.93	..	10.43	10.03	9.81	9.71	-0.01	0.35	0.41	-0.41 ± 0.06	12.66	-3.26	..	J16160814-5137079	
106	16 16 51.77	-51 14 28.46	..	10.77	10.18	9.82	9.49	-0.05	0.05	0.60	0.05 ± 0.07	12.66	-3.44	..	J16165176-5114284	
107	16 15 23.49	-51 38 42.21	13.43	11.01	10.24	9.84	9.48	0.06	0.20	0.69	0.04 ± 0.07	12.66	-3.51	..	J16152348-5138422	
108	16 19 59.03	-51 10 21.00	12.52	10.57	10.11	9.85	9.34	..	-0.65	0.46	0.18 ± 0.05	12.66	-3.27	..	J16195903-5110210	
109	16 18 32.21	-51 13 16.21	16.81	12.02	10.60	9.85	8.89	0.07	-0.44	1.22	-0.57 ± 0.26	12.66	-4.03	..	J16183221-5113162	
110	16 16 28.28	-51 05 49.79	..	10.76	10.18	9.88	9.62	0.02	0.20	0.55	-0.10 ± 0.08	12.66	-3.33	..	J16162828-5105497	
111	16 15 03.31	-51 32 09.88	10.42	10.04	9.91	9.91	9.79	0.13	-0.17	0.12	0.59 ± 0.04	11.04	-1.25	..	J16150330-5132098/TYC 8323-2297-1	
112	16 13 35.95	-51 05 11.59	..	12.13	10.68	9.91	9.49	0.06	1.08	1.25	-0.01 ± 0.15	12.66	-3.99	..	J16133595-5105115	
113	16 16 48.56	-50 23 13.24	..	10.53	10.12	9.93	9.55	0.05	-0.41	0.39	0.23 ± 0.05	12.66	-3.12	..	J16164856-5023132	
114	16 17 05.06	-50 47 25.74	14.01	11.20	10.37	9.94	..	0.06	0.20 ± 0.09	12.66	J16170505-5047257	
115	16 17 03.36	-51 10 25.14	16.92	12.09	10.66	9.94	9.23	0.14	0.22	1.19	0.73 ± 0.29	12.66	-3.91	..	J16170335-5110251	
116	16 17 03.33	-50 40 12.71	12.90	10.85	10.24	9.95	9.55	0.09	-0.18	0.54	0.18 ± 0.06	12.66	-3.25	..	J16170332-5040127	
117	16 18 48.06	-51 06 41.59	12.77	10.80	10.24	9.96	9.60	0.06	-0.11	0.51	0.12 ± 0.06	12.66	-3.21	..	J16184805-5106415	
118	16 19 22.85	-51 22 49.52	10.67	10.19	10.05	9.96	9.87	-0.03	-0.02	0.21	0.84 ± 0.04	10.30	-0.55	..	J16192284-5122495/TYC 8324-2022-1	
119	16 15 29.17	-51 40 13.23	12.72	10.94	10.29	9.96	9.60	0.06	..	0.58	0.10 ± 0.24	12.66	-3.27	..	J16152916-5140132	
120	16 13 18.66	-51 04 43.97	10.87	10.27	10.07	9.97	9.89	0.02	0.08	0.23	0.85 ± 0.04	10.29	-0.54	..	J16131865-5104439/TYC 8323-686-1	
121	16 16 06.16																		

TABLE 12
APPARENT MAGNITUDES OF O9 AND O5 STARS

Sp.	Class	$K_{s,abs}$ (mag)	A_{K_s} (mag)	DM (mag)	K_s (mag)
O5	I	-5.52	0.40	12.66	7.54
O9	I	-5.52	0.40	12.66	7.54
O5	I	-5.52	1.60	12.66	8.74
O9	I	-5.52	1.60	12.66	8.74
O5	I	-5.52	2.20	12.66	9.34
O9	I	-5.52	2.20	12.66	9.34
O5	I	-5.52	0.40	13.70	8.58
O9	I	-5.52	0.40	13.70	8.58
O5	I	-5.52	1.60	13.70	9.78
O9	I	-5.52	1.60	13.70	9.78
O5	I	-5.52	2.20	13.70	10.38
O9	I	-5.52	2.20	13.70	10.38
O5	V	-4.39	0.40	12.66	8.67
O9	V	-3.28	0.40	12.66	9.78
O5	V	-4.39	1.60	12.66	9.87
O9	V	-3.28	1.60	12.66	10.98
O5	V	-4.39	2.20	12.66	10.47
O9	V	-3.28	2.20	12.66	11.58
O5	V	-4.39	0.40	13.70	9.71
O9	V	-3.28	0.40	13.70	10.82
O5	V	-4.39	1.60	13.70	10.91
O9	V	-3.28	1.60	13.70	12.02
O5	V	-4.39	2.20	13.70	11.51
O9	V	-3.28	2.20	13.70	12.62

In the color-magnitude diagram (CMD), E6 ($A_{K_s} = 0.2$ mag) is located on the red edge of the first main sequence which is populated by stars in the Sagittarius-Carina arm. However, its Gaia DR2 parallax (0.31 ± 0.04 mas) suggests a distance of 2.9 kpc (Scutum-Crux arm), still consistent with a dwarf. WR 74 (P2) is located just above the second main-sequence peak with $A_{K_s} = 0.43$ mag and most probably belongs to G332.809-0.132 in the Scutum-Crux arm, as well as the new WN 8 (E4, $A_{K_s} = 0.5$ mag). The other observed early-type stars have A_{K_s} from 0.74 mag to 1.55 mag. The spectrophotometric properties of star E2 (Ofpe/WN 9, $A_{K_s} = 0.9$ mag) are compatible with the 3 kpc kinematic distance of the G332.809-0.132 molecular complex. The stellar cluster [DBS2003]160-161 (IRAS 16132 - 5039) is also at a similar distance, but its members are still embedded with $A_{K_s} = 1.2$ -1.7 mag (Roman-Lopes & Abraham 2004). Therefore, it appears that stars with A_{K_s} from 0.4 mag to 1.6 mag may belong to the G332.809-0.132 molecular complex of the Scutum-Crux arm. If we consider the early-type stars with $J-K_s$ color from 0.7 mag to 3.0 mag, i.e., with A_{K_s} from 0.4 mag to 1.6 mag, in the “Bridge” we count 108 stars (= 83 OB candidates + 16 free-free + 6 OB observed + 3 previously known OB stars and WRs) stars brighter than $K_s < 10$ mag (O9 V at 3.4 kpc) that are the potential ionizing stars of the G332.809-0.132 molecular complex. These numbers along with the sampled A_{K_s} and the expected magnitudes in Table 12, suggest that we have identified most of the supergiants in the region, and that those stars may already account for about 50% of the ionizing flux measured by WMAP (see Section 5). In Table 12 the apparent magnitudes of an O5 and O9 stars are calculated for $A_{K_s} = 0.4, 1.6, 2.2$ mag, and 3.4 and 5.5 kpc. These early-type stars are sparsely distributed on “The Bridge”, but rare in the northwestern sector (i.e., toward the direction of SNRs G332.0 + 00.2 and Kes 32, which are reported at a larger distance of 6-7 kpc), as seen in the Fig. 5. Note that in our exercise we consider stars brighter than $K_s =$

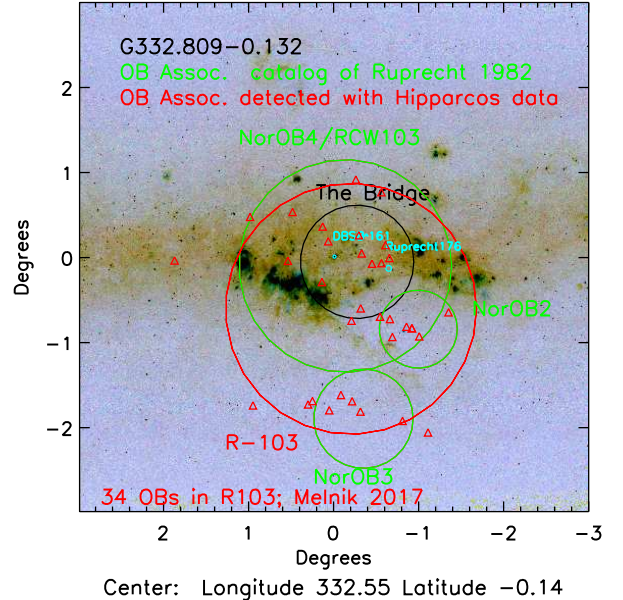


Fig. 9.— MSX composite image of “The Bridge” (area encircled by the black circle). The green circles show the Nor OB2, Nor OB3, and Nor OB4 associations listed by Ruprecht et al. (1982). The red circle show the RCW 103 association following the partitions of Blaha and Humphreys listed in Mel’Nik & Efremov (1995); the 34 OB members are marked with red triangles (Mel’nik & Dambis 2017).

10 mag. As demonstrated by Roman-Lopes et al. (2009), the IRAS 16132 - 5039 region contains obscured massive stars, with only the two brightest around this magnitude. The actual number of Lyman continuum emitters is greater than estimated. The G332.0 + 00.2 complex is unquestionably rich in evolved massive stars.

The complex also hosts a number of K-M I stars, with six of them listed by Skiff (2014). We are able to confirm five of those as associated with the G332.0 + 00.2 complex. By looking at the spatial distribution, we can see that they are located at the periphery of “The Bridge”. A few other candidate RSGs were identified in the central region.

6. HOW DOES OUR ANALYSIS COMPARE TO PREVIOUS KNOWLEDGE ON STELLAR ASSOCIATIONS AND CLUSTERS?

The kind referee has suggested considering known stellar clusters projected toward this line of sight, and so here we report on our search in the literature. It has long been known that this area of the sky was rich in massive stars and explosive supernovae. Historical information, though, was not correlated, and several authors reported independently about the beauty of this region and its content of massive stars. As shown in Section 5.6, this line of sight is quite complex because it crosses three spiral arms; furthermore, the morphology of the complex at mid-infrared light suggests strong patchiness of interstellar extinction.

In the case of G332.809-0.132, the extended HII region identified in the WMAP radio data (see 5) lies within the area of the Nor OB4/RCW 103 association (Alter et al. 1970; Ruprecht et al. 1982). A sketch of the Nor OB associations is shown in Fig. 9. This OB association is 150’ in size and encloses “The Bridge” area here considered, which comprises its central portion (diameter of 80’). The Nor OB4 associa-

tion is also mentioned by Ambartsumian & Kandalian (1989) as related to a region of recent star formation containing stellar associations. There are no associated articles before 1969. Nor stands for Norma (Ruprecht et al. 1982), as this line of sight is a tangent point to the Norma spiral arm at longitudes 332° (see our Fig. 6 and also the list of tangent points provided by Englmaier & Gerhard (1999)).

Westerlund (1969) reports about 36 OB stars in the neighborhood of the emission nebula RCW 103 ($331^\circ < l < 334^\circ$, $-2^\circ < b < +1^\circ$). Humphreys (1978) lists 26 OB stars in the same area. Their radial velocities are quite uncertain (e.g., 40 km s^{-1} variations are measured toward the same star) and vary from $+27$ to -80 km s^{-1} . Thirty-four OB stars and two stellar kinematic subgroups (six and seven stars) were identified in RCW 103 by Mel'nik & Efremov (1995), who assigned a kinematic distance of 3.2 kpc ($V_{lsr} = -48 \text{ km s}^{-1}$ with $\sigma = 30.5 \text{ km s}^{-1}$). Identified members are listed in Mel'nik & Dambis (2017) and their locations are shown in Fig. 9. Only 9 of these 34 OB members fall in the central area we analyzed (“The Bridge”). These members are marked in Table 8, have $A_{K_s} < 0.4$ mag and are among the 15 most distant OB stars previously known (parallactic distances from 2 to 4 kpc) – with average proper motions $\mu_{ra} = -2.026 \text{ mas yr}^{-1}$ with $\sigma = 1.5 \text{ mas yr}^{-1}$, $\mu_{dec} = -2.934 \text{ mas yr}^{-1}$ with $\sigma = 1.5 \text{ mas yr}^{-1}$. A recent search for star formations and infrared OB stars in the direction of this WMAP extended complex was carried out by Rahman et al. (2013), with two detected overdensities (RMM34a and RMM34b) of $6'$ and $17'$ in size, located on the left-side bright $8 \mu\text{m}$ emission east of the sled.

Ruprecht 176 and DBSB 161 are the only two known open clusters enclosed in “The Bridge” area (Kharchenko et al. 2016). DBSB 161 has already been described already above (see Section 5.6); it is located in the center of “The Bridge” at about 3 kpc, is still embedded ($A_{K_s} = 1.2\text{--}1.7$ mag), and rich in massive O stars (Roman-Lopes & Abraham 2004; Corti et al. 2016).

Ruprecht 176 is an older known open cluster. Kharchenko et al. (2016) estimate a distance of 2.7 kpc, $E(B-V)=0.48$ mag ($A_{K_s} \approx 0.13$ mag), and an age of 580 Myr. Sampedro et al. (2017) provides 438 individual members based on the motions of stars in the UCAC4 catalog, $E(B-V)=0.69$ mag ($A_{K_s}=0.2$ mag), a distance of 1.5 kpc, and age of 288 Myr. Newer Gaia data from DR2, using 130 members, have yielded a most likely distance (the mode of the likelihood) of 2.7 kpc (from 2.1 to 3.7 kpc), proper motions $\mu_{ra} = -2.644 \text{ mas yr}^{-1}$ with $\sigma=0.13 \text{ mas yr}^{-1}$, and $\mu_{dec} = -2.984 \text{ mas yr}^{-1}$ with $\sigma = 0.078 \text{ mas yr}^{-1}$; $\varpi = 0.335 \text{ mas}$ with $\sigma = 0.070 \text{ mas}$, and a radius of $2'.34$ (Cantat-Gaudin et al. 2018). With Gaia DR2, $A_V=1.68$ mag ($A_{K_s} \approx 0.14$ mag) and the age is lowered to 150 Myr (Bossini et al. 2019). Its parallactic distance, proper motions, and A_{K_s} are consistent with those of RCW 103 given by Mel'nik & Dambis (2017), and identical to values we measured for OBs on the second main sequences of the CMD in Fig. 8, however, using redder stars at $A_{K_s}=0.4$ mag. This indicates differential extinction and the need for parallaxes and velocities to assign distances. This brings the open cluster Ruprecht 176 into the Scutum-Crux arm, perhaps in its front side.

Bica et al. (2019) present a list of ~ 35 candidate clusters toward the “Bridge”. The bulk of them consists of tiny regions (radius $< 1'$) of strong diffuse mid-infrared emission, whose positions do not spatially correlate with those of selected OB stars. Those could represent very young stellar objects, the re-

sults of recently triggered star formation. Several of them may also reside in the background -90 km s^{-1} molecular cloud (5 kpc, Norma arm); for example, GLIMPSE 77 is located in the northern edge of “The Bridge”, has an $A_{K_s}=0.9$ mag, but a spectrophotometric distance of 5.2 kpc (Messineo et al. 2018; Morales et al. 2013) and belongs to the Norma arm; VVV CL065 is another embedded cluster in the -95 km s^{-1} cloud (Morales et al. 2013). [MCM2005b] 76, VVV CL066, [MCM2005b] 74, VVV CL064 are also embedded, but associated with molecular clumps at -50 km s^{-1} (Morales et al. 2013). In conclusion, the G332.809–0.132 complex is made of molecular clouds at $\approx -50 \text{ km s}^{-1}$ in the Scutum-crux arm; but, behind it, a conspicuous amount of clouds accumulates with V_{lsr} at $\approx -90 \text{ km s}^{-1}$ because of the tangent point to the Norma arm. Plus, there is a stellar population (not associated with clouds) belonging to the nearest spiral arm (Sagittarius).

In the present work, we have analyzed about 100 candidate early-type stars selected over “The Bridge” area, that are sparsely distributed, i.e., not in clusters, with $K_s < 10$ mag (O9 at 3.4 kpc) by aiming to detect evolved massive stars. The large size and patchiness of the interstellar extinction hamper a precise knowledge of the stratification of the various stellar populations. In Fig. 10, we display the Gaia DR2 proper motions and parallaxes of the candidate OB stars and show that the range of extinction $0.4 < A_{K_s} < 1.6$ mag samples stars at 3 kpc and beyond. An average $\mu_{ra} = -3.11 \text{ mas yr}^{-1}$ with $\sigma=0.91 \text{ mas yr}^{-1}$, and $\mu_{dec} = -3.68 \text{ mas yr}^{-1}$ with $\sigma = 0.82 \text{ mas yr}^{-1}$ are measured. These proper motions are consistent with that of the massive stars with free-free emission; indeed, for IRAS 16115–5044, $\mu_{ra} = -3.51 \pm 0.33 \text{ mas yr}^{-1}$ and $\mu_{dec} = -3.17 \pm 0.19 \text{ mas yr}^{-1}$; for P2 (WR 74), $\mu_{ra} = -3.47 \pm 0.07 \text{ mas yr}^{-1}$ and $\mu_{dec} = -3.86 \pm 0.05 \text{ mas yr}^{-1}$; for E2 (Ofpe/WN 9), $\mu_{ra} = -2.63 \pm 0.19 \text{ mas yr}^{-1}$ and $\mu_{dec} = -4.15 \pm 0.14 \text{ mas yr}^{-1}$; for E4 (WN 8), interestingly, $\mu_{ra} = -5.49 \pm 0.74 \text{ mas yr}^{-1}$ and $\mu_{dec} = -6.41 \pm 0.68 \text{ mas yr}^{-1}$, but errors are still large.

Gaia DR4 will release spectroscopic spectral types and improved parallaxes. With this information, it will be possible to assign type, motion, and distance to each individual bright massive star.

7. CS 78/NGC 6334

We observed the bright infrared star 2MASS J17213513–3532415 located at the center of the dust shell CS 78 and with a nearby pulsar. This nebula is listed among the bubbles detected by GLIMPSE (Churchwell et al. 2007), and it coincides with the $4'$ radio nebula, G351.70+0.66, detected by NVSS at 1.4 GHz (Condon et al. 1998), as shown in Fig. 11. This bubble is at the periphery of a large giant molecular complex NGC 6334 (e.g., Russeil et al. 2016).

7.1. The Nearby Pulsar B1718–35 and Distance to CS 78

The bright star is located a few arcsecs away from the B1718–35 pulsar (Minter 2008). This is an energetic young pulsar (spin down $4.5 \times 10^{34} \text{ erg s}^{-1}$, age = 176 kyr) at a distance of about 4.6 kpc (Manchester et al. 2005); the previously credited distance was 6.4 kpc (Gaensler et al. 2000). Minter (2008) detected OH absorption against the PSR B1718–35. There are only two other pulsars with such absorption. The OH radial velocity (from -1.5 to -1.9 km s^{-1}) is consistent with the radial velocity of the NGC 6334 complex (Brooks & Whiteoak 2001). OH absorption may arise in the interaction region of a molecular cloud with an SNR

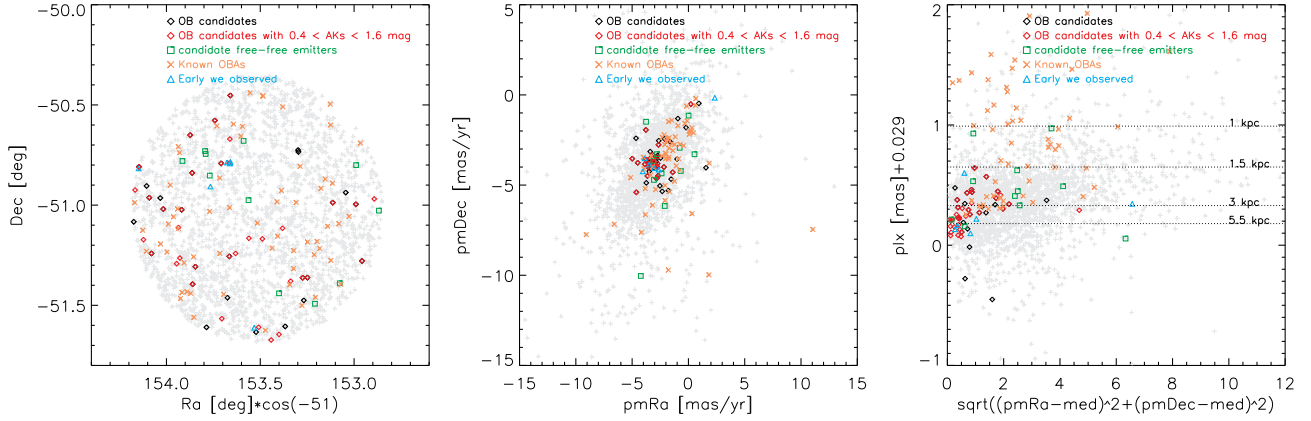


FIG. 10.— *Left panel:* Spatial distribution of stars in “The Bridge”. *Middle panel:* Proper motions. *Right panel:* ϖ values versus the distance in proper motion space from the median point of OB candidates. Distance values of 1, 1.5, 3, and 5.5 kpc are indicated with horizontal lines. In the three panels, only stars with UWE value within the limits of Luri et al. (2018) are plotted. Gray plus signs indicate 2MASS datapoints ($K_s < 10$ mag) in the Bridge. Black diamonds are the OB candidates from Table 11, and in red those with $0.4 < A_{K_s} < 1.6$ mag. Green squares mark the candidate free-free emitters from Table 10. Orange crosses indicate the previously known early-type stars from Table 8, cyan triangles the early-type stars observed in this work.

or an HII region. Minter concluded that the continuum object along the line of sight toward PSR B1718–35 was an HII region associated with the NGC 6334 complex. Indeed, for CS 78 (their G351.69+0.67), using radio continuum data Russeil et al. (2016) measured a thermal source ($\alpha = 1.2$), with a systemic $V_{\text{lsr}} = +3 \text{ km s}^{-1}$.

With H_α , radio data and OB spectrophotometric distances, Russeil et al. (2016) and Russeil et al. (2017) concluded that velocities from zero to -11 km s^{-1} belongs to the NGC 6334 complex. In H_α , they detected a foreground cloud at $+6 \text{ km s}^{-1}$ and a background at -25 km s^{-1} ($\approx 3.7 \text{ kpc}$); with CO data, larger velocities at -40 km s^{-1} – -125 km s^{-1} were also seen along the same line of sight, which correspond to distances of 4.67 and 6.97 kpc (Reid et al. 2009). Therefore, the pulsar B1718–35 is likely located in the -40 km s^{-1} cloud. Fukui et al. (2018) also published a new CO map of the NGC 6334 complex. These authors detected the main component centered at -4 km s^{-1} (NGC 6334), a secondary (shifted) component at -16 km s^{-1} , a foreground component at $+6 \text{ km s}^{-1}$ in the local gas close to the sun, and an additional component at -25 km s^{-1} more distant than NGC 6334.

7.2. The Star 2MASS J17213513–3532415

The Gaia parallax ($0.81 \pm 0.22 \text{ mas s}^{-1}$) has a fractional error still larger than 20%, and suggests a distance from 0.9 kpc to 1.5 kpc, that matches well that of the NGC 6334.

The 2MASS catalog reports high-quality measurements; furthermore, the 2MASS photometry is in excellent agreement with the DENIS photometry ($K_s = 6.73$ and 6.78 mag , $J = 10.13$ and 10.11 mag). Within the measurement errors, we can exclude variability (e.g., Messineo et al. 2004). By assuming an intrinsic $J - K = -0.02 \text{ mag}$, and adopting the extinction ratios of Messineo et al. (2005), we estimate $A_{K_s}(JH) = 1.54 \text{ mag}$ and $A_{K_s}(JK_s) = 1.81 \text{ mag}$. By assuming a distance of 1.35 kpc (see next Section), and an absolute K_s magnitude of -5.41 mag , from the dereddened flux densities, we estimate a BC_K of -0.75 mag and $M_{\text{bol}} = -6.16 \text{ mag}$, i.e., a luminosity $\log_{10} \frac{L_*}{L_\odot} = 4.36$. Dwarfs of B3–B5 types have M_{bol} from -4.0 to -2.2 mag , Ia supergiants (B3–B5) have $M_{\text{bol}} \approx -6.5 \text{ mag}$, Ib supergiants (B3–B5) have $M_{\text{bol}} \approx -5.8 \text{ mag}$, and a B3 giant has $M_{\text{bol}} \approx -4.5 \text{ mag}$ (Humphreys & McElroy 1984; Lejeune & Schaerer 2001; Koornneef 1983; Messineo et al.

2011).

We conclude, therefore, that star E1 is a B supergiant. Although, higher-resolution spectra are needed to characterize the stellar atmosphere of star E1; its SED shows an excess at mid-infrared wavelengths (Fig. 12), most likely due to a combination of free-free emission plus a dust component ($\approx 650 \text{ K}$).

There is ample ongoing discussion about the classification of B supergiants with emission lines (e.g., Humphreys et al. 2017; Smith et al. 2019; Clark et al. 2005). Spectroscopically, candidate LBVs and B[e] supergiants can appear similar. LBVs can only be classified with the help of long-term monitoring in order to verify their photometric variability and the presence of sporadic luminosity outbursts. B[e] stars are characterized by warm dust emitting longward of $1 \mu\text{m}$ (e.g., Clark et al. 1999; Humphreys et al. 2017). Known LBVs have initial masses from ≈ 30 to $\approx 100 M_\odot$, luminosities from $200,000 L_\odot$ to $5,000,000 L_\odot$, and are located on the instability strip near the Eddington limit. B[e] stars are fainter (typically from $30,000$ to $200,000 L_\odot$, 15 – $40 M_\odot$) with only narrow overlap in luminosities with the LBVs (e.g., Humphreys et al. 2017; Smith & Tombleson 2015). It is unclear if those low-luminosity stars, like 2MASS J17213513–3532415, are analogous to LBVs, or if they come from a different formation scenario (e.g., mass transfer in binary systems and stellar mergers) (e.g., Smith & Tombleson 2015).

7.3. CS 78 and Its Ionizing Source

CS 78 is likely associated with the NGC 6334 complex at about 1.35 kpc (Wu et al. 2014; Minter 2008; Russeil et al. 2016). The bright 2MASS J17213513–3532415 is located in the core of this bubble.

The morphology and high extinction of the bubble suggest that 2MASS J17213513–3532415 is the main ionizing source of the CS 78 bubble. The radio continuum flux at 1.4 GHz detected toward the nebula by NVSS is 89.8 mJy . By assuming a typical temperature of 7500 K for an optically thin thermal nebula (Martín-Hernández et al. 2003), we calculated a number of Lyman continuum photons (N_L) of $10^{45.88}$. When we consider an NVSS flux of 124 mJy (which includes two fainter NVSS sources at the edge of the nebula), we calculated $N_L = 10^{46.02}$. This number of photons is expected from a single B2–B3 supergiant (Panagia 1973), and this further con-

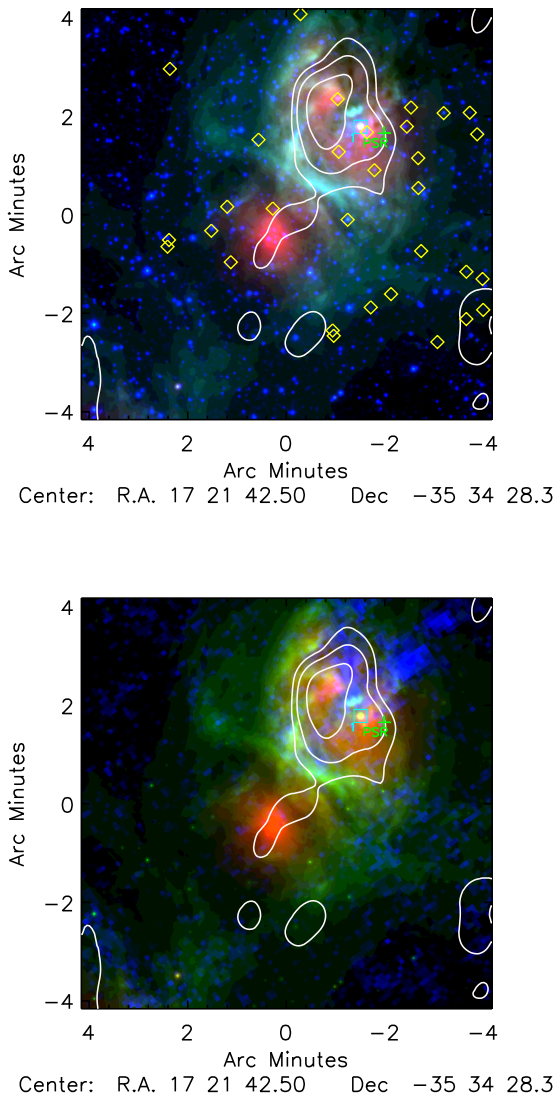


FIG. 11.— *Upper panel:* Composite image of CS 78; in blue the GLIMPSE $3.6 \mu\text{m}$ image, in green the GLIMPSE $8.0 \mu\text{m}$, in red the MIPS GAL $24.0 \mu\text{m}$. NVSS contours are overlaid in white color. The green cross marks the position of the pulsar B1718–35, the cyan square the star 2MASS J17213513–3532415. Yellow diamonds marks the GLIMPSE young stellar objects identified by Willis et al. (2013). *Upper panel:* Composite image of CS 78; in blue the ATLAS GAL image, in green the GLIMPSE $8.0 \mu\text{m}$, in red the MIPS GAL $24.0 \mu\text{m}$. NVSS contours are overlaid in white color. The green cross marks the position of the pulsar B1718–35, the cyan square the star 2MASS J17213513–3532415.

firms the luminosity class; for example, a B3 III star would only emit $10^{44.3}$. 2MASS J17213513–3532415, therefore, is the ionizing star of bubble CS 78.

The bubble is flagged as an incomplete ring (Churchwell et al. 2007), and is shown in Fig. 11. The $8 \mu\text{m}$ emission is due to PAH emission located at the edge of the photodissociation region (NVSS radio continuum source), which is filled with $24 \mu\text{m}$ emission (emission by heated dust). The entire NGC 6334 complex has been analyzed with GLIMPSE data to locate young stellar objects by Willis et al. (2013). A few are located in the direction of CS 78, indicating that star formation is still ongoing in the shell.

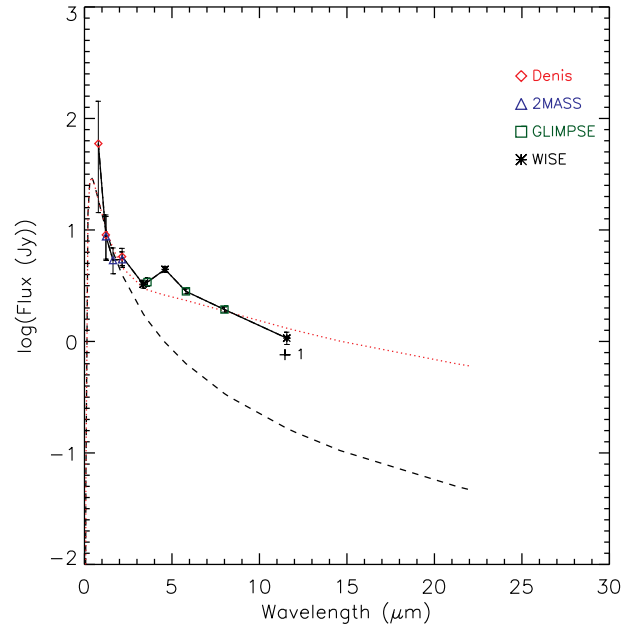


FIG. 12.— Stellar energy distribution (SED) of star E1. The long-dashed curve marks a blackbody curve, F_ν , of 21,500 K. The red dotted line is a modified blackbody curve, where a second blackbody of 650 K and a free-free emission has been added. Magnitudes from DENIS are marked with diamonds, from 2MASS with triangles, from GLIMPSE with squares, from MSX with crosses, and from WISE with asterisks.

8. CONCLUSIVE CONSIDERATIONS

We searched for massive OB stars in 1 of the 14 most prominent HII region complexes of the Milky Way detected with data from the Planck satellite (Rahman & Murray 2010). Of these, the G332.809–0.132 complex is relatively nearby (about 3 kpc away), and particularly rich in high-energy sources. Three SNRs and one TeV emitter, HESS J1616–508, are found along its line of sight. This associated molecular cloud complex comprises the Nor OB4/RCW 103 association. We focused our analysis on the central 80 pc of Nor OB4, which encloses the three SNRs. This is a rare coincidence; indeed, no SNRs among those listed in Green (2014) are associated with the giant HII regions of Conti & Crowther (2004). Forty-nine SNRs (17%) have their centroids projected on one of the 14 WMAP sources (Table 1 of Rahman & Murray 2010) (from 0 to 10 SNRs). Only 11 SNRs (4%) are projected on one of the corresponding 40 SF complexes identified at mid-infrared in Table 2 of Rahman & Murray (2010) (from zero to three SNRs). G332.809–0.132 is the only complex in Table 2 of Rahman with 3 SNRs.

Those three SNRs are found in the area covered by Nor OB4, providing evidence for a rich population of evolved massive stars and transitional objects toward this direction. In the molecular cloud GMC G23.3-0.3 (80 pc in size), which hosts four SNRs, Messineo et al. (2014) detected one rare candidate LBV in apparent isolation along with other evolved massive stars. Stellar clusters may have dissolved already, or the most massive stars may have been ejected, or have even been born in isolation. As noticed by Smith & Tomblason (2015), with a few exceptions (e.g. Eta Car is in the Tr16 cluster) LBVs are mostly found in isolation: AG Car, HR Car, Hen 3-519, HD160529, MWC 930 are located more than 20 pc away from an O-type star. It is clear that to find those spectacular stars we must look for bright stars in extended HII

regions.

Its richness in SNRs and the shaped mid-infrared emission of G332.809–0.132 are suggestive of feedback from massive stars. In its core, we found more than 200 early-type stars, about 110 early-type stars brighter than $K_s = 10$ mag (O9) and with $J-K_s$ color from 0.7 mag to 3.0 mag. By assuming supergiants, this number alone could account for 50% of the number of Lyman continuum photons measured towards G332.809–0.132. Therefore, we confirm that this region is rich in massive stars and transitional objects. Indeed, two WR stars were already known in the direction of this complex, WR74 (WN 7) and [SMG2009] 1059–34 (WC 8). Among the free-free candidates, IRAS 16115–5044 is reclassified as a candidate LBV. By targeting bright stars with colors typical of free-free emitters, we have added spectroscopic detections of another WR, a WN 8 star, and a rare transitional star, an Ofpe/WN 9. Those three WR stars have spectrophotometric properties consistent with those of supergiants at a distance

of about 3.4 kpc – $M_{bol} = -6.57$ (WC 8), -8.16 (WN 7), -9.16 (WN 8). For the Ofpe/WN 9 star, $M_{bol} = -10.45$ mag. Ofpe/WN 9 stars are transitional objects, perhaps dormant LBVs (Martins et al. 2007). For 3.4 kpc IRAS 16115–5044 has $M_{bol} = -8.8$ mag.

The spatial distribution of classical LBVs is expected to be statistically similar to that of WR stars (Aadland et al. 2018). Within the Nor OB4 association, we measured a typical separation of 3–5 pc between candidate free-free emitters and the closest OB candidates.

Another rare transitional object is reported here as the central ionizing star of CS 78. For an assumed distance of 1.35 kpc, 2MASS J17213513–3532415 has $M_{bol} \approx -6.16$ mag; with this faint magnitude it is likely to be a B[e] star, and not an LBV. Since, their formation, final fate, and relation to the high-mass LBVs are highly uncertain (Smith et al. 2019), it is of primary importance to increase the number of these peculiar B supergiants.

APPENDIX

A. PHOTOMETRIC DATA

We provide collected photometric information on the spectroscopically detected stars in the direction of G332.809–0.132 and CS 78 in Table A1.

B. SPECTRA OF LATE-TYPE STARS

We provide plots of the late-type stars spectroscopically detected in the direction of G332.809–0.132 and CS 78 in Figs. B1 and B2.

C. IDENTIFICATION CHARTS

In Figure C1 the VVV charts of the spectroscopically detected stars in the direction of G332.809–0.132 and CS 78 are illustrated.

D. SNRS AND STELLAR CLUSTERS

One of the first reports in the literature about the association of a stellar cluster and an SNR was written by Pauls (1977). SNR G127.1+00.5 coincides in position with the open cluster NGC 559 (note that the SNR was previously called G127.3+0.7 Pauls 1977). For the SNR a distance of $1.15_{+1.15}^{-0.25}$ kpc has been reported (Acero et al. 2016), while the cluster is at a distance of 2.2 kpc (Kharchenko et al. 2016) and has an age of 630 Myr. The SNR’s diameter is 45’. The cluster centroid is located within the remnant at 50% of the SNR’s radius (11’).

One year after the report of the serendipitous discovery by Pauls (1977), a review of clusters projected onto SNRs was published by Kumar (1978), who searched a list of 117 SNRs for positional coincidences with clusters and located two new coincidences. One was considered spurious based on distance measures, while the association of the SNR G291.0-0.1 with the cluster Trumpler 18 was considered to be real. However, nowadays, newer determinations place the cluster at 1.4 kpc (Kharchenko et al. 2016) and the SNR at 5 kpc (Acero et al. 2016).

Currently, a comprehensive Catalogue of Galactic Supernova Remnants is maintained by Dr. D. Green with the latest update in 2019⁹, while Acero et al. (2016, and references therein) list distances for 112 SNRs.

Kharchenko et al. (2016) provide a list of 3210 stellar clusters, which they detected with “a combination of uniform kinematic and near-infrared (NIR) photometric data gathered from the all-sky catalog PPMXL”. Parameters like distance and ages are uniformly determined. We cross-matched the positions of SNRs from Green (2019) with the positions of clusters by Kharchenko et al. (2016). We found a total of 90 cluster centroids located in projection within 48 SNRs. Independently estimated distance is required to confirm the physical association between the cluster and the SNR. By shifting the coordinates in the longitudinal direction and repeating the matching procedures, we estimated that more than 80% of the matches are random, and not physically meaningful. We limited checking relative to SNRs with a radius smaller than 25’ the 28 matches. These 28 clusters have estimates of distance (Kharchenko et al. 2016), but distance is known only for 13 SNRs (Acero et al. 2016). *Three matches appear real; BDSB-141 (10 Myr) is very likely associated with SNR G049.2-00.7, NGC 559 (630 Myr) with SNR G127.1+00.5 (see also Pauls 1977), and FSR-0891 (230 Myr) with SNR G189.1+03.0.*

Bica et al. (2019) collected Galactic candidate clusters from the literature to generate a catalog of 10,978 star clusters (from Digital Sky Survey and incremented with the 2MASS, WISE, VVV, Spitzer and Herschel surveys). We considered objects with diameters smaller than 1°, and found 37 possible matches with SNRs – i.e., with SNR centroids enclosed within the

⁹ <http://www.mrao.cam.ac.uk/surveys/snrs/>

TABLE A
I. INFRARED COUNTERPARTS OF THE SPECTROSCOPICALLY OBSERVED TARGETS.

ID	2MASS			DENIS			GLIMPSE				MSX				WISE				NOMAD			GAIA-DR2							
	2MASS-ID	<i>J</i>	<i>H</i>	<i>K_s</i>	<i>I</i>	<i>J</i>	<i>K_s</i>	[3.6]	[4.5]	[5.8]	[8.0]	<i>A</i>	<i>D</i>	<i>C</i>	<i>D</i>	<i>W1</i>	<i>W2</i>	<i>W3</i>	<i>W4</i>	<i>B</i>	<i>V</i>	<i>R</i>	<i>G</i>	VR	plx	pmRa	pmDec		
	(mag)	(mag)	(mag)	(mag)	(mag)	(mag)	(mag)	(mag)	(mag)	(mag)	(mag)	(mag)	(mag)	(mag)	(mag)	(mag)	(mag)	(mag)	(mag)	(mag)	(mag)	(mag)	(mag)	(mag)	(km s ⁻¹)	(mas)	(mas/yr)	(mas/yr)	
E1	17213513-3532415	10.13	8.30	6.78	14.68	10.11	6.73	5.48	..	4.48	4.29	5.62	4.43	4.05	17.61	6.11	..	0.81±0.22	-0.38±0.36	-2.77±0.24		
E2	16174291-5054251	7.64	6.63	6.05	10.84	7.17	5.96	5.84	6.74	5.23	5.07	5.03	5.72	5.25	5.12	3.92	12.37	..	0.57±0.14	-2.63±0.19	-4.15±0.14		
E3	16174204-5056372	7.78	6.68	6.08	11.40	7.43	5.62	6.70	6.04	5.43	5.37	5.22	5.58	5.17	5.43	4.99	17.02	13.69	12.85	..	0.88±0.19	-2.23±0.25	-5.31±0.20
E4	16201606-5058076	8.43	7.78	7.43	10.69	8.58	7.47	7.11	6.87	6.68	6.56	6.94	6.73	5.34	0.39	13.70	13.24	12.60	12.08	..	1.32±0.56	-5.49±0.74	-6.41±0.68		
E5	16170220-5047031	11.97	10.65	9.73	15.64	1.40	0.30	0.05	-2.51	17.21	17.77	..	0.19±0.18	-4.06±0.33	-4.24±0.20	
E6	16200902-5048588	10.43	10.23	10.10	11.23	10.53	10.06	9.99	9.94	9.84	9.44	12.90	11.98	11.40	12.06	..	0.31±0.04	2.34±0.06	-0.16±0.04		
E7	16170923-5047147	13.26	11.47	10.15	15.82	13.24	10.15	8.79	8.22	7.69	7.08	8.73	7.91	5.77	..	17.43	16.91	16.42	18.40	..	0.10±0.23	-3.03±0.39	-4.06±0.27		
E8	16170300-5047308	11.54	10.68	10.29	14.46	11.59	10.34	9.97	9.92	9.80	16.88	16.03	16.00	..	0.07±0.10	-3.89±0.17	-3.52±0.11
L1	16172975-5055396	5.58	4.47	3.87	9.00	5.74	3.66	3.65	3.45	3.52	3.51	3.36	..	3.69	3.29	3.47	2.61	13.91	13.50	11.86	10.18	..	1.73±0.20	-0.41±0.34	-3.58±0.21		
L2	16202085-5053372	9.31	6.04	4.41	..	9.20	3.86	3.31	2.61	..	1.53	-0.10	-0.32	-0.86	3.12	2.01	..	-1.26	19.04	..	0.74±0.52	-0.54±0.77	-3.26±0.53	
L3	16165866-5104016	8.44	6.10	4.95	4.27	4.51	3.96	4.01	3.60	2.41	2.11	..	4.39	3.74	2.92	1.74	16.78	..	-0.42±0.44	-3.71±1.13	-1.84±0.85	
L4	16181449-5056134	8.04	6.06	5.09	14.86	8.05	4.18	4.42	3.72	..	3.48	2.61	2.32	..	4.82	3.33	2.89	1.98	15.94	..	0.11±0.27	-3.53±0.48	-3.88±0.29	
L5	16182588-5102055	8.38	6.27	5.16	15.48	8.45	4.41	4.40	4.70	4.00	4.05	3.54	2.29	2.12	1.60	4.63	3.88	2.99	1.77	16.19	..	0.37±0.27	-3.53±0.44	-2.79±0.29		
L6	16173092-5058351	6.46	5.61	5.32	8.89	6.06	4.41	5.22	6.67	5.17	5.14	5.07	5.27	5.05	5.11	4.02	12.28	10.08	9.40	9.21	-24.24±0.37	0.61±0.04	-0.77±0.07	-1.70±0.05		
L7	16170875-5102172	6.55	5.77	5.43	8.73	6.14	4.88	5.22	..	5.23	5.23	5.13	5.57	5.38	5.36	..	12.14	10.33	9.45	9.31	-42.46±0.27	0.56±0.04	-1.21±0.07	-2.51±0.04		
L8	16165202-5105335	8.46	6.51	5.58	5.63	5.85	4.70	4.45	4.20	3.51	3.47	..	5.42	4.49	3.95	3.08	15.33	..	0.19±0.27	-2.80±0.49	-1.75±0.28	
L9	16171876-5101364	8.75	6.74	5.61	..	8.74	5.04	4.43	4.15	3.67	2.65	2.46	..	5.03	3.91	3.00	1.89	16.48	..	0.10±0.32	-3.68±0.61	-3.88±0.31		
L10	16165827-5050474	6.98	6.00	5.61	6.12	5.40	5.40	5.31	5.59	5.47	5.50	5.31	13.11	12.27	10.05	10.32	-19.60±0.56	0.54±0.08	1.24±0.13	-2.43±0.08		
L11	16171805-5057292	9.55	7.05	5.90	16.83	9.43	5.41	6.97	..	4.79	4.59	4.62	5.28	4.81	4.66	3.98	17.47±0.25	-4.32±0.49	-4.57±0.28	
L12	16164958-5051172	8.51	6.73	5.93	5.34	6.08	5.36	5.34	4.95	5.32	5.41	5.35	5.03	15.43	14.57	..	0.34±0.14	-2.89±0.29	-3.62±0.16	
L13	16170473-5059417	7.49	6.38	6.00	9.82	7.64	5.54	6.07	6.13	5.80	5.74	5.63	5.87	5.91	5.68	5.14	11.28	-7.18±0.25	0.67±0.14	-2.67±0.20	-4.80±0.15		
L14	16161669-5114598	8.31	6.81	6.11	5.88	6.35	5.59	5.58	5.49	5.86	5.72	5.07	3.38	13.83	..	-0.46±0.18	-3.77±0.26	-3.97±0.17		
L15	16190855-5045090	9.12	7.11	6.11	16.38	9.09	5.95	6.10	5.91	5.12	4.97	4.79	5.65	5.21	4.46	3.30	16.90	..	0.85±0.29	0.58±0.44	-1.45±0.30		
L16	16222857-5049280	9.42	7.36	6.24	6.45	9.36	6.24	5.57	6.09	5.18	5.06	4.92	5.72	5.28	4.67	2.64	17.02	..	-1.46±0.39	-4.48±0.52	-3.93±0.33		
L17	16172446-5103320	7.74	6.67	6.33	9.78	7.58	6.26	6.42	..	6.15	6.12	6.23	6.12	6.26	6.21	..	13.78	12.78	11.22	11.16	-43.41±0.23	0.54±0.09	-2.27±0.15	-1.57±0.10		
L18	16193796-5057298	10.46	7.75	6.36	16.54	10.35	6.16	5.48	5.92	4.95	4.88	5.64	4.96	4.29	1.80	17.76	..	15.63	19.60	..	-0.56±0.63	-2.64±1.33	-3.75±0.93		
L19	16191621-5102176	10.26	7.64	6.38	..	10.28	6.34	5.30	6.63	4.89	4.77	5.35	5.65	5.24	4.17	2.42	19.05	..	-0.53±0.46	-6.00±0.82	-4.79±0.51	
L20	16215861-5105148	10.04	7.66	6.39	..	10.15	6.46	6.66	5.54	5.16	4.94	5.03	6.06	5.35	4.51	3.43	19.31	..	0.22±0.68	0.04±1.14	-4.75±0.79	
L21	16173873-5059383	9.97	7.63	6.50	17.60	9.95	6.43	6.03	5.86	5.46	5.33	5.12	5.78	5.58	4.75	3.36	18.10	..	0.03±0.31	-3.66±0.56	-5.63±0.34		
L22	16184330-5056401	9.40	7.44	6.50	15.45	9.35	6.42	6.69	6.00	5.64	5.48	4.98	5.92	5.75	4.71	3.64	16.30	..	0.19±0.25	-4.63±0.38	-4.82±0.24		
L23	16181315-5102106	9.09	7.57	6.72	13.24	8.90	6.59	6.71	5.85	5.59	5.33	4.97	6.15	5.77	4.73	3.61	16.44	..	-0.38±0.26	-2.99±0.41	-4.11±0.27		
L24	16215678-5101145	9.19	7.51	6.78	14.02	9.13	6.73	6.83	6.60	6.29	6.22	6.34	6.46	6.33	3.64	15.33	..	-0.12±0.23	-2.49±0.30	-2.99±0.22	
L25	16170351-5055026	9.25	7.55	6.88	13.41	9.22	6.96	6.83	6.72	6.41	6.37	6.52	6.60	6.49	6.39	17.80	..	15.63	14.96	..	0.29±0.17	-4.86±0.28	-4.34±0.18		
L26	16222509-5048358	10.27	8.04	6.95	..	10.19	6.94	6.63	6.17	5.78	5.59	5.46	6.28	5.99	5.07	3.66	18.36	..	-0.89±0.36	-4.97±0.52	-5.02±0.34		
L27	16180145-5055588	9.42	7.69	6.97	13.87	9.33	6.98	6.68	6.70	6.38	6.36	6.64	6.64	6.04	4.06	18.28	15.26	..	0.10±0.19	-1.29±0.27	-2.46±0.20	
L28	16173617-5055236	9.40	7.71	7.03	13.55	9.27	7.01	6.87	6.79	6.52	6.48	6.68	6.74	6.78	17.26	15.06	..	0.13±0.16	-3.34±0.24	-1.99±0.17	
L29	16161970-5114017	9.56	7.84	7.07	6.73	6.64	6.39	6.43	5.53	6.58	6.57	5.92	3.86	15.65	..	-0.00±0.20	-3.67±0.28	-2.59±0.19	
L30	16174539-5058020	9.43	7.82	7.11	13.69	9.37	7.14	6.82	6.95	6.61	6.68	6.73	6.82	4.97	3.03	15.06	..	0.17±0.17	-4.58±0.24	-4.06±0.17		
L31	16173534-5057091	8.15	7.39	7.14	9.75	8.14	7.08	7.00	7.09	6.99	6.91	6.33	6.91	7.03	6.53	4.77	12.69	11.72	10.73	10.77	-57.69±0.74	0.57±0.09	-0.75±0.14	-3.88±0.11		
L32	16170651-5100058	10.67	8.25	7.14	17.83	10.57	7.12	6.88	6.47	6.17	6.13	6.43	6.41	6.28	5.57	18.46	..	-0.34±0.35	-4.89±0.62	-4.58±0.41	
L33	16192478-5108209	9.75	8.00	7.18	14.74	9.72	7.17	6.82	6.86	6.59	6.57	6.77	6.81	6.44	4.10	20.90	16.06	..	0.15±0.18	-3.56±0.28	-1.87±0.20		
L34	16164196-5106055	9.94	8.05	7.20	6.78	6.79	6.56	6.57	6.56	6.63	7.03	19.67	16.45	..	-0.02±0.22	-3.42±0.46	-2.87±0.23		
L35	16202293-5053290	12.17	8.83	7.20	..	11.97	7.12	6.70	..	5.63	5.74	6.15	6.01	5.71
L36	16165014-5112236	10.08	8.15	7.28	7.14	6.92	6.62	6.52	6.91	6.89	6.73	5.13	20.47	..	19.81	16.96	..	-0.32±0				

TABLE A
1. CONTINUATION OF TABLE A1.

ID	2MASS			DENIS			GLIMPSE				MSX				WISE				NOMAD			GAIA-DR2						
	2MASS-ID	<i>J</i>	<i>H</i>	<i>K_s</i>	<i>I</i>	<i>J</i>	<i>K_s</i>	[3.6]	[4.5]	[5.8]	[8.0]	<i>A</i>	<i>D</i>	<i>C</i>	<i>D</i>	<i>W1</i>	<i>W2</i>	<i>W3</i>	<i>W4</i>	<i>B</i>	<i>V</i>	<i>R</i>	<i>G</i>	VR	plx	pmRa	pmDec	
	(mag)	(mag)	(mag)	(mag)	(mag)	(mag)	(mag)	(mag)	(mag)	(mag)	(mag)	(mag)	(mag)	(mag)	(mag)	(mag)	(mag)	(mag)	(mag)	(mag)	(mag)	(mag)	(mag)	(km s ⁻¹)	(mas)	(mas/yr)	(mas/yr)	
L40	16192903-5042257	10.41	8.39	7.43	16.70	10.35	7.39	6.83	7.02	6.64	6.64	6.92	6.93	7.46	4.29	17.50	..	0.13± 0.27	-3.86± 0.42	-3.82± 0.29	
L41	16165636-5054263	10.91	8.59	7.46	6.89	6.83	6.54	6.47	6.30	6.79	6.79	6.24	4.54	18.80	..	0.26± 0.36	-2.29± 0.69	-2.32± 0.45	
L42	16215688-5103560	9.70	8.17	7.57	13.43	9.67	7.57	7.17	7.39	7.15	7.11	6.98	7.21	16.40	4.97	..	-0.08± 0.17	-3.98± 0.23	-7.05± 0.16	
L43	16180517-5054355	10.24	8.43	7.63	15.22	10.27	7.59	7.11	7.29	6.99	6.96	7.05	7.13	6.62	5.24	16.52	..	0.15± 0.21	-5.50± 0.34	-4.52± 0.22	
L44	16172904-5100234	10.42	8.50	7.63	15.89	10.34	7.56	7.08	7.14	6.92	6.94	7.05	7.09	6.77	5.24	17.57	20.63	17.06	..	0.17± 0.28	-2.89± 0.47	-3.75± 0.26
L45	16164039-5107327	8.35	7.80	7.68	7.64	7.72	7.66	7.54	7.55	7.66	7.31	6.63	11.32	10.41	9.84	10.08	-33.47± 0.43	1.10± 0.07	-0.54± 0.09	-4.54± 0.06	
L46	16172605-5102560	10.13	8.47	7.71	14.80	10.09	7.63	7.24	7.42	7.14	7.14	7.23	7.36	7.07	..	17.24	17.06	21.00	16.13	..	-0.20± 0.18	-2.27± 0.33	-3.60± 0.20	
L47	16164417-5104082	9.98	8.45	7.74	7.31	7.52	7.16	7.20	7.35	7.49	7.33	5.47	20.79	..	17.82	15.65	..	-0.08± 0.18	-1.01± 0.34	-1.01± 0.19	
L48	16202739-5054420	11.66	9.12	7.94	..	11.43	7.78	7.03	6.94	6.58	6.57	6.99	6.70	5.14	0.58	9.98	..	1.83± 2.32	-1.87± 2.13	-0.43± 2.11	
L49	16184348-5056111	10.43	8.72	7.95	14.84	10.33	7.91	7.49	7.61	7.36	7.30	7.46	7.48	6.45	5.10	16.98	16.24	17.24	16.25± 0.15	-4.51± 0.23	-2.38± 0.16	
L50	16181035-5101573	10.71	8.88	8.10	14.62	10.73	8.03	7.46	7.61	7.37	7.33	7.50	7.50	7.35	5.04	17.27	..	0.37± 0.24	-4.53± 0.41	-3.98± 0.28	
L51	16175105-5053143	11.43	9.20	8.32	17.24	11.34	8.33	7.69	7.78	7.55	7.47	7.78	7.78	7.09	18.37	..	-0.13± 0.32	-4.92± 0.47	-3.23± 0.36	
L52	16193774-5058136	12.45	9.73	8.40	..	12.42	8.35	7.45	7.37	6.96	6.95	7.47	7.10	5.41	2.50
L53	16175823-5100594	12.99	10.19	8.96	..	12.86	8.84	8.02	8.08	7.79	7.77	8.11	8.04	7.65	4.88
L54	16164846-5108393	11.43	9.68	9.01	8.49	8.66	8.46	8.41	8.54	8.57	7.80	5.69	21.00	7.36	..	-0.96± 0.35	-4.54± 0.43	-4.14± 0.30	
L55	16174477-5057451	12.27	10.20	9.35	..	12.28	9.26	8.62	8.81	8.53	8.60	8.77	8.80	7.05	4.86	9.02	..	0.31± 0.67	-10.13± 1.04	-0.60± 0.73	
L56	16201621-5058522	12.41	10.36	9.49	18.28	12.47	9.45	8.86	8.93	8.66	8.69	8.97	8.98	5.49	1.15	19.23	..	0.26± 0.45	-4.65± 0.80	-6.00± 0.55	
L57	16174628-5058235	13.54	10.85	9.68	..	13.45	9.60	8.74	8.80	8.49	8.59	8.77	8.65	6.35	4.23
L58 ^a	16170180-5047303	10.79	10.19	9.93	9.82	9.81	9.86	9.15	8.78	15.12	14.01	12.97	13.41	-41.33± 1.29	0.44± 0.02	-4.98± 0.04	-5.50± 0.03	
L59	16171437-5047188	15.90	11.77	9.99	9.99	8.81	8.73	8.32	8.40	8.88	8.47	..	2.38
L60	16200749-5047123	14.15	11.35	10.05	..	14.04	9.94	9.07	9.10	8.73	8.78	9.09	8.91	5.59	2.04
L61	16185783-5051538	12.99	10.95	10.09	..	12.89	10.03	9.45	9.48	9.17	9.21	9.48	9.43	6.47	3.67	9.85	..	0.97± 0.70	-5.00± 1.39	-3.56± 1.00	
L62	16200945-5049256	11.33	10.44	10.11	13.66	11.37	10.01	9.82	9.79	9.69	9.66	9.87	9.86	7.39	..	18.45	14.94	15.07	15.08	..	0.21± 0.08	-2.95± 0.12	-4.34± 0.08	
L63	16202826-5054493	11.71	10.57	10.16	14.19	11.70	10.06	9.91	9.97	9.86	10.13	16.63	16.62	15.40	15.75	..	0.18± 0.17	-2.17± 0.25	-2.57± 0.17	
L64	16173473-5055106	11.89	10.70	10.26	14.87	11.88	10.11	9.92	9.91	9.79	9.69	9.95	9.93	8.91	..	19.28	..	16.33	16.51	..	0.30± 0.11	-4.52± 0.20	-3.35± 0.12	
L65	16202094-5054467	14.35	11.57	10.29	..	14.19	10.22	9.41	9.45	9.12	9.27	9.15	9.14
L66 ^a	16201866-5055114	14.52	..	10.50
L67	16161247-5116217	14.27	11.64	10.51	9.65	9.60	9.27	9.53	9.22	5.13	1.97
L68	16202305-5052328	14.40	11.81	10.55	..	14.37	10.47	9.62	9.62	9.25	9.83	9.71
L69	16202632-5055100	15.48	12.30	10.77	..	15.47	10.69	9.70	9.64	9.31	9.21
L70 ^a	16171360-5048119	17.79	13.03	10.81	10.66	9.01	8.88	8.35	8.44	9.51	9.02	7.82	2.03
L71 ^a	16202470-5054044	16.14	12.76	10.94	10.77	9.65	9.63	9.27	9.60	9.54	9.24	5.56	1.89
L72	16170784-5046454	12.36	11.37	10.98	14.65	12.24	10.96	20.05	17.17	15.98	16.12	..	0.13± 0.08	-0.56± 0.12	-1.09± 0.08
L73 ^a	16202772-5054564	15.86	13.09	11.26	16.20	13.02	10.66	9.77	9.79	9.50	9.73
L74	16170437-5047164	13.26	12.45	11.78	14.54	13.38	11.86	10.95	10.90	10.57	17.35	16.14	15.32	15.77	..	3.20± 0.05	10.55± 0.09	-35.08± 0.06	
L75 ^a	16170610-5047314	17.06	13.57	11.84	11.69	10.52	10.29	10.06
L76 ^a	16200887-5048510	18.15	14.31	12.19	11.95	10.40	10.15	9.86	10.06
P1	16143723-5126263	15.05	12.79	11.54	10.49	10.04	9.84	9.53	10.59	10.04	8.86	5.84
P2	16161381-5136417	9.73	9.22	8.80	8.27	8.00	7.78	7.44	8.21	7.83	7.71	4.93	13.78	12.97	11.35	12.60	..	0.14± 0.05	-3.47± 0.07	-3.86± 0.05	
P3	16125464-5044510	7.08	6.17	5.79	6.83	6.22	5.64	5.57	5.05	5.68	5.51	4.73	13.55	11.33	10.67	10.30	-39.82± 0.36	0.33± 0.06	-1.02± 0.08	-1.45± 0.06	
P4	16151992-5026463	5.44	4.00	3.48	2.76	2.05	1.97	1.36	..	3.05	2.51	1.42	16.34	13.37	11.77	10.16	-49.68± 0.43	0.90± 0.12	-0.93± 0.18	-4.06± 0.12	
P5	16164067-5014370	5.53	4.47	3.97	3.99	3.58	3.31	3.54	3.55	3.27	..	3.85	3.58	3.47	2.62	13.63	12.78	11.23	9.66	..	1.36± 0.12	1.02± 0.17	0.98± 0.12	
P6	16191454-5024243	6.60	4.07	2.83	4.39	..	0.05± 0.29	-5.56± 0.43	-4.01± 0.28	
P7	16191948-5131264	5.57	4.20	3.84	4.13	3.65	..	2.99	2.21	2.37	1.65	3.62	3.52	2.56	1.63	13.89	12.13	10.10	9.67	-59.33± 0.58	1.01± 0.10	-2.82± 0.17	-4.40± 0.16	
P8	16202307-5104580	6.02	5.10	4.71	4.69	..	4.51	4.46	4.06	..	3.33	..	4.48	4.42	4.44	3.52	12.67	11.09	9.57	9.23	-42.74± 0.45	0.43± 0.04	-1.29± 0.07	-1.98± 0.04	

Messineo et al.

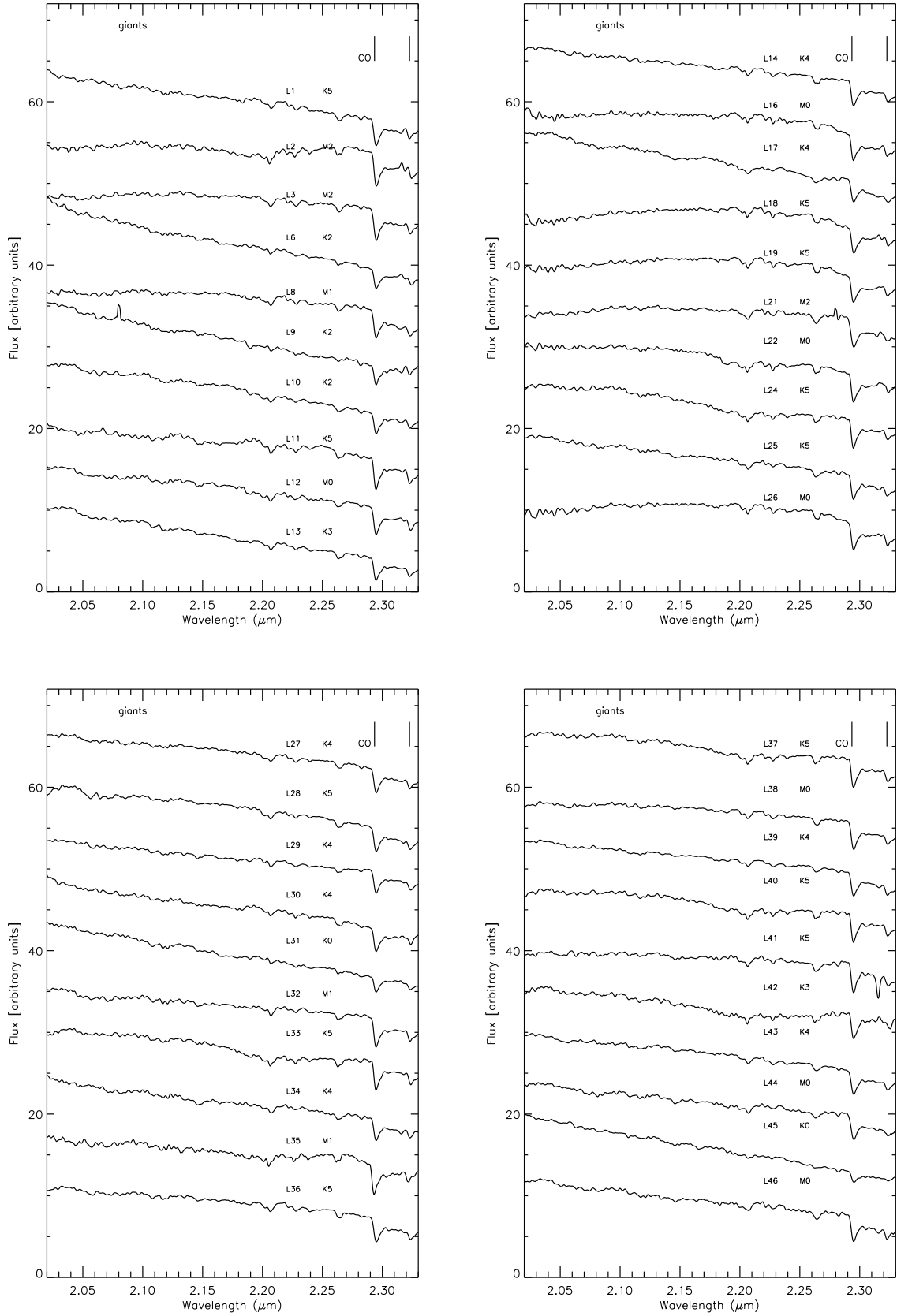


FIG. B.— 1. Dereddened *K*-band spectra (high-resolution mode) of giant stars in the direction of G332.809–0.132. AGB stars are shown in the last panel.

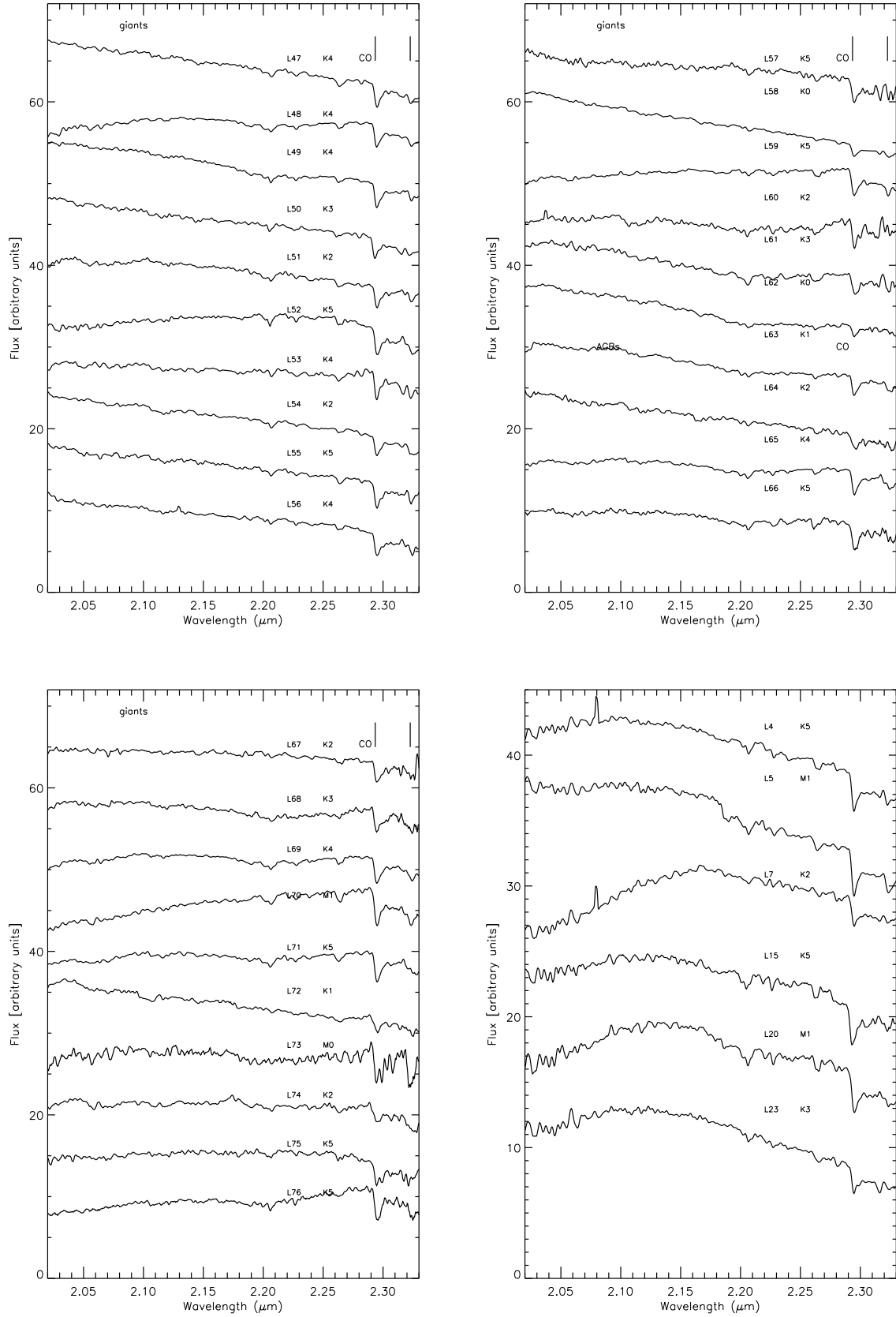


FIG. B.— 1. Continuation of Fig. B.1.

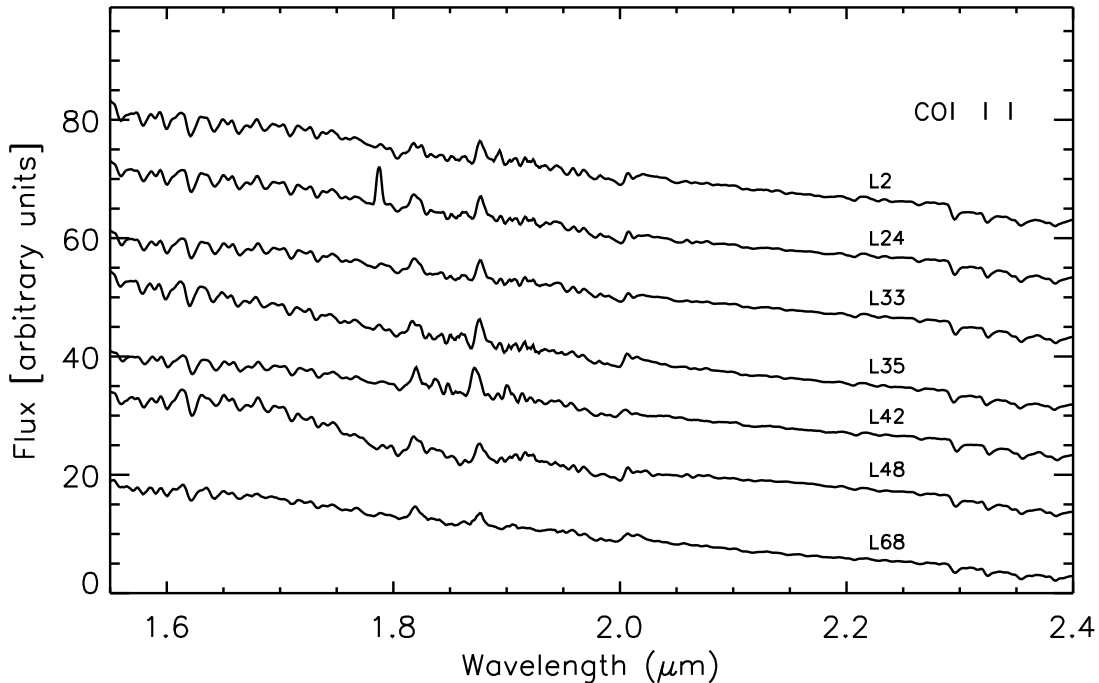


FIG. B.— 2. Dereddened *HK* spectra of stars also observed in the low-resolution mode.

cluster area. When shifting their coordinates in longitudes, we found from 25 to 42 false matches. By assuming a mean of 32, we deduce that 86% of the matches are by chance. Without distance (those are candidate clusters), one would first look for the positional coincidences. There are four entries with excellent matches (separations of SNR centroids and cluster centroids within 10% of the cluster radius); NGC 6834, NGC 3766, ASCC 64, and NGC 5281. Note that these four entries are also included in the Kharchenko’s catalog. All but NGC 6834 are random superpositions. NGC 6834 is located at a likely distance of 3.1 kpc (Mathew et al. 2014), but an estimate of the distance to SNR G065.7+01.2 is not available (Acero et al. 2016).

This publication makes use of data products from the Two Micron All Sky Survey, which is a joint project of the University of Massachusetts and the Infrared Processing and Analysis Center/California Institute of Technology, funded by the National Aeronautics and Space Administration and the National Science Foundation. This work is based [in part] on observations made with the Spitzer Space Telescope, which is operated by the Jet Propulsion Laboratory, California Institute of Technology under a contract with NASA. The DENIS project was supported, in France by the Institut National des Sciences de l’Univers, the Education Ministry and the Centre National de la Recherche Scientifique, in Germany by the State of Baden-Wuerttemberg, in Spain by the DGICYT, in Italy by the Consiglio Nazionale delle Ricerche, in Austria by the Fonds zur Foerderung der wissenschaftlichen Forschung and the Bundesministerium fuer Wissenschaft und Forschung. This research made use of data products from the Midcourse Space Experiment, the processing of which was funded by the Ballistic Missile Defence Organization with additional support from the NASA office of Space Science. This work makes use of the Naval Observatory Merged Astrometric Dataset (NOMAD). This work has made use of data from the European Space Agency (ESA) mission *Gaia* (<http://www.cosmos.esa.int/gaia>), processed by the *Gaia* Data Processing and Analysis Consortium (DPAC, <http://www.cosmos.esa.int/web/gaia/dpac/consortium>). Funding for the DPAC has been provided by national institutions, in particular the institutions participating in the *Gaia* Multilateral Agreement. This publication makes use of data products from WISE, which is a joint project of the University of California, Los Angeles, and the Jet Propulsion Laboratory/California Institute of Technology, funded by the National Aeronautics and Space Administration. This research has made use of the SIMBAD data base, operated at CDS, Strasbourg, France. This work was partially supported by the ESA fellowship, the ERC grant ERC Advanced Investigator Grant GLOSTAR (247078), the Fundamental Research Funds for the Central Universities in China, and USTC grant KY2030000054. MM thanks Maria Massi for useful discussions on free-free emitters, and Mike Rich for discussions on explosive environments.

REFERENCES

- Aadland, E., Massey, P., Neugent, K. F., & Drout, M. R. 2018, *AJ*, 156, 294
 Abeysekara, A. U., Archer, A., Aune, T., et al. 2018, *ApJ*, 861, 134
 Acero, F., Ackermann, M., Ajello, M., et al. 2016, *ApJS*, 224, 8

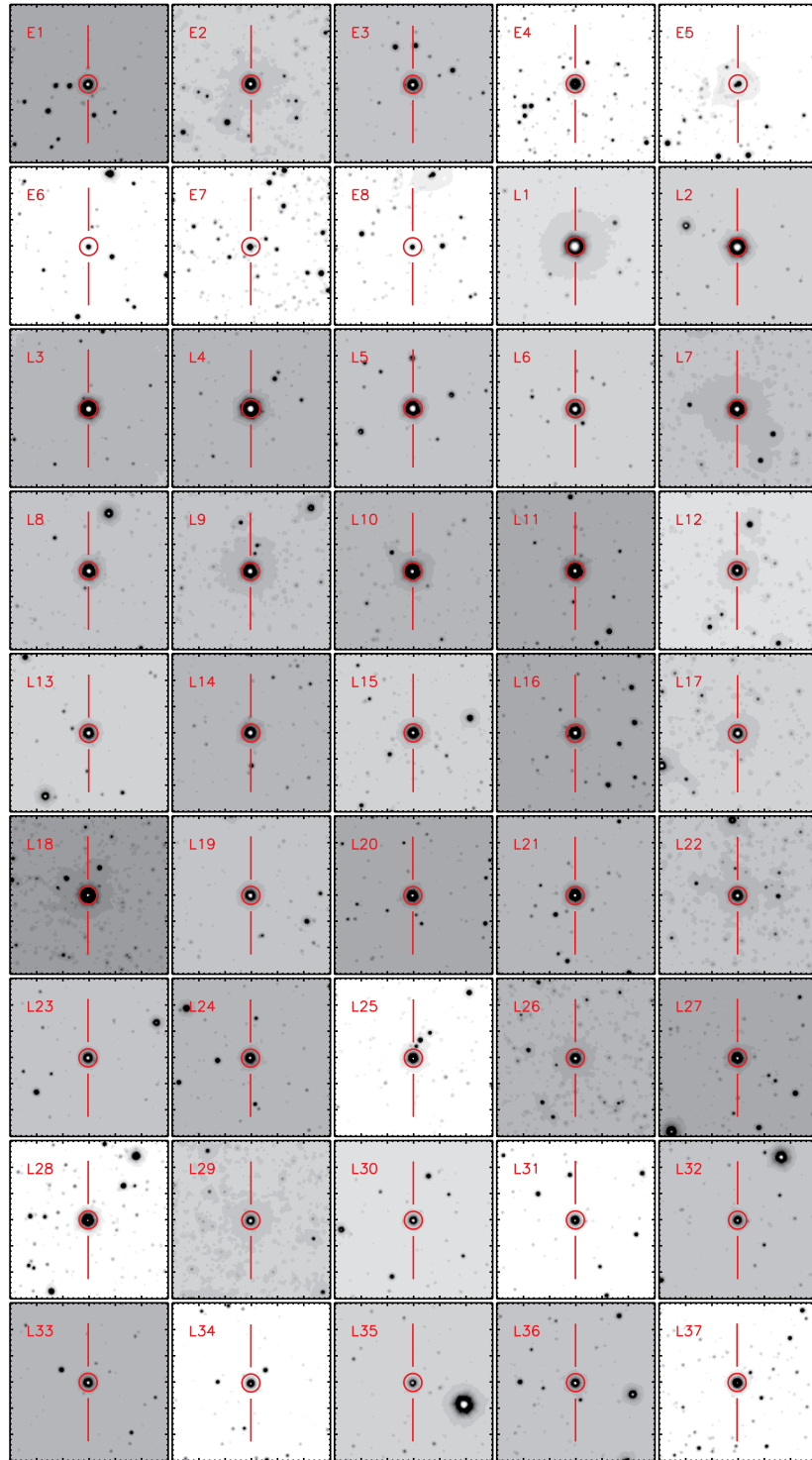


FIG. C.— 1. VVV K_s -band images ($\approx 1' \times \approx 1'$ large) of the spectroscopically detected stars in the direction of G332.809–0.132 and CS 78. North is up and east to the left. Targets are marked with circles. Identification numbers are as in Tables 2 and 4.

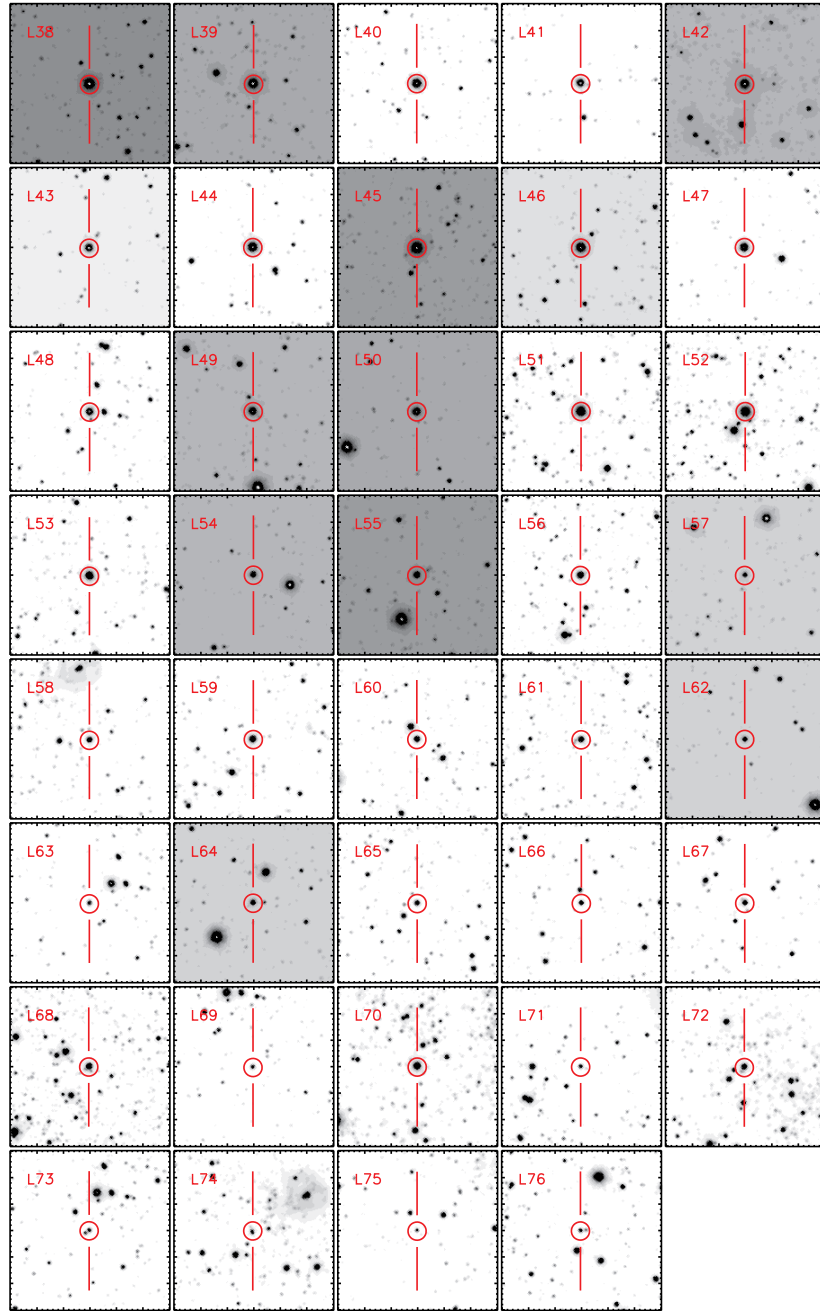


FIG. C.— 1. Continuation of Fig. C1.

- Aharonian, F., Akhperjanian, A. G., Bazer-Bachi, A. R., et al. 2006, *ApJ*, 636, 777
- Alter, G., Balazs, B., Ruprecht, J., & Vanysek, J. 1970, *Catalogue of Star Clusters and Associations* (Budapest: Akademiai Kiado)
- Ambartsumian, V. A. & Kandalian, R. A. 1989, *Astrofizika*, 30, 455
- Bica, E., Pavani, D. B., Bonatto, C. J., & Lima, E. F. 2019, *AJ*, 157, 12
- Blum, R. D., Depoy, D. L., & Sellgren, K. 1995, *ApJ*, 441, 603
- Blum, R. D., Ramírez, S. V., Sellgren, K., & Olsen, K. 2003, *ApJ*, 597, 323
- Borghese, A., Coti Zelati, F., Esposito, P., et al. 2018, *MNRAS*, 478, 741
- Borissova, J., Ramírez Alegria, S., Alonso, J., et al. 2016, *AJ*, 152, 74
- Bossini, D., Vallenari, A., Bragaglia, A., et al. 2019, *A&A*, 623, A108
- Brinkmann, W., Kawai, N., Scheingraber, H., Tamura, K., & Becker, W. 1999, *A&A*, 346, 599
- Bronfman, L., Nyman, L.-A., & May, J. 1996, *A&AS*, 115, 81
- Brooks, K. J. & Whiteoak, J. B. 2001, *MNRAS*, 320, 465
- Cantat-Gaudin, T., Jordi, C., Vallenari, A., et al. 2018, *A&A*, 618, A93
- Caswell, J. L. & Haynes, R. F. 1987, *A&A*, 171, 261
- Caswell, J. L., Murray, J. D., Roger, R. S., Cole, D. J., & Cooke, D. J. 1975, *A&A*, 45, 239
- Chang, C., Konopelko, A., & Cui, W. 2008, *ApJ*, 682, 1177
- Churchwell, E., Babler, B. L., Meade, M. R., et al. 2009, *PASP*, 121, 213
- Churchwell, E., Watson, D. F., Povich, M. S., et al. 2007, *ApJ*, 670, 428
- Clark, J. S., Davies, B., Najarro, F., et al. 2009, *A&A*, 504, 429
- Clark, J. S., Egan, M. P., Crowther, P. A., et al. 2003, *A&A*, 412, 185
- Clark, J. S., Larionov, V. M., & Arkharov, A. 2005, *A&A*, 435, 239
- Clark, J. S., Steele, I. A., Fender, R. P., & Coe, M. J. 1999, *A&A*, 348, 888
- Condon, J. J., Cotton, W. D., Greisen, E. W., et al. 1998, *AJ*, 115, 1693
- Conti, P. S. & Crowther, P. A. 2004, *MNRAS*, 355, 899
- Cordes, J. M. & Lazio, T. J. W. 2002, *arXiv astro-ph/0207156*
- Corti, M. A., Baume, G. L., Panci, J. A., et al. 2016, *A&A*, 588, A63
- Crowther, P. A., Hadfield, L. J., Clark, J. S., Negueruela, I., & Vacca, W. D. 2006, *MNRAS*, 372, 1407
- Cutri, R. M., Skrutskie, M. F., van Dyk, S., et al. 2003, *VizieR Online Data Catalog*, 2246
- Davies, B., de La Fuente, D., Najarro, F., et al. 2012, *MNRAS*, 419, 1860
- Davies, B., Figer, D. F., Kudritzki, R.-P., et al. 2009, *ApJ*, 707, 844
- Dutra, C. M., Bica, E., Soares, J., & Barbuy, B. 2003, *A&A*, 400, 533
- Englmaier, P. & Gerhard, O. 1999, *MNRAS*, 304, 512
- Epchtein, N., de Batz, B., Copet, E., et al. 1994, *Ap&SS*, 217, 3
- Figer, D. F., MacKenty, J. W., Robberto, M., et al. 2006, *ApJ*, 643, 1166
- Figer, D. F., McLean, I. S., & Morris, M. 1995, *ApJ*, 447, L29
- Figer, D. F., McLean, I. S., & Morris, M. 1999, *ApJ*, 514, 202
- Figer, D. F., McLean, I. S., & Najarro, F. 1997, *ApJ*, 486, 420
- Figer, D. F., Najarro, F., Geballe, T. R., Blum, R. D., & Kudritzki, R. P. 2005, *ApJ*, 622, L49
- Frank, K. A., Burrows, D. N., & Park, S. 2015, *ApJ*, 810, 113
- Fukui, Y., Kohno, M., Yokoyama, K., et al. 2018, *PASJ*, 70, S41
- Gaensler, B. M., Stappers, B. W., Frail, D. A., et al. 2000, *MNRAS*, 318, 58
- Gaia Collaboration, Brown, A. G. A., Vallenari, A., et al. 2018, *A&A*, 616, A1
- Gotthelf, E. V. & Halpern, J. P. 2008, *ApJ*, 681, 515
- Green, D. A. 1991, *PASP*, 103, 209
- Green, D. A. 2014, *Bulletin of the Astronomical Society of India*, 42, 47
- Green, D. A. 2019, *Journal of Astrophysics and Astronomy*, 40, 36
- Gvaramadze, V. V., Weidner, C., Kroupa, P., & Pflamm-Altenburg, J. 2012, *MNRAS*, 424, 3037
- H. E. S. S. Collaboration, Abdalla, H., Abramowski, A., et al. 2018, *A&A*, 612, A3
- Hamann, W.-R., Gräfener, G., & Liermann, A. 2006, *A&A*, 457, 1015
- Hare, J., Kargaltsev, O., Pavlov, G. G., Rangelov, B., & Volkov, I. 2017, *ApJ*, 841, 81
- Heger, A., Fryer, C. L., Woosley, S. E., Langer, N., & Hartmann, D. H. 2003, *ApJ*, 591, 288
- Ho, W. C. G. & Andersson, N. 2017, *MNRAS*, 464, L65
- Houk, N. 1978, *Michigan catalogue of two-dimensional spectral types for the HD Stars* (Ann Arbor, MI: Univ. Michigan)
- Humphreys, R. M. 1978, *ApJS*, 38, 309
- Humphreys, R. M., Gordon, M. S., Martin, J. C., Weis, K., & Hahn, D. 2017, *ApJ*, 836, 64
- Humphreys, R. M. & McElroy, D. B. 1984, *ApJ*, 284, 565
- Immer, K., Galván-Madrid, R., König, C., Liu, H. B., & Menten, K. M. 2014, *A&A*, 572, A63
- Kargaltsev, O., Pavlov, G. G., & Wong, J. A. 2009, *ApJ*, 690, 891
- Kharchenko, N. V., Piskunov, A. E., Schilbach, E., Röser, S., & Scholz, R. D. 2016, *A&A*, 585, A101
- Kleinmann, S. G. & Hall, D. N. B. 1986, *ApJS*, 62, 501
- Koornneef, J. 1983, *A&A*, 128, 84
- Kumar, C. K. 1978, *ApJ*, 219, L13
- Lejeune, T. & Schaerer, D. 2001, *A&A*, 366, 538
- Liu, X. W., Xu, R. X., van den Heuvel, E. P. J., et al. 2015, *ApJ*, 799, 233
- Luri, X., Brown, A. G. A., Sarro, L. M., et al. 2018, *A&A*, 616, A9
- Manchester, R. N., Hobbs, G. B., Teoh, A., & Hobbs, M. 2005, *AJ*, 129, 1993
- Martín-Hernández, N. L., van der Hult, J. M., & Tielens, A. G. G. M. 2003, *A&A*, 407, 957
- Martins, F., Genzel, R., Hillier, D. J., et al. 2007, *A&A*, 468, 233
- Martins, F. & Plez, B. 2006, *A&A*, 457, 637
- Martins, F., Schaerer, D., & Hillier, D. J. 2005, *A&A*, 436, 1049
- Massey, P. 2000, *PASP*, 112, 144
- Mathew, B., Varricatt, W. P., Subramaniam, A., Ashok, N. M., & Banerjee, D. P. K. 2014, *Research in Astronomy and Astrophysics*, 14, 1173
- Mauerhan, J. C., Van Dyk, S. D., & Morris, P. W. 2011, *AJ*, 142, 40
- Mel'nik, A. M. & Dambis, A. K. 2017, *MNRAS*, 472, 3887
- Mel'nik, A. M. & Efremov, Y. N. 1995, *Astronomy Letters*, 21, 10
- Messineo, M. & Brown, A. 2019, *ApJ*
- Messineo, M., Davies, B., Figer, D. F., et al. 2011, *ApJ*, 733, 41
- Messineo, M., Davies, B., Ivanov, V. D., et al. 2009, *ApJ*, 697, 701
- Messineo, M., Figer, D. F., Davies, B., et al. 2008, *ApJ*, 683, L155
- Messineo, M., Habing, H. J., Menten, K. M., Omont, A., & Sjouwerman, L. O. 2004, *A&A*, 418, 103
- Messineo, M., Habing, H. J., Menten, K. M., et al. 2005, *A&A*, 435, 575
- Messineo, M., Menten, K. M., Churchwell, E., & Habing, H. 2012, *A&A*, 537, A10
- Messineo, M., Menten, K. M., Figer, D. F., Chen, C. H. R., & Rich, R. M. 2018, *ApJ*, 862, 10
- Messineo, M., Menten, K. M., Figer, D. F., et al. 2014, *A&A*, 569, A20
- Messineo, M., Zhu, Q., Menten, K. M., et al. 2017, *ApJ*, 836, 65
- Minter, A. H. 2008, *ApJ*, 677, 373
- Morales, E. F. E., Wyrowski, F., Schuller, F., & Menten, K. M. 2013, *A&A*, 560, A76
- Mori, K., Gotthelf, E. V., Zhang, S., et al. 2013, *ApJ*, 770, L23
- Morris, P. W., Eenens, P. R. J., Hanson, M. M., Conti, P. S., & Blum, R. D. 1996, *ApJ*, 470, 597
- Muno, M. P., Clark, J. S., Crowther, P. A., et al. 2006, *ApJ*, 636, L41
- Murray, N. & Rahman, M. 2010, *ApJ*, 709, 424
- Najarro, F., Figer, D. F., Hillier, D. J., Geballe, T. R., & Kudritzki, R. P. 2009, *ApJ*, 691, 1816
- Najarro, F., Krabbe, A., Genzel, R., et al. 1997, *A&A*, 325, 700
- Oh, S., Kroupa, P., & Banerjee, S. 2014, *MNRAS*, 437, 4000
- Panagia, N. 1973, *AJ*, 78, 929
- Pauls, T. 1977, *A&A*, 59, L13
- Price, S. D., Egan, M. P., Carey, S. J., Mizuno, D. R., & Kuchar, T. A. 2001, *AJ*, 121, 2819
- Rahman, M., Matzner, C. D., & Moon, D.-S. 2013, *ApJ*, 766, 135
- Rahman, M. & Murray, N. 2010, *ApJ*, 719, 1104
- Ramírez, S. V., Stephens, A. W., Frogel, J. A., & DePoy, D. L. 2000, *AJ*, 120, 833
- Rea, N., Borghese, A., Esposito, P., et al. 2016, *ApJ*, 828, L13
- Reid, M. J., Menten, K. M., Zheng, X. W., et al. 2009, *ApJ*, 700, 137
- Roman-Lopes, A. & Abraham, Z. 2004, *AJ*, 127, 2817
- Roman-Lopes, A., Abraham, Z., Ortiz, R., & Rodríguez-Ardila, A. 2009, *MNRAS*, 394, 467
- Ruprecht, J., Balazs, B., & White, R. E. 1982, *Bulletin d'Information du Centre de Donnees Stellaires*, 22, 132
- Russell, D., Adami, C., Bouret, J. C., et al. 2017, *A&A*, 607, A86
- Russell, D., Tigé, J., Adami, C., et al. 2016, *A&A*, 587, A135
- Safi-Harb, S., Ribó, M., Butt, Y., et al. 2007, *ApJ*, 659, 407
- Saito, R. K., Minniti, D., Dias, B., et al. 2012, *A&A*, 544, A147
- Sampedro, L., Dias, W. S., Alfaro, E. J., Monteiro, H., & Molino, A. 2017, *MNRAS*, 470, 3937
- Shara, M. M., Moffat, A. F. J., Gerke, J., et al. 2009, *AJ*, 138, 402
- Shull, J. M. & Danforth, C. W. 2019, *ApJ*, 882, 180
- Skiff, B. A. 2014, *VizieR Online Data Catalog*, 1
- Skrutskie, M. F., Cutri, R. M., Stiening, R. 2006, *AJ*, 131, 1163
- Smith, N., Aghakhanloo, M., Murphy, J. W., et al. 2019, *MNRAS*, 488, 1760
- Smith, N. & Tombleson, R. 2015, *MNRAS*, 447, 598
- Stafford, J. N., Lopez, L. A., Auchettl, K., & Holland-Ashford, T. 2019, *ApJ*, 884, 113
- Steele, I. A. & Clark, J. S. 2001, *A&A*, 371, 643
- Storey, P. J. & Hummer, D. G. 1995, *MNRAS*, 272, 41
- Suárez, O., García-Lario, P., Manchado, A., et al. 2006, *A&A*, 458, 173
- Taylor, J. H. & Cordes, J. M. 1993, *ApJ*, 411, 674
- van der Hucht, K. A. 2001, *New A Rev.*, 45, 135
- van Genderen, A. M., Sterken, C., & de Groot, M. 1997, *A&A*, 318, 81
- Weldrake, D. T. F., Wood, P. R., & van de Steene, G. C. 2003, in *IAU Symposium, Vol. 209, Planetary Nebulae: Their Evolution and Role in the Universe*, ed. S. Kwok, M. Dopita, & R. Sutherland (San Francisco, CA: ASP), 129
- Westerlund, B. E. 1969, *AJ*, 74, 882
- Willis, S., Marengo, M., Allen, L., et al. 2013, *ApJ*, 778, 96
- Wolf, B. & Kaufer, A. 1997, *Astronomical Society of the Pacific Conference Series, Vol. 120, Spectral Variations of LBVs during Outbursts*, ed. A. Nota & H. Lamers, 26
- Wright, E. L., Eisenhardt, P. R. M., Mainzer, A. K., et al. 2010, *AJ*, 140, 1868
- Wright, N. J., Drew, J. E., & Mohr-Smith, M. 2015, *MNRAS*, 449, 741
- Wu, Y. W., Sato, M., Reid, M. J., et al. 2014, *A&A*, 566, A17
- Xing, Y., Wang, Z., Zhang, X., & Chen, Y. 2014, *ApJ*, 781, 64
- Zacharias, N., Monet, D. G., Levine, S. E., et al. 2004, *AAS Meeting*, 205, 48, 15